

Diss. ETH No. 20983

ENGINEERING APPROACHES FOR STUDYING MYOGENESIS

A dissertation submitted to
ETH ZÜRICH

for the degree of
Doctor of Sciences
(Dr. sc. ETH Zürich)

presented by
ELSA CHARLOTTA THOMASSON
MSc in Engineering Physics
Chalmers University of Technology
born on November 11, 1982
citizen of Sweden

accepted on the recommendation of
Prof. Dr. Janos Vörös, examiner
Dr. Gábor Csúcs, co-examiner
Dr. Aldo Ferrari, co-examiner

2013

*So eine Arbeit wird eigentlich nie fertig. Man muß sie für
fertig erklären, wenn man nach Zeit und Umständen das
Mögliche getan hat.*

JOHANN WOLFGANG VON GOETHE, "ITALIENREISE" (1787)

Acknowledgements

This is my opportunity to express my gratitude to the people who have contributed to the success of this thesis. I am very grateful for the advice, support and discussions that all of you have provided. Without you, the completion of this work would not have been possible.

Janos, six years ago you accepted me as a master thesis student in your brand new lab. I was a bit nervous when I wrote the application email because it was my first one for a project abroad. Five minutes later you called me on my mobile phone and offered me a master thesis position. Since then you have always taken your time whenever I had anything to discuss. Thank you for your guidance and advice, especially when my PhD project presented rough times. After all, you are the one who taught me that every problem has at least 50 solutions! My next thanks go to Tomaso and Aldo. I had a great time working together with both of you on the FluidFM project. Tomaso, you are one of the most structured scientists I have ever met and that certainly provided a very important contribution for our project. Aldo, is there anything you don't know? Your knowledge about your topic is better than any encyclopedia. To learn about, and work on the immune response together with you was a pure joy! I would also like to express my gratitude to Al for starting my initial PhD project and showing me how to run a cell lab. Your experience in proper aseptic techniques and handling of contamination was helpful as the lab grew larger. I further thank our collaborators in the Nanotechnology group, Department of Mechanical and Process Engineering, ETH Zurich as well as the people in the Microsystems For Space Technologies Lab EPFL, Neuchâtel for the fruitful work we did together. Dr. Gábor Csúcs is acknowledged for his very helpful input regarding image processing and for proof reading the manuscript on cytoskeletal support during myogenesis.

What would our research group do without the helpful people who dedicate their time to simplify our tasks? Thank you Esther for keeping track of our expenses and reimbursements, for making sure that we are supplied with everything necessary from work spaces to pens and for organizing several very nice Christmas dinners. Thank you Stephen Wheeler for all the tools you have constructed for my experiments. You always improved my designs so that the end result became at least ten times better than expected! My work in the clean room would not have gone as smoothly as it did without the help from Martin Lanz. Thank you for introducing me to the equipment and for your friendly suggestions when I needed to correct mistakes. Gosia and Anette, thank you for making sure that there was always enough ethanol and bleach in the cell lab and for repairing the autoclave over and over and over again. Thank you Dominik for the PDMS membrane construction tool and for participation in numerous LBB hat making occasions.

Norma, you are a fantastic person! Thank you for your cheerful and down to earth advice and support during my entire PhD time. Together with you, I learned how to handle the most extreme and sometimes even absurd situations. Thank you for the calendar and for the corrections! You are a very important person to me. Thank you for your friendship!

Thank you Leena for all the cool events we have been to together! Hiking, snowshoeing, skiing, climbing, volleyball and to my great surprise even the gym. Everything is fun when you are around! Your friendship is very important to me. Also, neither the LBB kitchen nor the cell lab would be even close to their current standards if it would not be for our Finnish super-girl.

Thank you Victoria for being an excellent lab manager and a very nice desk mate! Prayanka, no party starts before you are there. Thank you for your laughs and entertaining stories. Johnny Bravo, viva! Harald and Bernd thank you for the awesome group retreat in Innsbruck. Laszlo, thank you for bringing the Hungarian-Japanese-singing perspective of life to the group. Peter, thanks for the booze, the hiking, the organization of the cookie competition and for your very authentic interpretation of Popeye. Dario, thank you for the FluidFM tips. Pablo, thank you for being the most active wiki-page updater. Julianne, your power will never cease to astonish me! Vincent, thanks for the friendly greetings every time we pass each other in the corridor. Alex L, thanks for polishing the wine tasting skills of our group. Kaori, it was really cool going skiing together with you. Blandine, you have my eternal respect for your skills in table soccer. Raphi 1, it was great fun to work on the cell sheet project together. Raphi 2, thank you for showing me what it means to come from the country of clocks. When I had run 14 km over two mountains

and handed over the baton with my last forces before collapsing, you let me happily know that you appreciated my punctuality. Benji, thanks for your advice on statistics. Thanks to Idalia for bringing knowledge about particles to the group. Andreas Dahlin, LBB is not the same without your subtle jokes and thought through ideas about the role of the scientist in society.

Many thanks go to the LBB associates who operate outside our lab. Marcy, Rami, Gemma, Chris, Queralt, Nicolas and all the others from the CERL group are greatly acknowledged for good collaboration. Pascal and Mike, thanks for the FluidFM-tips! Sophie, Florian and Martina, it is very nice that you always join for the group events.

There are three people who have contributed extra much to the progress of my thesis through their independent minds and devoted work. A big thank you for my students: Loïc, Radu and Liting.

LBB does not look the same as when I first arrived. Many thanks for introducing me to the group and acting as good role models in most of the LBB activities go to the people who have already left: Brigitte, Blädi, Dorothee, Takumi, Robert, Marta, Mike, Ana, Bink and Orane.

A very very big thank you to all the people from LTNT!! Davide, Mirko, Severin, Simone, Bercan, Giulia, Nada, Wolfgang, Daniele, and all the others. Thank you for parties, Friday beers, climbing and a lot of fun. I had a great time working in your lab.

At this point I would like to thank my friends in Sweden and elsewhere, who have all been of great support during my PhD. I value your friendship very much. Cissi and Johanna, thank you for being there since we were 14 years old. Every time I come home I can barely wait until I have a chance to see you again. Thank you for always having time also when you don't, and always having new interesting topics to discuss. Klara and Martin, you are the best examples I know for how to get things done properly. The fact that we have lived far away from each other for a long time has never been an obstacle for us to meet regularly. You are the ones who showed me that if you want to go somewhere, you simply go there. Thank you for trusting me to be the godmother of Agnes. I am so happy about this intelligent little person. Linus and Darya, you moved to Switzerland! That was an unexpected and very welcome solution to us meeting more often. Thank you for all the fun we have had together both in Sweden and in Switzerland. Asta, not coming from the same country and not living in the same country, our chances of meeting often should be quite slim. But we do! I am really happy about all the time we have spent

together discussing everything from cool activities to basic views of life. I appreciate you very much and I have learnt a lot from you. The bird and the flower smiled at me throughout the entire writing process. Zhanel, thank you for showing me the beauty of piano playing and for bringing me and Tasos to Kazakhstan. It is great to know you!

Taso, being a member of the family, I guess you had to wait a little longer for your acknowledgement :-P. However, you are acknowledged for general awesomeness, for amazing filled peppers, for reading my entire thesis, for being a great colleague, for supporting me in everything that matters and for sending me an email stating that I'm awesome in ten different programming languages. All in all for being my team mate and my best friend in life. I trust you for everything except perhaps leaving you alone in the kitchen.

I would like to thank my entire family for their never ceasing support during my PhD. You are all very important to me. Knowing that you would always pick me up and put me back on track no matter in what state I end up is the most important comfort and security I have in life. Tack mamma och Stig, pappa och Mimmi, Ingrid, Agnes, André, Rikard, Bénédicte, Lucas, Félicia, farfar och Vega, mormor och morfar, farmor, Pia och Göran, Klasse, Gunilla, Nike och Dicte, Jazze, Yvonne, Henke med familj och Lisa.

ETH Zurich and the Swiss National Science Foundation (SNF) K-32K1-116532/1 are greatly acknowledged for funding.

Abstract

Muscle wasting disorders such as sarcopenia and muscular dystrophy cause severe degradation to life quality or even an early death. These disorders are not only severe, they are currently also incurable. Successful development of a cure requires a better understanding of muscle development. Three different perspectives of myogenesis are investigated within this thesis in three different parts. The first part unravels fundamental aspects of myogenesis. The second part is of engineering nature. The third and last part presents an application of myoblasts that could potentially be used in clinical practice.

The first part of this thesis is detailed in three chapters. In the first results chapter, structural investigation of adherens junctions and of the actin cytoskeleton provided insights in the process of myoblast fusion. Confocal laser scanning microscopy was used to capture images and cross sections from fixed and stained myoblasts during three different stages of myogenesis: 1) initial cell-cell contact formation, 2) myoblast-myoblast fusion and 3) the final stage of mature myofibers. The results indicated that an up to now unknown tubular cytoskeletal support was formed at the fusion site. This support appeared to be actin based and shared with the two fusing cells. Actin filaments from both cytoskeletons were linked through cadherins. A combined setup of atomic force microscopy and confocal laser scanning microscopy was used to image live myoblasts during fusion. The results indicated that a cytoskeletal support was already in place before cytosolic exchange took place. That is, before the fusion pore opened up. Counting of nuclei belonging to the different stages of myogenesis let us conclude that the fusion process was fast in comparison with all other stages. Finally, a proposed model of the mechanisms behind the cytoskeletal arrangements is presented. After studying the fusion stage of myogenesis we switched focus to another phase of muscle tissue formation: the initial stages of myoblast-myoblast contact formation.

In the following results chapter, force measurements between two myoblasts, performed with fluid force microscopy, are presented. The force-time dependence indicates that the initial cell-cell contact is established within the range of 2-3 seconds. The results further indicate that the force increases linearly with the square root of time up until a point when it stabilizes at a constant value. This, in turn, suggests that the contact force is mediated by freely diffusing adhesion molecules in the cell membrane. A force measurement was also performed on another cell system: weak adhesion of monocytes to a monolayer of human umbilical vein endothelial cells. That done, we moved on from measuring force interactions to studying the developmental mechanobiology of myoblasts.

In the third results chapter, the following hypothesis is suggested: stretch induced up-regulation of mechano growth factor is mediated via calcium influx through stretch activated calcium channels (SACs). This hypothesis was tested by subjecting proliferating myoblasts to uni-axial cyclic strain in the presence of SAC blockers. Although initial results were very promising, subsequent experiments indicated a large variability in the underlying mechanism. As a result, the hypothesis could unfortunately neither be proven, nor rejected.

The engineering part of this thesis is presented in the next results chapter, where novel approaches for stretching cells were developed. Up until now, most cell stretchers use mechanical means of actuation which can lead to overheating related problems of the motor in the hot incubator. Mechanical actuation also usually requires a large setup. In this thesis, the development of two types of cell stretchers are presented: one aiming to stretch cells in culture and one stretcher for single cells. The stretching principle of both are based on electrical actuation of dielectric elastomers. The first stretcher was built-up from acrylic dielectric elastomers and provided a uni-axial in-plane stretch of a colony of cells. Myoblast alignment and partial myoblast cell sheet detachment were achieved in this type of stretcher as a response to strain. The second design was built up from poly(dimethylsiloxane) (PDMS), a silicone dielectric elastomer. Ion implantation of gold particles into a PDMS membrane allowed for patternable electrodes. Using this technology, small stretching areas could be defined. This stretcher was consequently designed for single cell stretching.

In the last part of this thesis, a novel approach to cell sheet engineering is presented. The release platform consisted of a two-block system. The underlying block had cross-linked polyelectrolyte multilayers while the upper block was built up by polyelectrolyte multilayers kept in their native state. On top of the native block, a monolayer of fi-

bronectin was adsorbed to enhance cell attachment. By adding ferrocyanide to the system, the native block dissolved. This dissolution allowed for the detachment of viable myoblast cell sheets. Further experiments showed that the dissolution affects the bonds between the fibronectin layer and the native polyelectrolyte multilayers. Hence the conclusion was drawn that these viable myoblast cell sheets still had the extracellular matrix attached to them, but no residues of the polymers remained.

The results of this thesis do not only contribute to the area of muscle development, but also prepare for further studies. Further investigation of the cytoskeletal support during myoblast fusion would lead to important insights of the mechanisms behind myogenesis. The FluidFMTM technique opens up an avenue of possibilities in the study of cell-cell interactions in any cell system. The study of mechanobiology of muscle development would profit from a standardized stretching protocol which in turn could become reality with the development of new stretchers. The ion dissolution of polyelectrolyte multilayers for cell sheet engineering is an application that could develop in two different directions. With its versatility, this technique has the potential of eventually being used in clinical trials. The dissolution of polyelectrolyte multilayers could also be developed into a single cell harvesting method where the cells are still adhered to their extracellular matrix.

Zusammenfassung

Muskelerkrankungen wie zum Beispiel Sarkopenie und Muskeldystrophie schränken die Lebensqualität der Patienten stark ein oder führen sogar zum frühzeitigen Tod. Da für derartige degenerative Erkrankungen keine Heilung existiert, stellen sie sowohl für den Patienten als auch für die Gesellschaft eine hohe Belastung dar. Um eine erfolgreiche Therapie entwickeln zu können, muss man zuerst die Prozesse der Muskelentstehung und Entwicklung (Myogenese) besser verstehen. Die drei Teile dieser Dissertation untersuchen drei verschiedene Aspekte der Myogenese. Der erste Teil ist von fundamenteller Natur und befasst sich mit grundlegenden Aspekten. Der zweite Teil ist technischer Natur. Der dritte und letzte Teil zeigt eine Anwendungsmöglichkeit von Myoblasten, die möglicherweise in Spitälern verwendet werden könnte.

Der erste Teil dieser Dissertation ist in drei Kapiteln gegliedert. Das erste Resultatekapitel erlaubt Einblicke in den Fusionsprozess von Myoblasten mittels struktureller Untersuchungen von Adhärenzverbindungen und des Aktinzytoskelettes. Konfokale Raster Laser Mikroskopie wurde benutzt, um Bilder und Querschnitte von Myoblasten aufzunehmen. Dabei wurden drei verschiedene Stadien der Myogenese untersucht: Erster Zell-Zell Kontakt, Myoblast-Myoblast Fusion und die letzte Phase von ausgereiften Myofibrillen. Die Resultate deuteten an, dass an der Fusionsstelle eine bisher unbekannte, ringförmige Stütze für das Zytoskelett ausgebildet wird. Diese ringförmige Unterstützung scheint aktinbasiert zu sein und von beiden Fusionszellen geteilt zu werden. Die Aktinfilamente beider Zytoskeletten wurden durch Cadherine verbunden. Ein kombinierter Aufbau von Rasterkraftmikroskopie und Konfokaler Raster Laser Mikroskopie wurde verwendet um die Myoblasten direkt während dem Fusionsprozess abzubilden. Die Resultate deuteten an, dass eine mechanische Stütze des Zytoskelettes bereits vor dem Öffnen der Fusionspore und dem damit verbundenen Zytosolaustausch vorhanden war. Nachdem dem Auszählen der Zellkerne in den verschiedenen Phasen, kamen wir zu der Schlussfolgerung,

dass der Fusionsprozess im Vergleich zu den restlichen Phasen sehr schnell ablief. Am Ende dieses Kapitels schlugen wir ein Modell vor, das die Mechanismen der Zytoskelettausrichtung erklären könnte. Nach der Untersuchung der Fusionsstufe in der Myogenese haben wir den Fokus auf anderen Phasen der Muskelentwicklung gerichtet: die ersten Phasen von Myoblast-Myoblast Kontaktformation.

Im zweiten Resultatekapitel, zeigen wir Kräftermessungen zwischen zwei Myoblasten. Diese Messungen wurden mit der FluidFMTM Technologie durchgeführt. Auf Grund der gemessenen Zeit-Kraft Kurven vermuteten wir, dass der erste Kontakt zwischen Myoblasten lediglich 2-3 Sekunden dauert. Zudem deuten die Resultate an, dass die Kraft linear mit der Quadratwurzel der Zeit ansteigt, und schliesslich einen konstanten Wert erreicht. Daraus schlossen wir, dass die Kontaktkraft durch frei bewegliche Moleküle in der Zellmembran weitergegeben wird. Eine Kräftermessung wurde auch mit einem anderen Zellsystem durchgeführt. Wir charakterisierten die schwache Adhäsion von Monozyten auf einer Zellschicht von menschlichen Endothelialzellen aus der Nabelschnurvene. Nach Abschluss der Kräftermessungen gingen wir dazu über die Mechanobiologie der Muskelentwicklung zu untersuchen.

Im dritten Resultatekapitel stellen wir folgende Hypothese auf: Die Produktion des Mechanowachstumsfaktors wird durch dehnungsaktivierte Kalziumkanäle (SAC) reguliert. Zum Test dieser Hypothese setzten wir proliferierende Myoblasten zyklischen, uniaxialen Belastungen aus und gaben den Experimenten SAC-Blocker zu. Während erste Experimente unsere Hypothese scheinbar bestätigten, zeigte sich im weiteren Verlauf, dass der zugrundeliegende Prozess eine grosse Veränderlichkeit aufweist. Die Hypothese konnte also weder verifiziert, noch falsifiziert werden.

Das vierte Resultatekapitel beschreibt den technischen, entwicklerischen Teil dieser Arbeit. Neue Möglichkeiten zur Zelldehnung wurden in diesem Kapitel entworfen. Bisher werden die meisten Zelldehnungsgeräte mechanisch betrieben, was mögliche Überhitzungen zur Folge hat, da die Geräte oft in warmen Inkubatoren verwendet werden. In diesem Kapitel wird die Entwicklung von zwei alternativen Dehnungsgeräten vorgestellt. Der Antrieb erfolgt bei beiden Geräten durch elektrische Stimulierung von dielektrischen Elastomeren. Das erste Gerät wurde mit dielektrischen Akrylelastomeren gebaut und ermöglichte eine uniaxiale Dehnung einer Zellkolonie in der Ebene. Mit diesem Gerät war es möglich Myoblasten aufzurichten, oder eine partielle Ablösung einer Zellschicht zu erreichen. Das zweite Gerät wurde für das Dehnen einzelner Zellen entwickelt und basierte auf einem dielektrischen Silikonkunststoff, Polydimethylsiloxan (PDMS). Durch

den Einbau von Goldionen in das PDMS war es möglich eine leitfähige Elektrode zu erhalten. Mit dieser Technik war es möglich sehr kleine Dehnungsintervalle vorzugeben.

Der letzte Teil meiner Dissertation zeigt eine neue Methode der Zellschichtentwicklung mit Myoblasten. Das Substrat für die Freisetzung der Zellschicht basierte auf einem Zweiblocksystem. Der untere Block bestand aus chemisch verknüpften Polyelektrolytmultischichten (PEMs), während der zweite Block unvernetzt war. Auf dem unvernetzten Block wurde eine Schicht Fibronectin adsorbiert um die Zellhaftung zu erhöhen. Unter Zugabe von Ferrocyanid löste sich der unvernetzte Block auf. Dies führte zur Ablösung von überlebensfähigen Myoblastschichten. Weitere Experimente zeigten, dass die Auflösung der unvernetzten PEMs lediglich die Bindungen zwischen der Fibronectinschicht und dem unvernetzten PEM auflöst. Daher haftete an den abgelösten Zellen noch extrazelluläre Matrix jedoch keine PEM-Reste mehr.

Die Resultate, die in dieser Dissertation präsentiert wurden, leisten nicht nur einen Beitrag für das Forschungsgebiet der Myogenese, sondern bieten auch die Möglichkeit zu weiteren Studien. Man könnte beispielsweise das Verständnis der Myogenesemechanismen durch weitere Studien des Zytoskelettes während der Myoblastenfusion erweitern. Die Verwendung des FluidFMs bietet Möglichkeiten zum Studium der Zell-Zell Interaktionen vieler verschiedener Zellsysteme. Die Entwicklung neuer Dehnungsgeräte könnte zu Vereinheitlichung der Protokolle zur Dehnung von Muskelzellen führen. Hiervon würde das gesamte Forschungsgebiet der Mechanobiologie profitieren. Schliesslich könnte die vorgestellte Polyelektrolytplattform zur Zellschichtablösung in zwei verschiedenen Richtungen weiterentwickelt werden. Die vielseitigen mechanischen und physischen Eigenschaften der PEMs bieten die Möglichkeit, dass diese Methode letztendlich in klinischen Studien verwendet wird. Die Auflösung der PEMs könnte auch zur Ablösung einzelner Zellen verwendet werden, wobei die extrazelluläre Matrix an den abgelösten Zellen verbleibt.

Contents

1	On Muscle Cell Differentiation and Related Tools	3
1.1	Muscle Tissue Formation - Myogenesis	4
1.1.1	human muscle	4
1.1.2	stages of myogenesis	6
1.1.3	the importance of cadherin in the initial stages of myogenesis . .	8
1.1.4	the role of the actin cytoskeleton during muscle tissue formation .	9
1.1.5	IGF-1 and its isoforms in myoblasts	10
1.1.6	the second messenger Ca^{2+} in proliferating and differentiating myoblasts	12
1.1.7	ion channels and their role in myogenesis	13
1.1.8	mechanobiology of muscle development	15
1.2	Stretching Approaches	17
1.2.1	cell stretchers	17
1.2.2	dielectric elastomers (DEs) and artificial muscle	20
1.3	Cell Sheet Engineering	23
1.3.1	cell types and applications	23
1.3.2	methods of harvesting	24
1.4	This Thesis	26
2	Scope of the Thesis	29
3	Materials and Methods	31
3.1	Materials	31
3.1.1	cell culture and cell sample preparation	31
3.1.2	cell sample analysis	33
3.1.3	polymers and other materials	35

3.2	Methods	35
3.2.1	cell culture	35
3.2.2	fixing and staining protocols	36
3.2.3	RNA extraction	37
3.2.4	cDNA synthesis	37
3.3	Instruments	37
3.3.1	imaging techniques	37
3.3.2	probing techniques	41
3.3.3	other instruments	44
4	Structural Interpretation of Myogenesis	47
4.1	Cell Culture Methods and Imaging Techniques	48
4.1.1	myogenic cultures and sample preparation	48
4.1.2	imaging with CLSM and AFM	48
4.1.3	nuclei count	49
4.2	Investigation of a Cytoskeletal Structure at the Fusion Site	49
4.2.1	making cell-cell contacts through adherens junctions	49
4.2.2	the cadherin-actin complexes are found at the periphery of the fusing cells adjusting to a rounded cell shape at the site of fusion .	50
4.2.3	a cytoskeletal structure supports the rounded shape at the fusion site prior to the opening of fusion pores	51
4.2.4	the basic functional unit of muscle tissue: the myofiber	52
4.2.5	fusion is a fast event	53
4.2.6	proposed model of cadherin-actin complex function during fusion	55
4.3	Chapter Conclusions	57
5	Cell-cell Contact Forces Measured with Fluid Force Microscopy	59
5.1	Setup and Data Processing of FluidFM TM Cell-Cell Contact Measurements	60
5.1.1	cell sample preparation	60
5.1.2	FluidFM TM procedure	62
5.1.3	processing of FluidFM TM data in MATLAB	62
5.2	Time Dependence of Initial Myoblast-Myoblast Contact Formation	64
5.2.1	measuring contact forces with FluidFM TM	64
5.2.2	initial myoblast-myoblast contact forces and dissociation energies increase linearly with the square root of time	66
5.2.3	monocyte adhesion to TNF- α treated HUVEC monolayers	69

5.2.4	initial myoblast-myoblast contact is mediated by freely diffusing adhesion molecules in the cell membranes	70
5.3	Chapter Conclusions	71
6	Calcium Mediated IGF-1 Expression as a Response to Stretch	73
6.1	Preparation and Analysis of Myoblast Stretching Experiments	74
6.1.1	preparation of cell samples	74
6.1.2	preparation of ion channel blockers	75
6.1.3	channel blocker test	75
6.1.4	stretching C2C12 myoblasts	75
6.1.5	QRT-PCR analysis	75
6.2	Subjecting Myoblasts to Stretch and Channel Blockers	76
6.2.1	channel blockers and myotube formation	76
6.2.2	stretch with streptomycin	77
6.2.3	stretch with nifedipine	79
6.2.4	stretch with BAPTA AM	80
6.2.5	MGF expression as a response to stretch	81
6.2.6	the non-trivial task of setting up a stretching experiment	82
6.3	Chapter Conclusions	84
7	Devices Designed to Stretch Cells in Culture and Single Cells	87
7.1	Creation of Devices for Cell Stretching	88
7.1.1	creation of acrylic DEA	88
7.1.2	creation of single cell stretcher	89
7.1.3	cell culture	90
7.2	Design and Performance of DEA Cell Stretchers	91
7.2.1	characterization of acrylic DEA	91
7.2.2	myoblast behaviour when subjected to stretch in acrylic DEA	93
7.2.3	Single Cell Stretcher	94
7.2.4	advantages and disadvantages of DEAs	99
7.3	Chapter Conclusions	100
8	Myoblast Cell Sheet Engineering	103
8.1	Construction of a PEM Platform for Cell Sheet Engineering	104
8.1.1	PEM assembly and fibronectin adsorption	104
8.1.2	cell culture and cell sheet harvesting	105

8.1.3	viability test	105
8.1.4	reattachment of the harvested cell sheet	105
8.1.5	QCM setup	106
8.2	Harvesting of a Viable Cell Sheet by Dissolution of PEMs	107
8.2.1	dissolution of (HA/PLL) _n with FC leaves no residues behind . . .	107
8.2.2	detachment of myoblast cell sheet by dissolution of PEMs	108
8.2.3	myoblast migration and differentiation in a reattached cell sheet .	110
8.2.4	viability of the harvested cell sheet	110
8.2.5	why does it work?	111
8.3	Chapter Conclusions	113
9	Conclusions and Outlook	115
	References	119
	Curriculum Vitae	147

Abbreviations

BSA - Bovine Serum Albumin
DAPI - 4',6-diamidino-2-phenylindole
DE - Dielectric Elastomer
DEA - Dielectric Elastomer Actuator
DM - Differentiation Medium
DMEM - Dulbecco's Modified Eagle Medium
DMSO - Dimethyl sulfoxide
dNTP - Deoxyribonucleotide triphosphate
DTT - Dithiothreitol
dsDNA - Double-stranded DNA
ECM - Extra Cellular Matrix
FBS - Foetal Bovine Serum
FC - Ferrocyanide
FN - Fibronectin
GAPDH - Glyceraldehyde 3-phosphate dehydrogenase
GM- Growth Medium
HA - Hyaluronic acid sodium salt
HEPES - 2-hydroxyethyl)piperazine-1-ethanesulfonic acid
HS - Horse Serum
HUVEC - Human Umbilical Vein Endothelial Cells
IGF - Insulin-like Growth Factor
MGF - Mechano Growth Factor or IGF-1Eb
oligo(dT) - deoxy-thymine nucleotides
PBS - Phosphate buffer saline
PDMS - poly(dimethylsiloxane)
PEI - Polyethyleneimine

PEMs - Polyelectrolyte multilayers

Pen Strep - Penicillin Streptomycin

PLL - Poly(L-lysine)

PLL-*g*-PEG - Poly(L-lysine)-graft-poly(ethylene glycol)

PMMA - Poly(methyl methacrylate)

ssDNA - Single-stranded DNA

TCPS - Tissue Culture PolyStyrene

CHAPTER 1

On Muscle Cell Differentiation and Related Tools

Four billion years ago, life started on Earth. Two to three billion years later, the first symbiosis between cells led to more complex organisms. Rather recently, about 200000 years ago, humans started to populate the world. From the perspective of evolutionary history, we are nothing but large, highly sophisticated complexes of symbiotic cells. As such, all bodily functions originate from cellular events that are precisely orchestrated to act in a synchronized manner. Such a machinery requires a refined communication system in order to function. At first glance, the tools that cells use to interpret and propagate signals appears infinite. Lists of hormones and growth factors, receptors and altered force equilibria, intra and extracellular messengers, some crucial, some redundant, could fill an entire encyclopedia. A closer look, however, brings all signals cells respond to and exert, down to two categories; chemical and mechanical stimuli [1–3]. The goal of this chapter is to introduce you to the state of current knowledge of cellular and molecular events during muscle formation -with focus on the role of the mechanical environment- and to tools related to this process. This introduction is divided into three parts: The theoretical background of myogenesis, the toolbox of stretching approaches and finally cell sheet engineering as a promising application of the knowledge of cell behavior. In the end of this chapter, the main aspects of this thesis are summarized.

1.1 Muscle Tissue Formation - Myogenesis

1.1.1 human muscle

Skeletal muscle, See Figure 1.1(a) is the only tissue in the body that allows for contractions controlled by the somatic nervous system [4, 5]. The contractile apparatus, the sarcomere, consists of an actin-myosin network that shortens upon sliding and thereby causes contraction [6]. Sarcomeres are the functional units of myofibers [7]. Myofibers, in turn, are elongated syncytia that constitute the basic unit of muscle tissue [8, 9]. The muscle tissue comprises several types of myofibers, classified on the basis of their specific muscle protein expression [7, 10, 11].

Dormant, so called satellite cells, are present and reside under the basal lamina of the myofibers [12–15]. Upon injury, see Figure 1.1(b), satellite cells get activated and change into proliferating motile cells, called myoblasts [16, 17]. When a sufficient pool of myoblasts is established, the mononucleated cells commit to differentiation. Thereby they withdraw from the proliferation cycle and fuse to form multinucleated cells, called myotubes. The latter ones eventually develop into myofibers [18]. The process of muscle tissue formation is called myogenesis [19]. In the following paragraphs, the different stages of myogenesis will be presented.

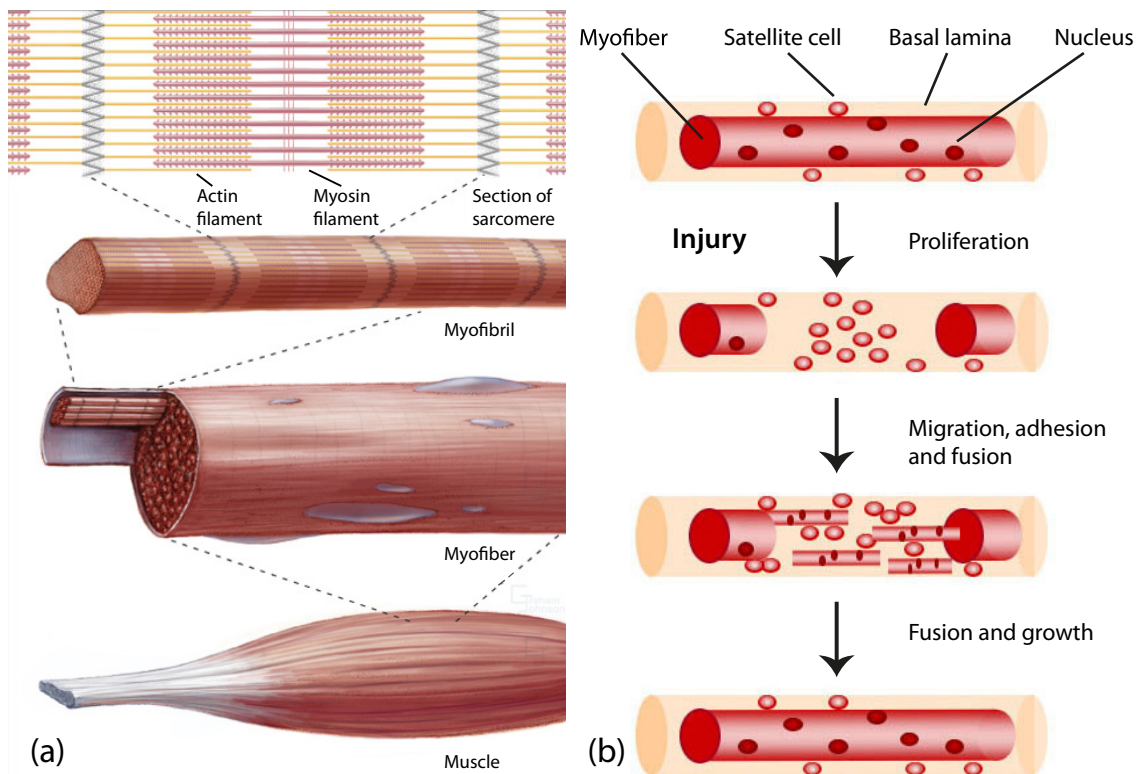


Figure 1.1: This figure shows a close up of muscle tissue architecture (a) and the process of muscle tissue repair upon injury *in vivo* (b). In (a) muscle tissue is built up from myofibers. The myofibers in turn, consist of smaller entities called myofibrils. The myofibril is a collection of highly organised contractile units called sarcomeres. The contractile function of sarcomeres originates from interactions between actin and myosin filaments. In (b) satellite cells get activated and become proliferating myoblasts. When a sufficient pool is established, the myoblasts commit to differentiation. Thereby they exit the proliferation cycle, migrate, adhere and align with other mononucleated muscle cells or pre-existing myotubes, with which they finally fuse. As nascent myotubes grow, they eventually repair the injury and the myofibre regains its functionality. (a) is reproduced from [9] and (b) from [12].

1.1.2 stages of myogenesis

Given the intrinsic difficulties of *in vivo* studies in humans, most of the knowledge we have today of muscle development has been discovered in model systems. The most studied model systems are the drosophila fly, the zebrafish (*Danio Rerio*) and the *C. elegans* nematode, as well as experimental systems of rodent cell lines and primary cells [12, 20–24]. In this part of the chapter, the aim is to give an overview of myogenesis as we know it today. The process can be divided into the following stages:

- proliferation
- migration and contact formation
- alignment and fusion
- nascent and mature myotubes

For a good visualisation of these stages, the reader is referred to the following review [25]. The focus of this text lies on discoveries made in mammalian cell cultures and in the drosophila model *in vivo* system.

proliferation

The first step of muscle development is the proliferation of myoblasts. Not yet committed to the differentiation pathway, proliferating myoblasts are still considered a part of muscle tissue formation. Their task is to establish a pool of cells, large enough that the required amount of myofibres can form. Additionally, proliferating myoblasts synthesize their own ECM in preparation for the forthcoming development into muscle tissue [26]. The composition of the ECM from both a chemical and mechanical point of view, turns out to be crucial in the context of differentiating cells [27, 28].

The proliferative phase stops upon increase in cell numbers, for example through contact inhibition. The myoblasts then change their expression of myogenic factors. This leads them to arrest the cell cycle in the G0/G1 phase [29–32]. In **cell culture**, differentiation can also be induced by decreasing serum content in the medium to which the cells are exposed, which is known to be tightly coupled with cell cycle arrest. Indeed, a decrease of serum concentration implies less growth factors, which in turn works inhibitory on proliferation [33–35]. Upon exiting the proliferation cycle, the myoblasts commit to differentiation and enter the next stage of myogenesis: migration and contact formation.

migration and contact formation

After cell cycle arrest, the first visually detectable characteristics of a differentiating myoblast is migration in the search for other cells in order to form tissue [36]. In cell culture, this migratory stage is also characterized by cells aggregating in islands, while forming cadherin mediated initial cell-cell contacts.

In *drosophila*, differentiating myoblasts belong to two separate groups with different functionalities: Founder Cells (FC) and Fusion Competent Myoblasts (FCM). FCs appear through division of progenitor cells. FCs then attract FCMs through attractant proteins, among others: Roughest (Rst) and Dumbfounded (Duf), two transmembrane proteins belonging to the Immunoglobulin superfamily [37, 38]. FCs adhere to FCMs through adhesion proteins: Hibris (Hbs) and Sticks-and-Stones (Sns), both of them having affinity to Rst and Duf [39–41].

Once myoblast-myoblast contact formation is formed, the next step is initiated: alignment and fusion.

alignment and fusion

The alignment and fusion of myoblasts follows the initial contact formation. All cell types are capable of **membrane** fusion. In fact, fusion with vesicles, endocytosis and exocytosis, is the major tool that the cell uses in order to exchange material with its environment. **Cell-cell fusion**, however, is limited to only a few cell types; for example yeast, sperm-oocyte and muscle cells [20, 42–46].

The alignment and fusion process is initiated as follows: After myoblast-myoblast contact is established, as the initial cell-cell contacts mature, larger areas replace the original points of contact. The muscle cells align, often but not always, along their long axes and fuse to form multinucleated tubes.

In *drosophila*, actin is accumulated into a specific structure, termed focus, at the site of fusion [47–49]. The actin focus is asymmetrically located and biased to the FCM. From this focus, invasive actin protrusions directed towards the FC, have been observed prior to opening of the fusion pore [50]. This actin core is surrounded by a ring-like structure called fusion-restricted myogenic-adhesive structure (FuRMAS) consisting of Sns and Kirre proteins [51, 52]. Following the disappearance of the actin focus, a fusion pore opens up, joining the two adjacent membranes [53].

In addition to studies of the *drosophila in vivo* system, *in vitro* studies of rodent myoblast fusion have also been performed to a certain extent. It has been concluded that myoblasts from the same pool of cells fuse with each other without the presence of an FC [54, 55]. Vesicle trafficking has been observed at the fusion site [56], as well as fusion pores [12]. Most of the known studies of mammalian myoblast fusion concentrate on understanding the signaling pathways governing the event, using biochemical or molecular biology approaches [57–62]. In particular, the role of small signalling G-proteins RhoA, Rac1 and cdc42 have been studied to a large extent in the context of myoblast fusion [63–67]. Additionally, studies have elucidated the function of regulatory molecules as well as their position at, or close to, the fusion site [56, 68–70].

Moreover, for determining the localization of fusion pores, cytoskeletal elements and fusion proteins, imaging methods such as atomic force microscopy (AFM), confocal microscopy and electron microscopy have also been used [56, 71–75]. However, the exact details of the fusion process remain largely unknown.

nascent and mature myotubes

When the fusion of two cells is complete, a so called nascent myotube is formed. A nascent myotube is a pre-stage of the mature myotube and contains 2-4 nuclei [54, 76]. As more cells align and fuse with the myotube, a mature myofiber, i.e. the contractile unit of muscle tissue, develops [22].

Under standard cell culture conditions *in vitro*, the first nascent myotubes are visible after 3-4 days in differentiation medium. After 6-8 days, the large fibres with tens of nuclei start to appear [77, 78]. The diameter of the nascent myotubes is mainly determined by the diameter size of one nucleus, around 12 μm , while a mature myotube can grow more than 3 times as large before it starts contracting and detaches from the substrate [79].

1.1.3 the importance of cadherin in the initial stages of myogenesis

As already mentioned, recognition and adhesion are crucial steps leading to fusion during myogenesis. The first cell-cell contacts are mediated by adherens junctions and desmosomes. In both cases a transmembrane adhesion protein, cadherin, is responsible for the connection between the two adherent cells. Cadherins are the most common cell adhesion

proteins. All cell types express at least one member of the cadherin superfamily which consists of N-cadherin, M-cadherin and VE-cadherin among others. The extracellular part of cadherin is folded into five or six beta-strand based so called **cadherin repeats**. These repeats are domains which allow for calcium dependent adhesion to another cadherin oriented in the opposite direction [8, 80–84].

The importance of cadherin during myogenesis has been studied and reviewed [85, 86] to a large extent. Mege *et al.* showed that N-cadherin mediated cell-cell adhesion was required for chicken embryo myoblast fusion [87]. Charrasse *et al.* investigated the involvement of N-Cadherin in the localization of Rho GTPases and β -catenin [88]. Matsuda further elucidated the role of N-cadherin in myoblast alignment when subjected to mechanical stretch [89]. In essence, there seems to be no doubt that the presence of N-cadherin is crucial for muscle tissue development. However, the role of M-cadherin has been subject to debate. Its involvement had already been studied for more than a decade [90–93] when Hollnagel *et al.* claimed that M-cadherin serves no required function during muscle tissue development, that could not be replaced by over expression of N-cadherin [94]. Even though the topic has been subject to further investigation after that [95], the question whether the functions of M-cadherin during myogenesis are fully redundant, has not been answered.

Cadherin mediated adhesion takes place according to the following process. The cadherin protein diffuses freely in the cell membrane ($1\text{--}2\text{ cm}^2/\text{s}$ [96]) until it is paired with another cadherin from an adjacent cell [97]. Delanoe-Ayari *et al.* proposed a mechanism by which the cadherins could aggregate at certain positions in the membrane through diffusion [98]. Once adherens junctions are formed, cadherins will next associate with an actin filament bundle through a catenin complex. This way the actin cytoskeletons from two adjacent cells become linked together [8, 80].

1.1.4 the role of the actin cytoskeleton during muscle tissue formation

Together with cadherin, actin has been shown to have a crucial role in myogenesis. Actin filaments can be assembled in a number of different ways. Examples seen in most eukaryotic cell types are spiky protrusions called filopodia, flat networks called lamellipodia and contractile stress fibers [2, 9]. Assembling in any of these three structures, **actin** is the tool that the cell uses for motility and cell shape maintenance. As such, the actin cytoskeleton

is primarily nucleated at the plasma membrane [8]. Myosin allows for the assembly of actin filaments into a contractile network that generates tension forces. This gives rise to a cytoskeleton under constant tension, starting at the various points of attachment [99].

Additionally, it has been shown that actin has a crucial role in myogenesis in the drosophila model, where actin based invasive protrusions at the site of fusion have been reported [49, 51, 52, 100]. Also myogenesis in mammalian cells is partially dependent on actin providing not only a structural element [71] but also enabling vesicle encapsulated cargo transport to the fusion site [73, 100–102]. Duan *et al.* investigated the adhesion site of differentiating rat myoblasts and found an actin wall being prominent after one day of culture in differentiation medium. This wall would disassemble after four days (Duan and Gallagher 2009). All in all, it has been shown that actin has a crucial role during myogenesis, but all details have not yet been unraveled.

1.1.5 IGF-1 and its isoforms in myoblasts

So far the process of myogenesis and the importance of the structural components cadherin and actin during muscle tissue formation, have been described. In this part of the chapter, focus will move on to the role of Insulin-Like Growth Factor 1 (IGF-1) as a chemical messenger during myogenesis.

In the 50's, the current technology to measure growth hormone was based on *in vivo* tests. As needs of a more sensitive and convenient method arose, Daughaday aimed to set up an *in vitro* system. Daughaday and Salmon could show that treatment with growth hormone of hypophysectomized rats, induced an increased sulphation in their cartilage *in vivo*. However, this effect failed to occur in their *in vitro* studies. Daughaday and Salmon concluded that an intermediate factor, induced by growth hormone, is responsible for the observed effect in rats. They called this substance **sulphation factor** [103, 104].

At first, the work of Daughaday and Salmon was met with disbelief by the scientific community. Lack of a practical assay as well as failure to find a tissue from which they -with existing technology- could extract the activity, led to poor interest from both colleagues and competitors to take up on the research of this hypothetical substance. Since then, decades have passed and the existence of the sulphation factor, later renamed to **somatomedin**, was established. Technologies such as radioimmunoassays, transgenic animals, in situ hybridisation, immunohistochemistry as well as isolation and sequencing have allowed for the study of splice variants; their sequences and location of expression.

Today somatomedin is usually referred to as **Insulin-like Growth Factor (IGF)**, which consists of two ligands: IGF-1 and IGF-2 [105]. The focus of this chapter lies on IGF-1 and its role in myogenesis.

In human muscle, three known isoforms of IGF-1 are expressed; IGF-1Ea, IGF-1Eb and IGF-1Ec. Figure 1.2 shows a schematic view of the splicing of the IGF-1 gene. IGF-1Ea is the same type as the one expressed and released by the liver and is supposed to play an important role in the development of several different tissues [106]. The function of IGF-1Eb in humans is not known. IGF-1Ec, termed IGF-Eb in rodents, is called Mechano Growth Factor (MGF) in both to avoid confusion [107–110].

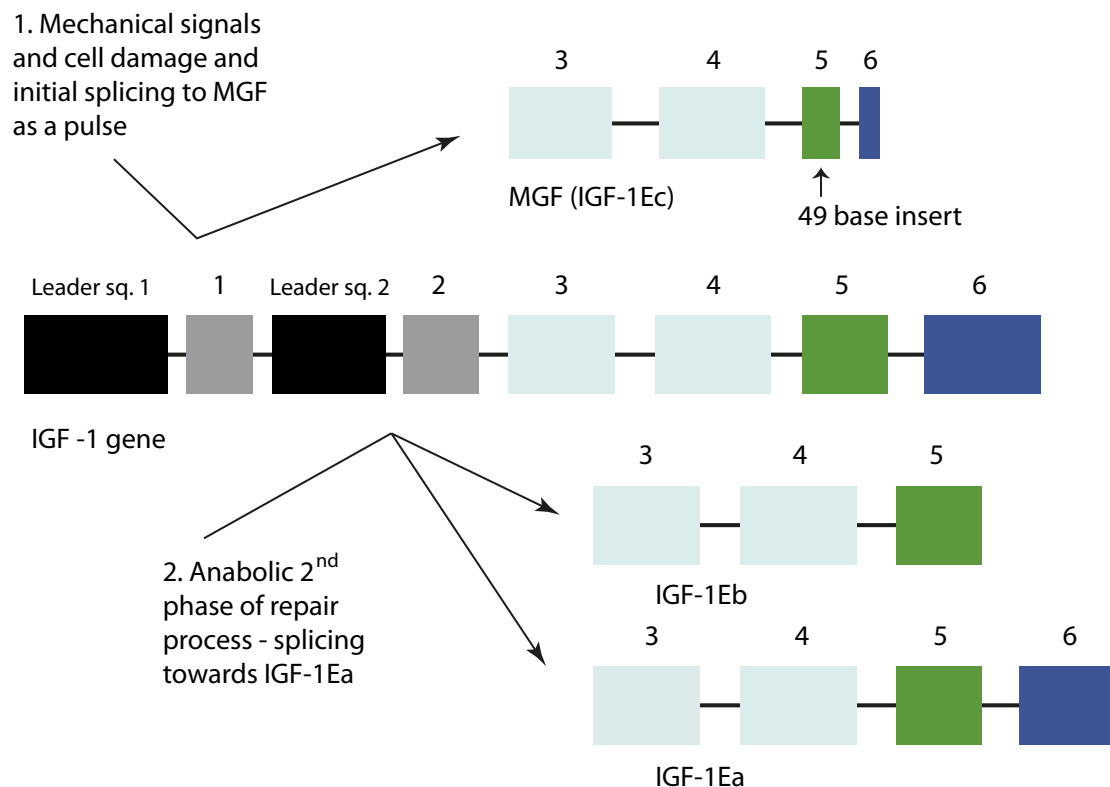


Figure 1.2: This Figure shows a schematic view of the splicing of the IGF-1 gene in human muscle. MGF is expressed as a response to mechanical signals and cell damage and promotes proliferation but inhibits differentiation. At a later stage the splicing of the IGF-1 gene switches to favor the expression of IGF-1Ea which promotes differentiation. Reproduced from [107].

Upon muscle damage, the expression of MGF peaks [111]. MGF expression turns out to be caused by changes in the mechanical environment, such as stretch [112, 113]. The

mechanical environment and its effect on myogenesis is covered in Chapter 1.1.8. As the MGF expression goes down, the splicing towards IGF-1Ea and IGF-1Eb is favored [114–116]. We recall from Chapter 1.1.1 that satellite cells, residing under the basal lamina, get activated upon injury and start proliferating. Once a sufficient pool of cells has been established, they exit the cell cycle and commence the differentiation path. Indeed, it has been shown that MGF enhances proliferation and inhibits differentiation of myoblasts *in vivo* and *in vitro* [117–120]. IGF-1Ea on other hand has shown to promote both [121, 122]. Hence the timing of the expression makes physiological sense. The expression and release of the IGF-1 splice variants are mastered by the muscle cells as a tool for communication within their own tissue. As the different splice variants of IGF-1 bind to IGF receptors in myoblasts, specific signaling pathways are activated which in turn cause the needed cell behavior [123].

Since decades, the research community is agreed on the basic functions of IGF, not to mention its existence. However, the topic still raises doubts and causes animated discussions. For example, in 2010 a discussion between Stewart and Pell, and Flueck and Goldspink arose. The disagreement concerned whether IGF is the main regulator of muscle hypertrophy or not. Stewart and Pell referred to developmental and genetic studies when claiming that it is, while Flueck and Goldspink argued from the perspective of mechanobiology where they claimed to have seen evidence of the opposite [124–128]. The discussion attracted attention from scientists in another research group, who decided to contribute with their opinion on the matter [129]. The involved people did not reach consensus, but remained faithful to their original opinion regardless of the impact of the counter-arguments.

1.1.6 the second messenger Ca^{2+} in proliferating and differentiating myoblasts

The importance of calcium in bodily functions has been a research topic since the 19th century. In 1883 Ringer saw that the Ca^{2+} in the water provided by New River Water Company, London, was necessary for heart contractions [130]. Since then it has been established that calcium is one of the most important second messengers in all living organisms, mediating parts of signaling processes governing practically all known cellular events. By altering local electrostatic fields with its charge, the Ca^{2+} ion has the capacity to change protein shape and charge upon binding [131, 132]. In order to produce a

signaling cascade mediated by calcium, the cell has to create controllable concentration differences. A major part of the cell energy is invested in this activity. Using ion pumps, the cell maintains a 20000 fold gradient between the extracellular space (in the range of mM) and the intracellular space (in the range of 100 nM). When calcium is needed in a certain location, two sources can be used. Either intracellular repositories where release occurs through ryanodine receptors or inositol 1,4,5-trisphosphate receptors [133–135] or the extracellular space, where influx is controlled by selective ion channels [136–138].

Calcium acts as a second messenger in many signaling processes at all stages of myogenesis. It has been shown that neither proliferation, nor fusion can take place, should the intracellular, or extracellular calcium concentration decrease below critical values. Przybylski *et al.* showed that the intracellular calcium concentration must be greater than 0.8 pmoles/cell and the extracellular calcium concentration cannot be lower than 0.2-0.4 mM for myoblast fusion to occur *in vitro*. However, if the extracellular calcium concentration was let below 0.9 mM, the intracellular concentration fell below its critical value [139]. Also, for the fully developed myofibre, contraction would not be possible in the absence of calcium. Further details about specific processes during and after myogenesis where calcium is involved falls outside the scope of this introductory chapter, but can be found in the following literature [140–151].

1.1.7 ion channels and their role in myogenesis

The calcium ion is one of the most important second messengers in the body in general and during myogenesis. The concept of signaling is based on maintenance of differences in calcium concentration (Chapter 1.1.6). The potential that arises allows for controlled enrichment of calcium in otherwise depleted areas. Upon interacting with proteins, a signaling cascade can take place.

The flux of calcium is controlled by ion channels. These channels can be either passive, hence allowing passage at all times, or **gated**. Gated ion channels are usually not wider than two atoms at its narrowest part. Upon activation, the proteins forming the channel change their conformation. Thereby the gating pore opens up and allows for passage. Ion channels are specific for which ions that can pass. In the case of cations, the most important channels orchestrate potassium, sodium and calcium fluxes.

There are several different types of gated ion channels, for example voltage gated, ligand gated and mechanically gated ion channels. Voltage gated channels are sensitive

to membrane potential. A voltage sensor propagates energy from the detected voltage to the pore which then opens up [152, 153]. There are many types of ligand gated ion channels and they can be activated through a diversity of substances. Depending on the type, the activation can be intra- or extracellular. In the case of intracellular binding, the ligand is usually a second messenger such as potassium, calcium or sodium [154–156]. The mechanically gated ion channels are activated by tension in the surrounding lipid bilayer [157, 158]. Gated ion channels as a group allow for passage of potassium, sodium and calcium. Each individual channel, however, is selective for a specific cation [152, 154, 159–161].

The mechanically gated ion channel was first found in chick skeletal muscle in the 1980's [162]. Since then it has been given many names; mechanosensitive channels (MSC), mechanogated channels, pressure-sensitive, pressure-induced, mechanical channels or **stretch activated channels (SACs)** [157, 163]. Several studies have shown that SACs are involved in myogenesis and muscle functionality [164–166]. Moreover, it turns out that the necessary influx of calcium during myogenesis is partially or fully mediated by SACs [102, 167, 168].

ion channel blockers

Ion channel blockers are appreciated tools for studying cell behavior orchestrated by ion channels. There exist several different types of blockers, some being specific for a certain type of ion channel, while others can interact with several different types. The most specific channel blockers are found in nature. Spiders, snakes, scorpions etc. have developed venom to shut down the nervous systems of both predators and preys by specifically blocking ion channels. The tarantula venom turns out to specifically block SACs. The peptide responsible for this action, GsMTx4, was identified and isolated by the Sachs lab [169].

Pharmacological blockage of ion channels tends to be non-specific when the choice of agent falls upon non-nature derived substances. The lanthanide gadolinium is commonly used to block SACs but the results have to be interpreted with caution because of non-specific interaction [169, 170]. Several members of the mycin family of antibiotics are popular SAC blockers. Streptomycin and neomycin are most commonly used. Ruthenium red is another example of a SAC blocker, but all of them suffer from non-specificity. Gadolinium and streptomycin are expected to also block voltage gated channels [132, 171,

172]. For voltage gated channels the list of available blockers is longer [140, 173–179]. Nifedipine is a commonly used blocker with specificity for voltage gated ion channels [180]. It is further possible to chelate the intracellular calcium storage. BAPTA-AM is a cell-permeant chelator commonly used for this purpose [181, 182].

1.1.8 mechanobiology of muscle development

Cells act in response to stimuli. These stimuli, which can be either of chemical or mechanical nature, induce a signaling cascade that eventually leads to an event taking place. Here, I will introduce the concept of mechanobiology and the role of mechanical stimuli in muscle development.

It has been shown that many cell types in our body respond to mechanical stimuli [183–193]. Examples are fibroblasts, chondrocytes, osteocytes, endothelial cells, smooth muscle cells and skeletal muscle cells [194–196]. Fibroblasts, being a part of connective tissue, have a vital role initiated by mechanical stimuli during development and wound healing. Chondrocytes respond to compression rather than tension during cartilage formation. Osteocytes are functional in an environment of constant mechanical input; torsion, tension, compression, while endothelial cells, forming the inner lining of the blood vessel respond to fluid shear stresses. Finally, both smooth muscle cells and skeletal muscle cells proliferate, differentiate and organize the architecture of the tissue guided by **mechanical forces**. For a comprehensive overview of responses to mechanical input in different cell types, the reader is referred to this excellent review by Wang *et al.* [197].

The mechanical stimuli a cell responds to will always propagate through, or be a property of, the ECM. Hence, physical movements of the ECM will cause mechanotransduction and so will the stiffness of the ECM. A number of cellular entities have been found to play a role in the different types of signaling transduction that are induced by mechanical loads [184]. Figure 1.3 shows a schematic view of some of the most studied pathways of mechanotransduction. The mechanical stimuli directly communicates with an entity that resides in the cell membrane. From the left we see SAC, G-protein, integrin and receptor tyrosine kinases (RTK). They act on their own or together. G-proteins are localized close to integrins, hence close to the site of mechanical stimulation. Upon conformational changes they start signaling cascades leading to cell growth. Integrins, constituting the attachment sites to the ECM, are the mediators that first sense mechanical load. They can start signaling cascades on their own through cytoskeletal links, or

passively allowing mechanical deformation of the cell membrane to propagate to other signaling entities nearby. RTKs are transmembrane proteins that play a role in integrin mediated signaling.

All these transmembrane mediators start signaling cascades through the cytoskeleton (**mechanical signaling transduction**) or through intracellular signaling molecules (ICSM) (**chemical transduction**). Transcription factors (TF) get activated down stream and gene transcription, leading to specific cell behavior, takes place. The cell action could be secretion of ECM products or cytokines, or DNA synthesis which leads to cell division.

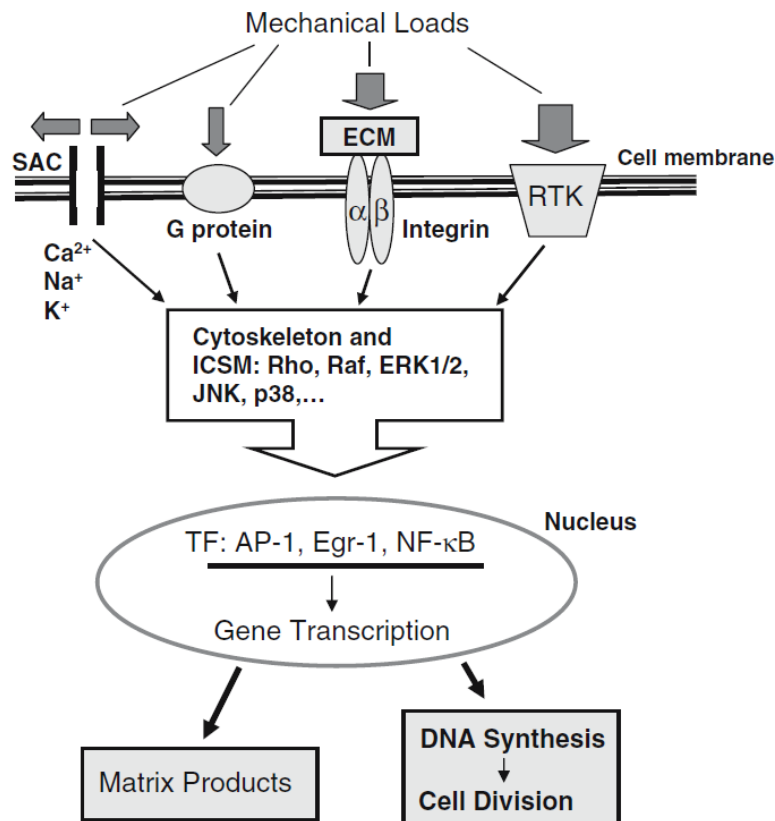


Figure 1.3: A schematic view of mechanotransduction pathways in the cell. Mechanical loads stimulate mediators, among them SACs. These mediators start a signalling cascade eventually leading to cell behavior. Reproduced from [197]

Being a tissue with the task of creating movement based on contraction, muscle tissue is constantly subjected to mechanical load *in vivo*. As such, it has not only evolved to adapt to its own produced environment, but also to make use of it. Muscle fibers are aligned according to a precise design that allows for contraction. Indeed it is also this contraction (experienced as stretch at the level of myofibers) that guides developing (new or healing) fibers to align according to a functional structure [198].

The myogenic program is also regulated by mechanical input [161, 199–202]. A bulk of studies have concluded that *in vitro* cyclic mechanical stretch stimulates proliferation but inhibits differentiation. Moreover, it turns out that MGF expression is up-regulated in myoblasts subjected to cyclic stretch [203–207]. This fits well into the picture, keeping in mind that MGF also promotes proliferation as discussed in chapter 1.1.5. Additionally, the expression of IGF-1Ea (promoter of differentiation of myoblasts) is increased as a response to both cyclic stretch and ramp stretch. IGF-1 expression is increased *in vivo* as a response to exercise [208–216].

1.2 Stretching Approaches

Up until now, the theory of myogenesis and several important factors that regulate this process have been described. The focus will now switch to the tools that have been developed in order to subject cells to stretch.

1.2.1 cell stretchers

Given the intrinsic difficulties of studying cell and tissue response to mechanical load *in vivo*, most of the knowledge we have of mechanobiology originates from *in vitro* studies. In order to mimic the *in vivo* situation, or sometimes to single out specific parameters from it, cell stretchers have been constructed. Results of cell behavior under stretching conditions have been reported based on home made stretchers or commercially available ones with different cell types and applications.

stretching paradigms

The most common mechanical loads used in the laboratories are compressive loads, fluid shear stresses and stretch [217–219]. When stretching cells, the most commonly used load paradigms are radial, uni-axial and bi-axial (Figure 1.4) [219].

Radial stretch was first introduced by Hasegawa *et al.* in 1985. A convex template was designed to induce a curvature on the bottom of a Petri dish upon applying pressure. The strain was not calculated but they claimed that it was uniform [220]. Later on, the

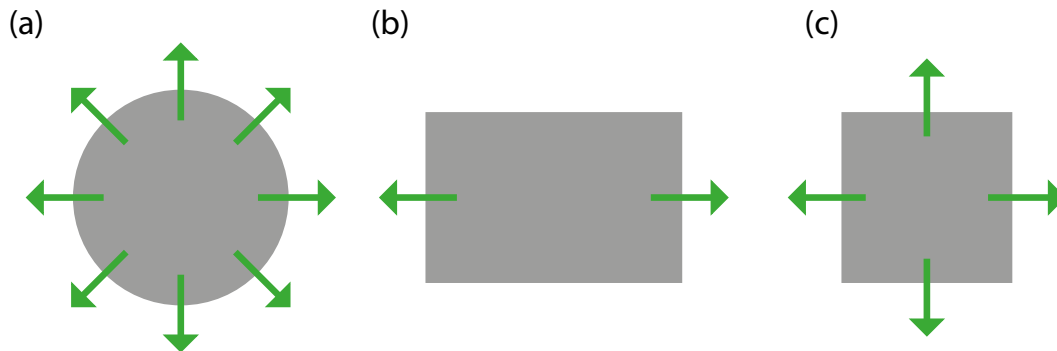


Figure 1.4: A schematic view of the most common stretching paradigms: radial (a), uni-axial (b) and bi-axial (c).

average strain of this type of device was estimated taking arc length and spherical distention into account [221] as well as by simple observation of changes in the substrate area induced by stretching [222]. More research groups have developed radial stretchers based on the platen driven mechanism [223–227].

Another approach of radial stretch is vacuum driven. In 1985 Banes *et al.* developed cell culture dishes with flexible bottoms. Downward stretch was achieved by applying vacuum from below the dish. The vacuum application was monitored by a PC which could control vacuum magnitude, waveform and frequency. The device was commercialized in 1987 as Flexercell[®] [228]. The Flexercell[®] is the most frequently used system until now. In 1995 a new version entered the market, the BioFlex-II[®] with increased diameter to thickness ratio of the stretching membrane. This improvement changed the formerly inhomogeneous radial strain to a homogeneous one. A similar approach to the vacuum induced stretch is pressure driven. The set-up is the same as for vacuum driven except that pressure is applied and the membrane therefore bends upwards [229]. Ellis *et al.* 1995 used this method for ultrafast stretch responses at strain rates up to 70 % for the study of injury response in rat cortical astrocytes [230].

The vacuum and pressure induced radial cell stretchers gained immediate acceptance by the research community. With time, however, unwanted side effects started to cause worry. The strain was heterogeneous by design. The periphery would not stretch with the same rate as the center. In order to solve this problem, new designs evolved with the stretching membrane staying in the same plane. Avoiding the out of plane buckling gave a homogeneous radial strain. Schaffer *et al.* and Hung *et al.* independently designed frictionless vertically pulsating circular ring platens. These ring platens did not have a

convex shape, but a flat one. When rising the piston, the membrane slid and remained flat [231, 232]. Versions of this design, driven by a DC motor as well as manually manoeuvred, were developed afterwards [233, 234]. In 1997 a new module for the Flexercell[®] was invented (Flexcell, inc.) which allowed for in-plane friction less stretch with vacuum.

Uni-axial stretch was tried out in the laboratories before the radial stretch. Static loading systems [235, 236] as well as oscillatory ones [237] were invented in the beginning of the 80's. The uni-axial stretching systems quickly became motor driven and automated so that frequency, strain and waveform could be chosen. A technique of clamping the substrate in two ends was the most common one [223, 238–240]. With this conceptual design in the background, many variations have been developed and tested. For home made solutions the uni-axial stretch is by far the most appreciated one [203, 241–248]. Commercially developed solutions also exist. B-Bridge international has developed and commercialized a uni-axial cell stretcher (STREX) based on mechanical stretch of a silicone membrane [249].

Bi-axial stretch has only exceptionally been used, as it in practice gives a very similar stretching pattern to radial stretch. The strain is inhomogeneous everywhere on the surface except for the exact middle, which implies obstacles in experimental design [250].

Stretchers providing radial, uni-axial or bi-axial stretch all endeavor to provide a mechanical environment which is easy to interpret. In difference to the *in vivo* situation, these techniques allow for *in vitro* 2D studies with controllable stretching parameters. Monotonous cyclic stretch over night in only one direction does not remind of physiological conditions, but gives a measurable and reliable insight in cell behavior when exposed to exactly this paradigm.

mechanical stimulation and tissue engineering

Until today, cell stretchers have mainly been used to elucidate cell behavior under mechanical stress as opposed to static conditions. As already reviewed in chapter 1.1.8, there are many different cell types that respond to the mechanical environment, among others endothelial cells, fibroblasts, myoblasts, chondrocytes and osteocytes. The knowledge of their behavior when subjected to mechanical load is growing and applications, where cells are used as tools rather than material for fundamental research, have started to emerge.

It turns out that many cell types align according to stretch [248, 251–253]. Also, differentiation is orchestrated partially by mechanical signals. Therefore, in tissue engineering, stretching has become an important tool in the design of parts of organs and of entire ones [197, 254–257].

1.2.2 dielectric elastomers (DEs) and artificial muscle

Dielectric elastomers (DEs) have been used for stretching purposes in fields other than cell stretching [258–261] and belong to the group of electroactive polymers (EAP). EAPs are polymers that change shape or size when stimulated by an electric field. The material properties that DEs have in common are low Young's modulus and high resistivity. However, the dielectric constant and the stress-strain relationship differ from DE to DE [262].

A major application of DEs is actuation. Dielectric elastomer actuators (DEA) function according to the principle described in Figure 1.5. The DE is sandwiched between two stretchable electrodes. Upon applying a voltage, the set-up functions as a capacitor and opposite charges are built up in the electrodes. Since the DE has a high resistivity, the current going through can be neglected until the breakdown voltage of the material is reached. As a consequence, the accumulated charges give rise to attractive forces (orange arrows) that squeeze the DE. Being an elastomer, the DE responds with deformation and extends in the lateral direction (green arrows). What we achieve is an in-plane stretching response to voltage application. Assuming constant volume the Maxwell stresses in each direction are $\sigma_{zz} = -\frac{1}{2}\epsilon_0\epsilon E^2$ and $\sigma_{xx} = \sigma_{yy} = \frac{1}{2}\epsilon_0\epsilon E^2$ where σ_{ii} is the Maxwell stress, ϵ_0 is the permittivity in vacuum, ϵ is the dielectric constant of the material and E is the electric field applied in the z-direction [263, 264].

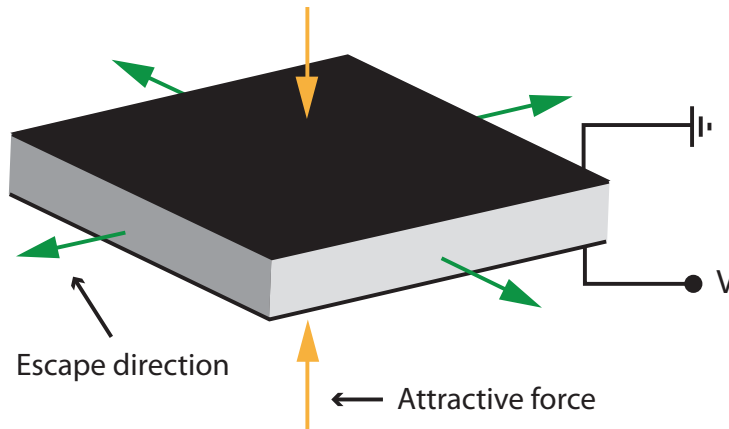


Figure 1.5: Working principle of electrical actuation of a DE. The polymer is sandwiched between two carbon black printed electrodes. As voltage is applied over the electrodes, attractive forces (orange arrows) arise and squeezes the elastomer which, as a consequence, escapes in the lateral directions (green arrows) causing a stretch event.

stretchable electrodes

For the actuation of DEs to work, there are two requirements on the sandwiching electrodes. Firstly, they have to be stretchable, preferably with a Young's modulus less than or equal to the Young's modulus of the DE. Secondly, The electrodes have to remain conductive when deformed. There are several engineering solutions to achieve stretchable electrodes [265].

Adding conductive fillers in an insulating matrix is a commonly used solution. The conductive filler is constituted of nanoparticles, often carbon black or metal particles. The matrix should be as soft as possible and the concentration of filler as low as possible in order to not stiffen the electrode more than necessary. Conductive composites display so called percolation, a transition phenomenon from insulator to conductor. The critical volume percentage of filler is the so called percolation threshold. All values below that will render an insulator and all values above, a conductor [266–268]. Carbon black can also be stamped directly on the DE and it will function as a stretchable electrode without a matrix. This way it is possible to **pattern** the electrode [269].

Metal electrodes have also been patterned directly on top of the DE with photolithography. The design can differ but the main concept is redundancy in the stretch direction. Examples are buckling electrodes [270] and lines of metal within the electrode patterned

parallel to each other and staying in contact through sliding upon stretch [271]. Additional methods include dip coating of polyelectrolyte multilayers with attached gold nano-clusters and gold ion implantation into the elastomer. The approach of using polyelectrolyte multilayers is advantageous from the perspective of stiffness. The polyanion and polycation solutions do not contribute to an increase in Young's modulus. The advantage of the ion implantation is that patterning is possible down to μm scale [272, 273].

acrylic and silicone based DEs

The choice of DE material depends on the application [274]. Kornbluh *et al.* have summarized the most commonly used DEs for actuation and their properties with focus on acrylic and silicone based DEs [275]. However, there is a number of material properties wanted in any DE [275]:

- high bulk resistance and low electrical loss factor for high efficiency
- low viscoelastic damping for high efficiency
- good electrical fatigue properties for high durability
- good mechanical fatigue properties and low creep
- good tolerance to temperature and humidity (for applications)
- ease of processing into thin uniform films with few defects for manufacturability and high yield

Acrylic as a DE was discovered in 1999 [276]. It turned out to be a very suitable material for actuation. The acrylate elastomer used in VHBTM 4910 from 3MTM has a high dielectric breakdown strength as well as a high dielectric constant. The most important application of acrylic DEs is the artificial muscle. Artificial muscle has nothing to do with real muscle tissue, but is based on the actuation response of acrylic DEs. By rolling or stacking Dielectric Elastomer Actuators (DEAs), deformation of a large entity can be achieved. Sheets can buckle, cylinders can expand or contract. This technology can be used in a variety of applications including robots [258–261]. Another example of an application of acrylic DEs is tunable optical elements [277].

Another class of materials in DEAs are silicone based. They have the advantage of higher temperature resistance than acrylic ones. Silicones also have a lower rates of moisture absorption. It remains to be shown whether these properties give a better actuation performance than the acrylic DE in challenging environments. Other parameters are comparable, with the exception of pre-stretch which is achievable to a higher rate in acrylic material. Examples of when silicone has been used is for ion implantation [273, 278–280] and for electrothermal actuation [281].

1.3 Cell Sheet Engineering

The third and last part of this chapter focuses on an application of knowledge of cell behavior. This application is cell sheet engineering. The term tissue engineering was first mentioned by Langer *et al.* 1993 when proposing a new approach for treating organ deficiencies that otherwise could not be healed [282]. The first methodology to be investigated and successfully used was the degradable scaffold, into which stem cells could be placed to proliferate and eventually create tissue, following the architecture of the template [283]. An experiment that received great attention at the time was an engineered ear growing on the back of a rat [284]. Examples of successful clinical applications are tissue engineered bone [285], bladder [286] and arteries [287, 288]. There are, however, problems with this method. The tissue-engineered constructs with biodegradable scaffolds are placed into the host and filled with proliferating cells and ECM. The scaffold itself may have unwanted properties, for example non-physiological stiffness. Deposited ECM may also lead to fibrosis [289].

In an aim to remove the biodegradable scaffold fully from the tissue engineering protocol, the approach of cell sheet engineering was proposed in the 90's by the group of Okano [290]. In cell sheet engineering, a monolayer of cells is grown on a specifically chosen substrate that allows for cell growth, and when cell-cell contacts are established, detachment from the culture surface, preferably with the ECM still attached to the sheet, is induced. The harvested monolayer of cells consists solely of bodily derived components.

1.3.1 cell types and applications

Cell sheet engineering quickly proved to be successful in clinical trials. All cell types with the capability of forming stable cell-cell contacts are suitable for creating a cell

monolayer. In some applications a different cell type than the one of the host tissue may provide a better result. An example of that is skeletal myoblasts used for cardiac repair [291].

The Okano lab has achieved most of the successful clinical trials in that field. One impressive example is the cell sheet construct used for repair of ocular trauma. Vision partially or fully disappears when the cornea is wounded. Severe conditions include Stevens-Johnson Syndrome, ocular pemphigoid and burns. Healthy corneal epithelial cells were isolated from the limbus, grown to a monolayer and harvested. The construct replaced the damaged cornea and vision was restored [292]. Corneal endothelial as well as retina pigmented epithelial cell sheet transplantations are currently tested in animal models [289].

Another remarkable achievement enabled with cell sheet engineering is the treatment of cardiomyopathy. Skeletal myoblast sheets were harvested and layered before application directly to the diseased part of the heart. No sutures were needed and the myopathy was healed. Further cardiac patches have been engineered with cardiomyocytes in order to have the pulsative contraction functionality [293–298].

Further applications are periodontal regeneration, bladder augmentation, esophageal ulcerations, epithelial patches, the sealing of lung air leaks and diabetes type 1 [283, 299–301]. More sophisticated tissue constructs are now being developed. Patterning techniques with smart materials and layering allows for 3D constructs of co-cultures for liver and kidney repair [299, 302]. Another method of 3D engineering is rolling. Myocardial tubes were created by wrapping sheets from rat cardiomyocytes around a rat aorta. After four weeks of transplantation in place of the abdominal aorta in rat the myocardial tube presented synchronized pulsations [303, 304].

Based on the success in clinical trials, the technique of cell sheet engineering will become publicly available in the foreseeable future. The companies Emmaus Medical, Inc. and CellSeed, Inc. are working on commercializing the technology of cell sheet engineering of corneal epithelial cells in US and Europe. The clinical trials in France are nearing completion and the companies will now apply for the European Medicines Agency's authorization for commercialization.

1.3.2 methods of harvesting

In cell sheet engineering, the design of the substrate is the critical part. It has to allow for cell attachment and growth during the phase of monolayer build-up. It also has to

allow for detachment in the phase of cell sheet harvesting. For this purpose polymers turn out to be a suitable class of materials given their often tunable properties. Before cell sheet engineering was introduced as a concept, the main method of cell harvesting was to use proteolytic enzymes such as trypsin and dispase. The enzymatic activity breaks all cellular attachments, both to the ECM and to other cells. In order to harvest an intact cell sheet, a different method had to be engineered. Here the two most famous solutions are presented. Both utilize polymers.

poly(N-isopropylacrylamide) (PNIPAAm)

The first solution, which is still the one used in clinical trials, employed a temperature responsive polymer, Poly(N-isopropylacrylamide) (PNIPAAm), [305]. PNIPAAm undergoes a phase transition at 32 °C. Above this temperature, the polymer coils due to hydrophobic interaction. The shrunk polymer allows cells to reach the bottom surface and adhere. However, below 32 °C, isopropyl side groups of PNIPAAm turn hydrophilic and thereby attract water molecules. The hydration of these side groups causes the polymer to swell and the increase in thickness lifts the cells from the surface, causing the adhesion bonds to the surface to break, but not the cell-cell adhesions. In short, when the cell culture dish is taken out of the incubator and put in room temperature, detachment occurs and the cell sheet can be harvested. This method is reliable, but also has its drawbacks. The preparation of the surface requires expensive tools and the grafting density is critical. Too low density does not cause the cell sheet to lift off, too high does not allow cell attachment in the first place. The optimal density turns out to be $1.4 \mu\text{g}/\text{cm}^{-2}$ (ca. 20 nm thickness) [289, 296, 304, 306, 307].

polyelectrolyte multilayers (PEMs)

Recently in our lab, another approach using polymers for cell sheet engineering was developed by Guillaume-Gentil *et al.*. This solution was based on polyelectrolyte multilayers (PEMs)[308]. The technique of building up PEMs by alternate deposition of polyanions and polycations on a surface was first described by Iler [309] in the 1960's. Frequent usage started in the 1990's with Decher *et al.* [310, 311]. Functionalizing surface coatings with this so called layer by layer (LBL) technique has two main advantages: ease of preparation and versatility. The preparation techniques (dip-coating or spraying) require

no expensive tools and are easy to handle. The mechanical, physical and chemical properties can be tuned. The choice of polyanion and polycation will determine the shape of the construct. The electrostatic interaction will be determined by the pK_a of the polymers in combination with the pH, ionic strength and temperature of the solvent. PEMs also allow for bio-functionalization which enables cells to grow on these substrates [312, 313]. With their highly tunable properties, PEMs have been used for various different applications ranging from ion separation to biomedical [312, 314–321].

Guillaume-Gentil *et al.* developed two different harvesting methods based on two different properties of PEMs; their tunable stiffness and their dissolution upon application of a current. In a monolayer of cells, two types of adhesion are involved; cell-ECM adhesion and cell-cell adhesion. As the monolayer matures, the cell-cell contacts grow stronger and intracellular contraction forces originating from the cytoskeleton increase at these sites. If the cell-ECM adhesion is weak due to low stiffness, the high contraction forces, enabled by the cell-cell contacts, will eventually force the cell-ECM contacts to break. Through their tunable mechanical properties, PEMs can provide the entire spectrum of cell adhesion, from excellent to none at all. By assembling a PEM construct that provides low cell adhesion, **spontaneous cell sheet detachment** occurs once the cell-cell contacts have become strong enough [308].

The mechanism of **electrochemical dissolution** of PEMs is hypothesized to be based on a pH change which in turn neutralizes the polyanions or the polycations (depending on whether positive or negative voltage is applied). By applying a potential, a cell sheet can be harvested on demand. Growing cells on top of a PEM construct means that they will detach when the construct dissolves. This technique also allows for patterning of cell sheets [322, 323].

Other methods of cell sheet harvesting are specific digestion of the cell substrate [324–327] and Magnetic force-based tissue engineering [328–331].

1.4 This Thesis

In light of the scientific background introduced in this chapter, this thesis is divided into three main parts that all concern muscle cells and some aspect of their growth and development. The first and largest part is of a fundamental nature. A structural analysis of cytoskeletal changes during myoblast fusion leads to a proposed model of the role

of actin filaments and adherens junctions as a support for the fusion site. Furthermore, initial myoblast-myoblast contact forces are monitored with the aid of the FluidFMTM technology. Finally a hypothesis suggesting that stretch induced up-regulation of MGF is mediated via calcium influx through SACs is tested.

The second part is of an engineering nature. The aim is to develop tools for the study of cells subjected to mechanical load. A stretcher for colonies of cells as well as a single cell stretcher are designed. Both are based on the actuation technology of DEs.

The third and last part concerns tissue engineering application of myoblast growth and development. Myoblast cell sheets are engineered using dissolution of PEMs with ferrocyanide.

CHAPTER 2

Scope of the Thesis

The introduction presented in Chapter 1 showed that research related to myoblasts is broad. Scientists working in conceptually different fields are doing research on muscle cells and their development. One of these fields is the fundamental one, where the aim is to answer scientific questions regarding myoblast behavior and muscle development. Another area is of engineering nature. As such, it is occupied with designing and constructing tools for subjecting cells to a pre-defined mechanical environment. The third field of research that was covered in the introduction is of applied nature. Cell sheet engineering was presented as a promising technique for tissue engineering and regenerative medicine. Indeed, myoblast cell sheets have proven to heal cardiomyopathy in clinical trials. Successful tissue engineering depends on the understanding of cell behavior and development as well as knowledge about the properties of relevant materials.

In this work we have aimed to contribute to all these three fields. Our fundamental research has been concentrated on cytoskeletal arrangements during fusion, forces during initial myoblast-myoblast contact formation and mechanotransduction of myoblasts. We have further developed devices to stretch cells. Finally we have engineered myoblast cell sheets by designing a novel platform.

In the first results chapter (Chapter 4) we investigated rearrangements of the actin-cadherin complex in mouse myoblasts *in vitro* in a 2D culture during myogenesis. Our findings suggested that the adherens junctions, established during initial cell-cell recognition and contact, might migrate within the cell membranes to form a tubular structure in the early stages of myoblast differentiation, resembling a mechanism previously described only for epithelial cells. Using live imaging of myoblasts with atomic force microscopy

and confocal laser scanning microscopy in combination, we further achieved results suggesting that the cytoskeleton arranged itself into a tubular structure before the fusion pore opened up. By counting nuclei of myoblasts at different stages during myogenesis we concluded that the fusion process was a fast event in comparison with the other stages. We finally proposed a mechanism by which a migration of adherens junctions may take place in order to create a tubular shape at the site of fusion.

In the second results chapter (Chapter 5) we used fluid force microscopy to probe the time dependence of myoblast-myoblast contact formation. We showed that we can probe myoblast-myoblast contact forces with the fluid force microscopy technology. Our data suggested that the contact forces and dissociation energies increased proportionally to the square root of time up until a certain time point when they stabilized at a constant force or energy. Based on the theory of Brownian motion, we suggested that the system which we were studying was a system of freely diffusing adhesion molecules in the cell membranes that interacted upon collision and thereby contributed to the adhesion force. We further tested the fluid force microscopy technology on a different cell system: monocyte adhesion to an endothelial monolayer in a state of inflammation.

In the third results chapter (Chapter 6) we hypothesized that stretch induced up-regulation of MGF is mediated via calcium influx through stretch activated calcium channels (SACs). We tested this hypothesis by stretching myoblasts in the presence of SAC blocker, voltage gated ion channel blocker and intracellular calcium storage chelator. MGF and IGF-1Ea expression were analyzed with real-time PCR.

The fourth results chapter (Chapter 7) presents engineering solutions for putting cells in a stretching environment. We created cell stretchers based on electrical actuation of acrylic DE. These stretchers were able to produce uniaxial strain up to 20%. Myoblasts were stretched in these stretchers. Cell alignment as well as partial cell sheet detachment could be observed as a response to stretch. We further designed a single cell stretcher based on actuation of PDMS as a DE.

In the fifth and final results chapter (Chapter 8) we used dissolution of PEMs as a platform to create myoblast cell sheets. The tunable chemical and mechanical properties of PEMs made them excellent candidates for constructing a surface that should provide both cell attachment and cell sheet detachment. We achieved harvesting of viable cell sheets. Additional experiments showed that the extra cellular matrix was still attached to the sheet but no polymer residues were left behind.

CHAPTER 3

Materials and Methods

This chapter lists the materials and the protocols as well as describes the instruments used throughout this thesis. Additional protocols related to a specific results section can be found in Chapter 4-8.

3.1 Materials

3.1.1 cell culture and cell sample preparation

Table 3.1 and Table 3.2 list the materials used for cell culture and cell sample preparation.

Material	Provider
C2C12 myoblasts	American Type Culture Collection (ATCC)
Cryo preservation medium, Recovery TM	Invitrogen Life Technologies
Cell Culture Freezing Medium, Liquid	
1 °C/min Freezing Container, Mr. Frosty	Nalgene
T75 cell culture flasks, SPL Polystyrol	Semadeni
DMEM (with 4.5 g/L Glucose, L-glutamine and pyruvate)	Invitrogen Life Technologies
CO ₂ independent DMEM, No L-glutamine	Gibco Invitrogen
FBS (Origin South America)	Gibco Life Technologies
HS (Heat inactivated, origin New Zealand)	Gibco Life Technologies

Table 3.1: Materials used for cell culture and cell sample preparation

Material	Provider
Trypsin-EDTA, 0.25% trypsin (1X)	Gibco Life Technologies
Pen Strep (10 000 units/mL penicillin, 10 000 μ g/mL streptomycin)	Gibco Life Technologies
Streptomycin sulfate salt (non-sterile powder)	Sigma-Aldrich
Ruthenium red	Sigma-Aldrich
Gd ³⁺ (GdCl ₃ ·6H ₂ O)	Sigma-Aldrich
Nifedipine (1,4-Dihydro-2,6-dimethyl-4-(2-nitrophenyl)-3,5-pyridinedicarboxylic acid dimethyl ester, MW=346.33)	Sigma-Aldrich
BAPTA, AM	Molecular Probes Life Technologies
Pluronic [®] F-127	Molecular Probes Life Technologies
DMSO, Dimethyl sulfoxide BioReagent, for molecular biology, $\geq 99.9\%$	Sigma-Aldrich
PBS (pH 7.4 (1X), no CaCl ₂ and no MgCl ₂)	Gibco Life Technologies
HEPES	Sigma-Aldrich
NaCl	Sigma-Aldrich
Ultrapure water	MilliQ Gradient, A 10 system, Millipore Corporation
Formaldehyde (37 wt% solution in water)	Sigma-Aldrich
Triton-X 100 (t-Octylphenoxypolyethoxyethanol)	Sigma-Aldrich
BSA	Sigma-Aldrich
Anti-PAN Cadherin primary antibody	Sigma-Aldrich
Secondary antibody Alexa Fluor 488, goat anti-rabbit IgG	Molecular Probes Life Technologies
Rhodamine-Phalloidin (Phalloidin-Tetramethylrhodamine B isothiocyanate)	Sigma-Aldrich
Mounting medium, Vectashield H 1200 (containing DAPI)	Vector Laboratories
CellTracker [™] Green CMFDA (5-Chloromethylfluorescein Diacetate), Special Packaging	Invitrogen Life Technologies
LIVE/DEAD [®] Viability/Cytotoxicity Kit, for mammalian cells	Invitrogen Life Technologies

Table 3.2: Continuation: Materials used for cell culture and cell sample preparation

preparation of solutions

- GM - 80% DMEM and 20% FBS
- DM - 95% DMEM and 5% HS
- HEPES 2 - 10 mM HEPES and 150 mM NaCl in ultrapure water
- Fixation and permeabilization medium - 4% formaldehyde, 0.1% Triton-X 100 in PBS
- Blocking solution - 20% FBS and 5% BSA in PBS
- Rhodamine-Phalloidin -
Phalloidin-Tetramethylrhodamine B isothiocyanate 0.13 $\mu\text{g/ml}$ diluted in PBS Buffer with 0.1% Triton X-10 and, 1% BSA

3.1.2 cell sample analysis

Primers were ordered from Microsynth. Table 3.3 shows the primers used in this thesis.

Description	Sequence
GAPDH Forward	5' ACGGCAAATTCAACGGCACAG 3'
GAPDH Reverse	5' GGGGGCATCGGCAGAAGG 3'
MGF Forward	5' TGCCCAGCGCCACACT 3'
MGF Reverse	5' TTCGTTTTCTTGTTTGTCTGATAGG 3'
IGF-1Ea Forward	5' AAAGCAGCCCGCTCTATCC 3'
IGF-1Ea Reverse	5' GTGTTCTTCAAATGTACTTCCTTCTGAG 3'

Table 3.3: Primers used in this thesis

The materials used for cell sample analysis are shown in Table 3.4.

Material	Provider
RNeasy Mini Kit	Qiagen AG
Qiashredder	Qiagen AG
RNase free DNase	Qiagen AG
Oligo(dT) ₂₀ Primer	Invitrogen Life Technologies
10 mM dNTP PCR Grade	Invitrogen Life Technologies
SuperScript® III Reverse Transcriptase, also includes 0.1 M DTT and 5X First Strand Buffer	Invitrogen Life Technologies
epT.I.P.S. Eppendorf Biopur	Vadaux-Eppendorf
Fast optical 96-well reaction plate with bar- code, 0.1 ml	Applied Biosystems
Fast SYBR Master Mix 50 ML	Applied Biosystems Life Technologies

Table 3.4: Materials used for cell sample analysis

3.1.3 polymers and other materials

Polymers and other materials used throughout this thesis are displayed in Table 3.5.

Material	Provider
PEI (branched), MW=25 000, 408727	Sigma-Aldrich
PLL hydrobromide, MW=15 000-30 000	Sigma-Aldrich
HA from bovine vitreous humor, MW ~300 000	Sigma-Aldrich
PDMS, Sylgard 184	Dow Corning
PDMS, Sylgard 186	Dow Corning
Montageband Transparent	Scotch 3M
Double-sticky tape 25 mm x 55 m 9460/50	Scotch 3M
PLL-g-PEG, MW of PLL=20, MW of PEG=2, grafting ratio=3.5	SuSoS Surface Technology
FC, potassium hexacyanoferrate(II) trihydrate (ferrocyanide, $\text{Fe}(\text{CN})_6^{-4}$)	Sigma-Aldrich
Carbon black, Ketjenblack EC-300J	Ketjenblack International Corporation
Copperband, smooth coated with zink	Distrelec

Table 3.5: Polymers and other materials in this thesis

3.2 Methods

3.2.1 cell culture

C2C12 myoblasts were stored in cryo preservation medium in liquid nitrogen at a passage number lower than P6 and at a density of 10^6 cells/ml. Freezing of C2C12 was done by putting the vials in a slow freezing device, mr. Frosty, and then into -80°C . Thawing was done quickly by agitating the vial in a 37°C water bath. The myoblasts were seeded at a density of $5 \cdot 10^5$ cells per T75 flask and grown in GM in a humidified cell culture incubator at 37°C and 5% CO_2 .

Myoblasts were trypsinized and passaged 1:10 before they reached a confluence of 70% which happened within two days after last passaging.

Cell counting was done with an automated cell counter, Cell countess (Invitrogen Life Technologies). Monitoring of cell growth was done with a wide field microscope capable of phase contrast imaging, equipped with a halogen lamp, a mercury lamp, filters for TRITC, FITC, and DAPI as well as a camera, Hoffman Modulation (Phase) Microscope (Leica Microsystems). All work with living cells was done in a sterile environment under a laminar flow box.

3.2.2 fixing and staining protocols

Cell samples were washed with PBS once and incubated in fixation and permeabilization medium in the fridge for 30 minutes. Afterwards the samples were washed with PBS three times.

After fixation and permeabilization, cells were incubated in blocking solution for 1h at room temperature. To stain for cadherin, the samples were incubated with anti-pan cadherin antibody at a 1:200 dilution ratio in 3% BSA/PBS, overnight at 4 °C. Afterwards the cells were incubated with a secondary antibody, Alexa Fluor 488 goat anti-rabbit IgG at a 1:1000 dilution ratio in 3%BSA/PBS for 1 hour at 4 °C. The actin filaments were stained with Rhodamine-Phalloidin, 0.13 μ g/ml diluted in 0.1% Triton X-100, 1% BSA/PBS, for 30 min at room temperature. The samples were then mounted on objective glass slides, 76x26 mm Menzel-Gläser, with mounting medium.

Live staining of C2C12 myoblasts in suspension with CellTrackerTMGreen followed the protocol supplied by the manufacturer. The following steps were performed: a stock solution (SS): 10 mM CellTrackerTMGreen in DMSO and a working solution (WS): 2 μ M (2 μ l SS in 10 ml DMEM) were prepared. Cells were trypsinized and centrifuged (5 minutes, 800 rpm). The supernatant was discarded and the cells resuspended in DMEM at 37 °C only to be centrifuged again (5 minutes, 800 rpm), the supernatant was discarded and resuspended in WS at 37 °C. The cell suspension was let to incubate in its centrifugation tube, in a humidified cell culture incubator, for 30 minutes. Afterwards they were centrifuged (5 minutes, 800 rpm), the supernatant was discarded and cells were resuspended in GM at 37 °C. The stained cells were seeded.

3.2.3 RNA extraction

The culture medium was removed from the samples and the living cells were washed once with PBS. 350 μ l per sample (10 cm^2) RTL lysis buffer (provided in the kit) was pipetted directly onto the cells and the viscous liquid was put in a 1.5 ml centrifuge tube. The RNA could be extracted right away, or the lysate could be stored in -80°C . In case of storage, the lysate was thawed out. Afterwards it was put into a QIAshredder spin column and centrifuged in a mini-spin from Eppendorf for 2 minutes at $14.4 \cdot 10^3$ rpm. 350 μ l 70% ethanol was added to the lysate and mixed by pipetting. From here on, the protocol was followed as instructed by the manufacturer of the RNeasy minikit with the recommended additional DNase on-column digestion step using RNase free DNase. The RNA samples were stored for short term in -80°C or analysed directly. The RNA purity was determined with the NanoDrop spectrophotometer as explained in Chapter 3.3.2. For all RNA handling epT.I.P.S. Eppendorf Biopur pipette tips were used.

3.2.4 cDNA synthesis

For the reverse transcription of the RNA samples, 1 μ g of total RNA was mixed with 1 μ l Oligo(dT), 1 μ l 10 mM dNTP mix and enough RNase free water (provided in the RNeasy Mini Kit) to bring up the volume to 14 μ l. The sample was incubated for 5 min in 65°C , cooled for 1 minute and centrifuged briefly (15 s, 10^4 rpm mini-spin Eppendorf). 4 μ l 5X First Strand Buffer, 1 μ l 0.1 M DTT and 1 μ l Superscript III Reverse Transcriptase were added to the solution. The vial was centrifuged (15 s, 10^4 rpm), placed at 50°C for 1 hour and finally let at 70°C for 15 minutes. After a minute of cooling condensation was brought down by centrifugation (15 s, 10^4 rpm). This cDNA sample was further analysed by PCR as described in Chapter 3.3.2.

3.3 Instruments

3.3.1 imaging techniques

Confocal Laser Scanning Microscopy (CLSM)

The basic concept of confocal microscopy was first invented in the 1950's by Marvin Minsky in an attempt to image biological events in living systems [332]. Since then, the

technique has developed to become one of the most used imaging methods in biology and material science. It has proven to be extra powerful in combination with fluorescence microscopy.

Figure 3.1 shows the working principle of the CLSM system using epifluorescence. A laser emits light (orange) at one or several well defined wave lengths. The light is collected with an optical set-up and separated by the excitation filter (a) which only allows a specific wavelength to pass. The light is next reflected by a dichroic mirror (b) and focused by the objective (c) onto a chosen point in a 3-dimensional transparent fluorescent sample. Emitted light from the sample with the exact opposite direction of the incident light will again be collected by the objective (c), pass through the dichroic mirror (b) and fit precisely to pass through a pinhole (d). Finally an emission filter (e) serves to allow only the expected emission wavelength to pass to the photomultiplier detector (PMT). Emitted light originating from any other point in the sample (blue) will not pass through the pinhole and consequently not be recorded by the detector.

The pinhole is the component that makes the system a confocal one. A thin slice of a sample (down to $0.8\ \mu\text{m}$ in thickness) can be imaged by scanning in the horizontal directions (x and y) at a desired depth (z). By varying the z-position, a 3-dimensional stack can be constructed. [333, 334]

In this thesis a LSM 510 (Zeiss) equipped with a Plan-Apochromat 63x/1.40 Oil DIC M27 was used. Argon, diode 405 and DPSS 561 lasers were combined with appropriate filter settings to enable imaging of the three different dyes in separate channels. The resolution of the images was set to 1024×1024 pixels and the size was $143\ \mu\text{m} \times 143\ \mu\text{m}$. In the z-stacks the size of one slice was $0.3\ \mu\text{m}$. For the live cell imaging the settings were identical except for the resolution being 512×512 .

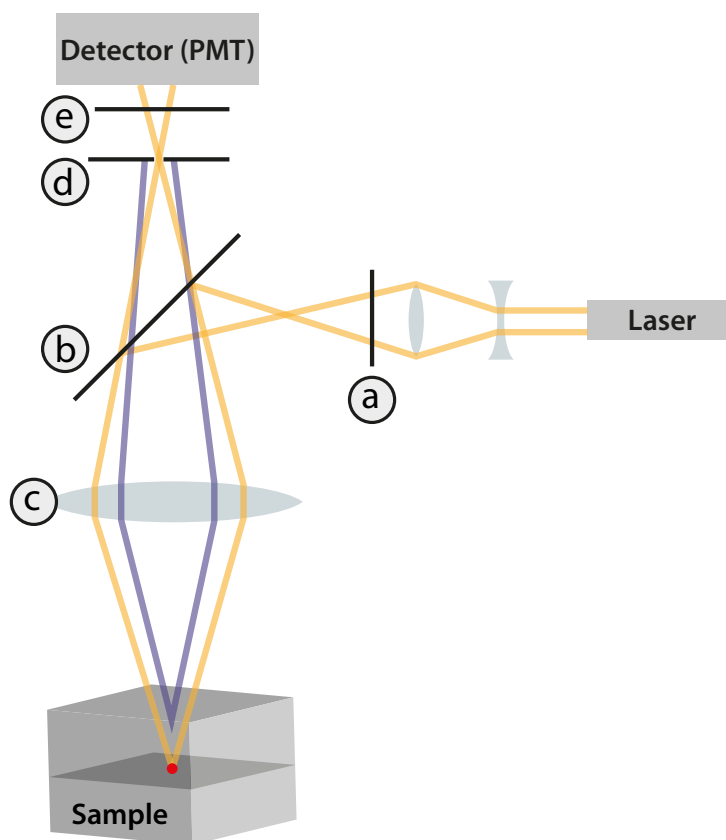


Figure 3.1: Working principle of CLSM. An epifluorescent set-up splits the incident light at the sample from the emitted light. The light path (orange) goes through an excitation filter (a), reflects at a dichroic mirror (b) and is focused by the objective onto a specific point in the sample. The emitted light from the sample finds its way again through the objective (c) and through the dichroic mirror to precisely pass through the pinhole (d) and an emission filter (e) where it finally is recorded by a photomultiplier detector. The core of the confocal technology: the pinhole, does not allow passage of emitted light from any other location (blue) than the predefined one.

Atomic Force Microscopy (AFM)

In 1986 Binning *et al.* introduced the first AFM and reported a sensitivity down to 10^{-18} N, a lateral resolution of 30 Å and a vertical resolution below 1 Å [335]. Today the AFM is used for various applications in physics, material science, biology and chemistry with the most common being force interaction measurements of molecular systems and topographical imaging of structures down to the Ångström level [336–343].

Figure 3.2 shows the working principle of AFM. A laser beam is reflected on a cantilever (a) and recorded by a position sensitive photo detector (b). A sharp tip (c) positioned under the cantilever is in direct contact with the sample. Bending of the cantilever corresponds to a force that the tip exerts on the underlying substrate. Following a calibration procedure, this force can be measured by the deflection of the laser beam on the position sensitive photo detector [344].

A piezoelectric crystal controls the z-position of the entire cantilever. When receiving feedback from the photo detector, the crystal can assure that the force is kept constant while scanning a surface. Another mode of topographical imaging is to keep the height constant and let the force vary. The so called tapping mode or intermittent contact mode allows for imaging of sensitive surfaces with the tip only partially being in contact. With the system controlling both position and force, force distance curves can be measured in various systems. [345, 346]

In this thesis an AFM (Nanowizard I, JPK, Germany) was used. Topographical imaging of living C2C12 myoblasts was done in contact mode with cantilevers having a stiffness of 0.06 N/m (CSC38, MikroMasch). The scanning speed was 20 $\mu\text{m/s}$ and the set-point 0.2 V. To provide a cell friendly atmosphere while imaging, the samples were put in a BioCell (JPK, Germany) that kept the temperature constant at 37 °C. To keep the samples at physiological pH, DM was prepared from CO₂ independent DMEM (Invitrogen Life Technologies).

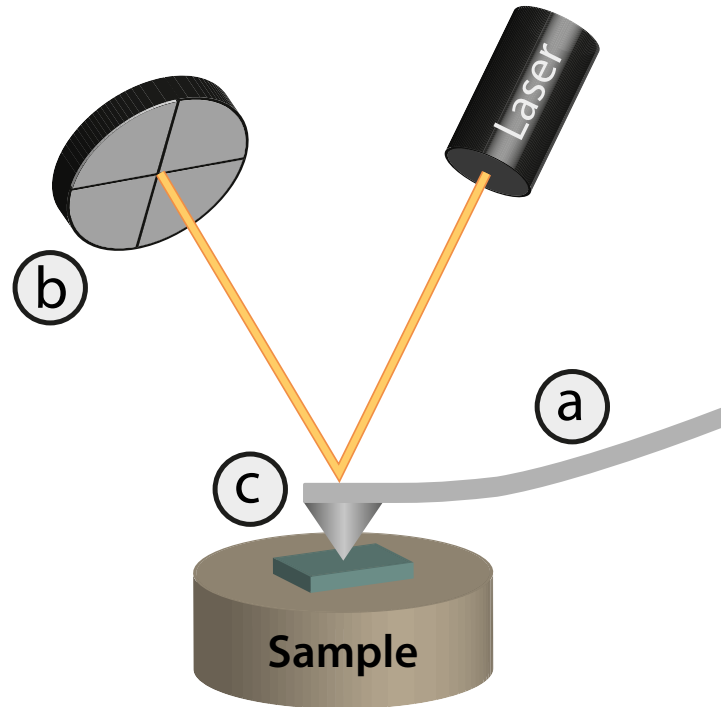


Figure 3.2: Working principle of AFM. A laser beam is reflected on a cantilever (a) and recorded by a position sensitive photo detector (b). A sharp tip (c) positioned under the cantilever is in direct contact with the sample. The detector records bending of the cantilever which can be linked to the force exerted by the tip onto the sample.

3.3.2 probing techniques

Fluid Force Microscopy (FluidFM™)

The integration of a microfluidic system in an AFM tip, FluidFM™, was presented by Meister *et al.* in 2009 [347]. The technology is based on hollow cantilevers through which liquid can be ejected or aspirated and allows for injection and extraction of cells as well as displacement and electro physiology. The pick and place of cells was established by Dörig *et al.* [348]. The process is described in Figure 3.3.

In this thesis, FluidFM™ tips were used in combination with the AFM (Nanowizard I, JPK, Germany). The tip was plasma cleaned as described in Chapter 3.3.3, 20 μl of water was added in the reservoir and a tubular system with a syringe at the end was

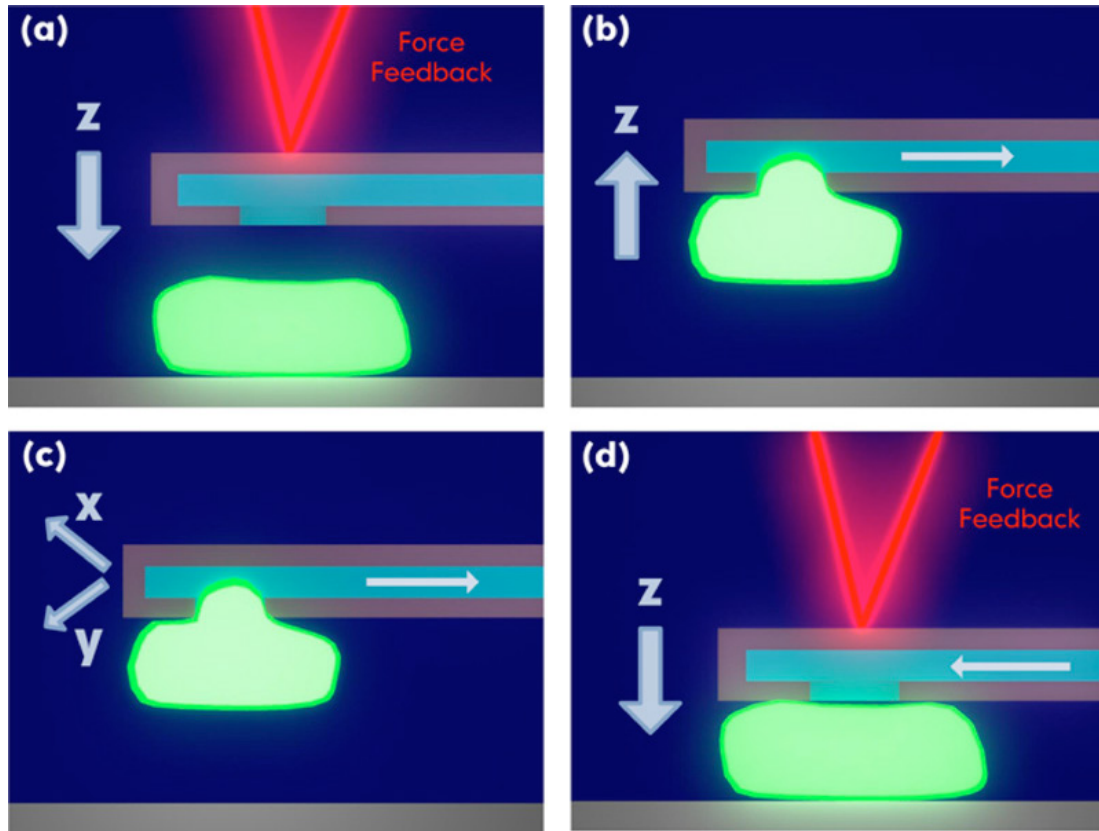


Figure 3.3: Pick and place of a cell with FluidFMTM. The cantilever approaches the cell by force feedback control (a). Suction provides immediate adhesion of the cell to the cantilever. By retracting the cantilever the cell is picked up from the surface (b). By movements in the x-y plane a new position can be chosen (c). The placement of the cell in the new position takes place by approach to the surface and subsequent release through ejection (d). Reproduced from [348].

attached. The tip was clamped to a home made transparent plastic tip holder that fit into the AFM and flow through was established by applying pressure to the syringe. The tip was immersed in 0.2 mg/ml PLL-g-PEG/HEPES 2 for one hour in order to avoid cell adhesion during the experiment. The size of the hole of the cantilever was 8 μm in diameter for the myoblast experiments and 4 μm in diameter for the monocyte pick-up.

Calibration was performed in liquid on a polystyrol petri dish. The company estimated a stiffness of 3 N/m for all FluidFMTM cantilevers. Myoblast cell-cell detachment forces were measured by 1) picking up a cell by applying suction to the tip, 2) approaching the other cell on the surface until a given set point force was reached (50nN for myoblasts and 20 nN for monocytes), 3) giving the cells a specified adhesion time and 4) measuring the force distance curve while retracting the tip (30 $\mu\text{m/s}$) with the cell attached to it.

Quantitative Real-Time Polymerase Chain Reaction (QRT-PCR)

In difference to traditional PCR, run on a gel, the QRT-PCR allows you to measure not only the abundance of a certain DNA segment in a sample but also its relative or absolute concentration. The basic working principle however is the same. Each heat cycle consists of a denaturation step where the dsDNA melts, an annealing step where primers anneal to each of the targeted ssDNA and an elongation step where DNA polymerase synthesizes a new DNA strand complementary to the template. This cycle is normally repeated around 30-40 times when a plateau is expected to be reached due to shortage of dNTPs. [349]

In QRT-PCR the two most important readout systems are based on a dsDNA binding dye, such as SYBR Green, and a probe-based system, such as TaqMan (Applied Biosystems Life Technologies), respectively. In both cases the increase in fluorescence signal is reported during the PCR run. Since dsDNA binding dyes are not selective, but bind to all dsDNA in the sample, a melting curve should be performed after the PCR run is done to assure that the reported gene expression indeed belongs to the chosen target gene and this one alone. [350]

A so called threshold level is set at the steepest part of the exponentially increasing curve of the reporter dye. At this point the threshold cycle C_t will be determined and used for quantification, keeping in mind that the total amount of amplified DNA doubles every cycle. Relative DNA levels are calculated using the $\Delta\Delta C_t$ method, while absolute quantification requires a standard curve. [351, 352]

For the experiments in this thesis the PCR machine used was StepOnePlus Real-Time (Applied Biosystems Life Technologies). The cDNA samples were diluted 10x with RNase free water (supplied in the RNeasy Mini Kit) so that there would be an amount of cDNA corresponding to 1 μg RNA per 200 μl . All primers were diluted to a concentration of 5 μM in RNase free water (provided in the RNeasy Mini Kit). A fast optical 96-well reaction plate was used for the PCR run. A mixture of 10 μl master mix, 2 μl template, 1 μl forward primer, 1 μl reverse primer and 6 μl RNase free water was put in each well of the well plate. The choice of a dsDNA binding dye technology required that not more than one primer set was present in each well. There were three technical replicas. The PCR runs had 40 cycles and ended with a melt curve stage.

Quartz Crystal Microbalance with Dissipation (QCM-D)

QCM-D is a biosensor capable of *in situ* measurements of masses and viscoelastic properties of adsorbing molecules at a surface with a sensitivity down to a few ng/cm². The resonance frequency of an oscillating quartz crystal changes relative to the adsorbed mass on its surface. A decrease in frequency corresponds to an increase in mass whereas a change in dissipation is related to the viscoelastic properties of the adsorbed layer. [353, 354] The QCM-D used in this thesis was a QCM-D E4 (Q-sense AB).

NanoDrop spectrophotometer

A spectrophotometer measures the concentration of a solute by recording the transmission spectrum of specific wavelengths passed through the solution. The wavelength at which a difference in transmitted light is recorded indicates what substance is present. For measuring the weight concentration of the total RNA, a NanoDrop ND-1000 UV-Vis Spectrophotometer (NanoDrop products) was used. 1 μ l of RNase free water (provided in the RNeasy Mini kit) was used to create a baseline and then 1 μ l of RNA sample was used for the measurement.

3.3.3 other instruments

plasma cleaner

A plasma cleaner is a reactor that ionizes a provided gas, most commonly air, oxygen or argon at pressures less than 1 torr. By putting a sample through a plasma cleaning procedure, it is bombarded with ions and radicals in order to remove carbonated compounds adhered to the surface. In the particular case of PDMS, the treatment causes an oxidation of the surface which turns hydrophilic. [355, 356]

The plasma cleaner used in this thesis was a PDC-32G (Harrick Plasma) with an inlet valve for air. The plasma treatment was always done at a pressure of $5 \cdot 10^{-2}$ mbar with the RF level adjusted to "high". For FluidFMTM tips the duration of the treatment was set to 10 seconds while for PDMS compartments the treatment lasted 2 minutes.

cell stretcher

For stretching C2C12 myoblasts a STREX Cell Strain Instrument ST-140-10 (B-Bridge) was used. This cell stretcher induces uni-axial mechanical stretch to elastic compartments allowing for 2D cell growth. There are different stretching patterns, such as sawtooth, ramp and square, available at different speeds and strains. The compartment used for cell growth was produce in our lab by moulding PDMS. The area of cell growth was 10 cm².

Structural Interpretation of the Cytoskeletal Support Requiring Adherens Junctions at the Fusion Site during Myogenesis¹

In 1998, Adams *et al.* published that E-cadherin together with the actin cytoskeleton play a major role during epithelial cell cluster formation. The first cell-cell contact is mediated through E-cadherin puncta which work as bridges to connect branches of actin filaments present in adjacent cells. Eventually the two adherent cells share one cortical actin network. In order to preserve stability at the site of adhesion, E-cadherin is distributed over the area and linked to actin filaments oriented along the axis of cell-cell contact [357].

While it has been shown that both actin and cadherin are crucial components during myoblast fusion, the full picture of the rearrangements of the cadherin-actin complex at the fusion site is not yet clear. Could a process similar to the one observed in epithelial cell clustering take place also during myoblast fusion? In the present work we investigated how the cadherin-actin complex facilitates the fusion process by confocal imaging of immunostained C2C12 myoblast cultures at different stages of myogenesis. The C2C12 mouse muscle cell line was chosen because it represents a universally accepted *in vitro* model for the study of muscle differentiation in mammals. We further investigated whether the first fusion pore opens up during or after the rearrangement of the cadherin-actin complex by imaging live myoblast fusion with a combined setup of AFM and confocal laser scanning microscopy (CLSM). Additionally we did a statistical study to investigate whether the fusion event is a fast or a slow process in comparison with the other stages of myogenesis.

¹Parts of this chapter were submitted to *Cytoskeleton* as Elsa Thomasson, Liting Yu, Gabor Csucs, Janos Vörös and Gemma Palazzolo, Structural Interpretation of the Cytoskeletal Support Requiring Adherens Junctions at the Fusion Site during Myogenesis.

4.1 Cell Culture Methods and Imaging Techniques

4.1.1 myogenic cultures and sample preparation

Three independent early-passage (P3) cultures of C2C12 myoblasts were incubated in parallel for two days in GM in a humidified incubator with 7% CO₂ in air at 37 °C. Then myoblasts were harvested and 9 samples per batch (giving a total of 27 samples) were prepared by plating myoblasts on glass slides (24 mm in diameter, thickness 1, Menzel-Gläser) at a density of 1500 cells/cm² in GM. After 6 hours the medium was changed to DM in order to induce differentiation. After 3, 4 and 7 days in culture, samples 1-3, 4-6 and 7-9 respectively from each batch were fixed, permeabilized, stained for cadherin, actin and nuclei and finally mounted on objective glass slides as described in Chapter 3.2.2.

The cell sample preparation for the AFM imaging required instead of live staining. Before seeding, 50% of the cells were stained with CellTrackerTM Green CMFDA according to the protocol described in Chapter 3.2.2. The two populations were mixed and seeded at the same concentration as above in order to create a co-culture. After three days in DM the samples were imaged live.

4.1.2 imaging with CLSM and AFM

Stained samples were imaged with a CLSM (LSM 510, Zeiss, Germany) equipped with a Plan-Apochromat 63x/1.40 Oil DIC M27. Argon, diode 405 and He-Ne 561 lasers were combined with appropriate filter settings to enable imaging of the three different dyes in separate channels. The resolution of the images was set to 1024x1024 pixels and the size was 143 μm x 143 μm . In the z-stacks the size of one slice was 0.3 μm . For the live cell imaging the settings were identical except for the resolution being 512x512 pixels as well as the CLSM being combined with the AFM.

For topographical imaging of living myoblasts we used an AFM (Nanowizard I, JPK, Germany) with contact mode cantilevers (0.06 N/m, CSC38, MikroMasch). The scanning speed was 20 $\mu\text{m/s}$ and the setpoint 0.2 V. To provide a cell friendly atmosphere while imaging, the samples were put in a BioCell (JPK, Germany) that kept the temperature constant at 37 °C. To keep the samples at physiological pH, DM was prepared from CO₂ independent DMEM (Invitrogen Life Technologies).

4.1.3 nuclei count

10 images per sample of 26 samples were taken which gave 260 images in total. Myoblasts were divided into 4 different groups: "making contact", "in fusion process", "nuclei in myotubes" and "not differentiating". Nuclei were counted by eye in each picture and sorted into the different groups. In total, approximately 4500 nuclei were counted in order to provide a rigid statistical representation. Statistical analysis was performed in MATLAB (The Math-Works, USA). The differences between myoblasts in fusion process and nuclei in myotubes for each time point were examined using the paired T-test ($\alpha = 0.05$). The measurements reported are expressed as average values ± 1 standard deviation ($n = 3$ biological replicas). The confidence interval for the statistical test is reported with one asterisk symbolizing $p < 0.05$. We made an estimation of the fusion time by linearly extrapolating between the data seen at day 4 and day 7. The amount of nuclei that should have been incorporated into a myotube during these three days would be expected to be in the range of the total amount of nuclei observed in myotubes at day 7 minus the total amount of nuclei seen in myotubes at day 4. Given the density of observed fusion events at day 4 and assuming that this density remains somewhat similar during these three days, the time of one fusion event can be estimated by multiplication of the total time and the observed amount of fusion events, and then divided by the amount of nuclei incorporated into a myotube since day 4.

4.2 Investigation of a Cytoskeletal Structure at the Fusion Site

4.2.1 making cell-cell contacts through adherens junctions

C2C12 myoblasts were grown for 3 days in DM and afterwards fixed, permeabilized and stained for cadherin, actin filaments and nuclei. The samples were imaged with CLSM. The images showed that a big majority of the cells made cell-cell contacts via adherens junctions. There was a well-defined stress fiber network and the shape of the cells was rather flat. In most cases there were several contact points per cell but no continuous contact area to the neighbor. The arrows in Figure 4.1 show two examples of adherens junctions where cadherin contact sites (green) are supported by assembled stress fibers (red). We hypothesize that these cells had entered the first stage of differentiation towards

muscle tissue. In order to differentiate and fuse, making cell-cell contact is an essential prerequisite, although it is not the only one. In fact we have observed cells making contact and afterwards separating (data not shown).

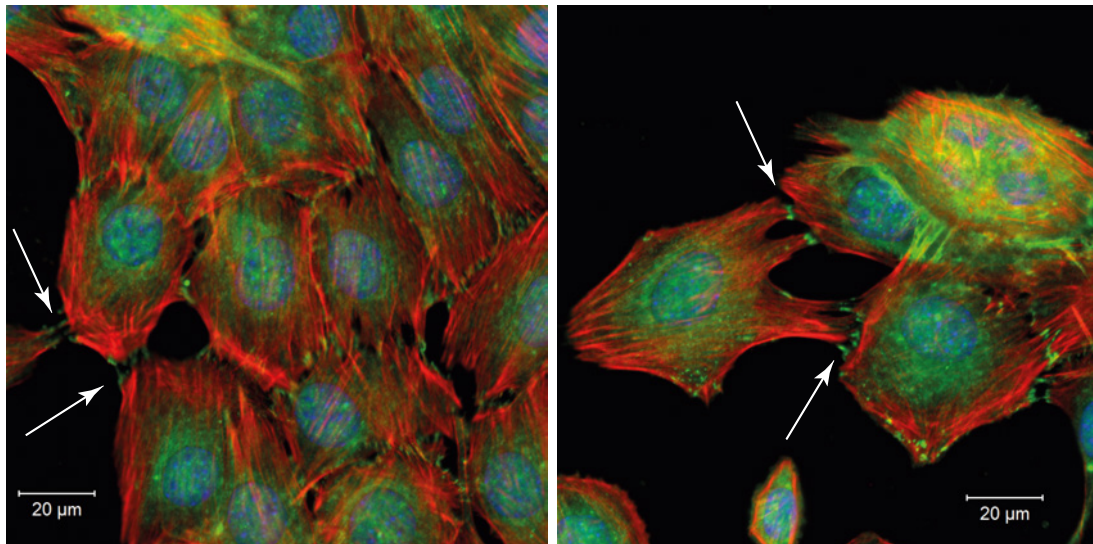


Figure 4.1: Flat myoblasts making cell-cell contact during the first stage of myogenesis. The arrows indicate two examples of adherens junctions where cadherin contact sites are supported by assembled stress fibers. Actin filaments red, cadherin green, nuclei blue.

4.2.2 the cadherin-actin complexes are found at the periphery of the fusing cells adjusting to a rounded cell shape at the site of fusion

As described above, a majority of the cells made cell-cell contact. In this subsection we will focus on a small fraction of cell couples which had started the fusion process. Figure 4.2(a) shows two fusion events at different stages. Cross section (a) reveals a well-established contact site between two cells. The adherens junctions (green) are many and provide an almost continuous contact line between the two cells. The shape is flat, as also described above, which indicates that this cell couple had not yet exited the first stage of differentiation. In cross section (b) a different scenario can be observed. The adherens junctions did not form a flat line close to the substrate but rather conformed to a rounded shape. This indicated that the cell membranes at the site of contact had started to shape according to a more tubular structure. In this particular case the fusion site formed adjacent to a nucleus. Figure 4.2(b) shows an example further away from the nucleus.

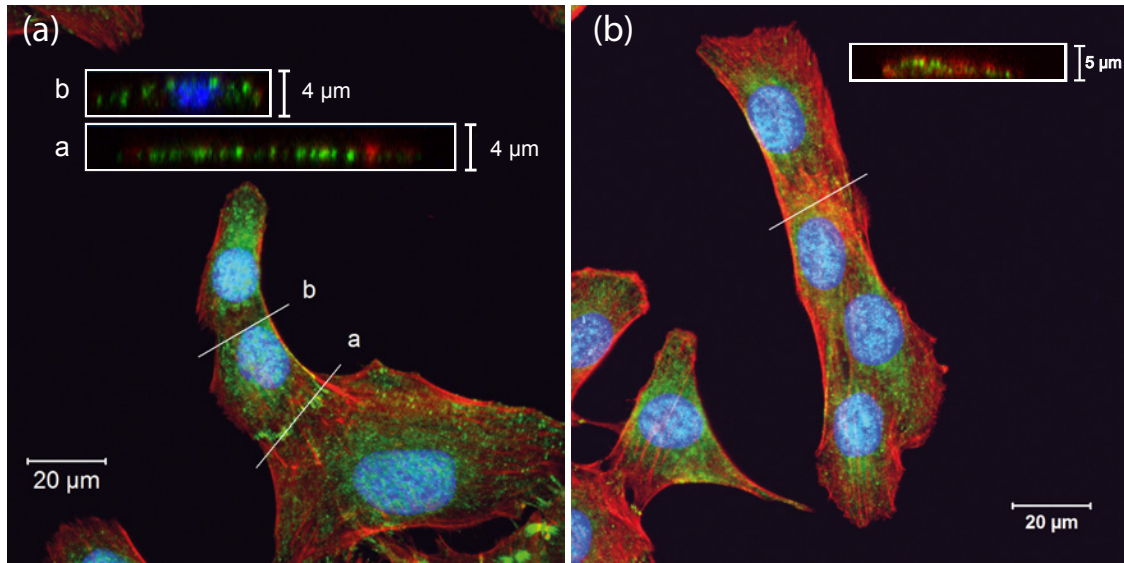


Figure 4.2: Cells in the beginning of the fusion process. In a, cross section (a) shows a well-developed cell-cell contact site in the first stage of muscle differentiation. The adherens junctions are found in the same plane. Cross section (b) shows a cell couple where the cadherin follows a rounded shape. This indicates that the cell membranes at the site of contact had started to shape according to a more tubular structure. It further shows that the adherens junctions are found at the periphery of this rounded shape. In b, the cross section between the two uppermost nuclei show cadherin puncta elevated from the surface in the same manner as in a. In this case the fusion site is slightly further away from the nearest nucleus showing that this cytoskeletal arrangement can support the height further away from the stabilizing nucleus as well.

4.2.3 a cytoskeletal structure supports the rounded shape at the fusion site prior to the opening of fusion pores

A co-culture of 50% CellTracker™ Green stained C2C12 myoblasts and 50% non-stained counterpart was grown for 3 days in DM. The samples were imaged live with a setup of AFM combined with a CLSM. Figure 4.3 shows an AFM image (height a and error signal b) and its corresponding CLSM image c of a number of fusing cells. The arrows in Figure 4.3(a), (b) and (c) show the fusion site. The AFM height image, 4.3(a), indicates that there was a continuum of cells and no division point. In the AFM image, 4.3(b), rod like structures are visible at this spot. However, according to the CLSM image, 4.3(c), the same site separated two cells; one with a cytosol stained with CellTracker™ Green and one with an untreated cytosol. I.e. what topographically appears to be a fully fused cell couple did not yet share cytosol. The diffusion constant of CellTracker™ Green in the cytosol is expected to be at least $3.4 \times 10^{-8} \text{ cm}^2 \cdot \text{s}^{-1}$ [358]. This means that the dye would diffuse into the entire cell body in tenths of a second, which is only a fraction of the 30 minutes spent to capture the AFM image and additional 3 minutes to subsequently

acquire the CLSM image. The fact that the dye was seen in one cell but not in the other can only mean that the fusion pore did not open up yet.

When a cell is imaged with an AFM, essentially the cytoskeleton, being the supporting structure under the soft cell membrane, represents what is detectable. If the cytoskeleton would be interrupted at some location, it would be visible in the AFM image as a hole or a well. Therefore, Figure 4.3 shows what appear to be cytoskeletal filaments that run continuously between the two cells. We assume that the cells are in a fusion process based on previous reports of this stage of differentiation [73, 74]. Indeed, the rounded/tubular shape observed in newly formed myotubes (Figure 4.4) is supported by a cytoskeletal structure. These findings indicate that a fusing myoblast couple first arranges its cytoskeletal structure into the shape the fused cells will have once the process is completed. Only after this support has been established the process of fusion pore opening starts. The phenomenon we just described for myoblast fusion has strong similarities with the behavior of epithelial cells making cell-cell contact [357], thus suggesting that the clustering process of epithelial cells as well as the differentiation of myoblasts share a common mechanism in the initial stages.

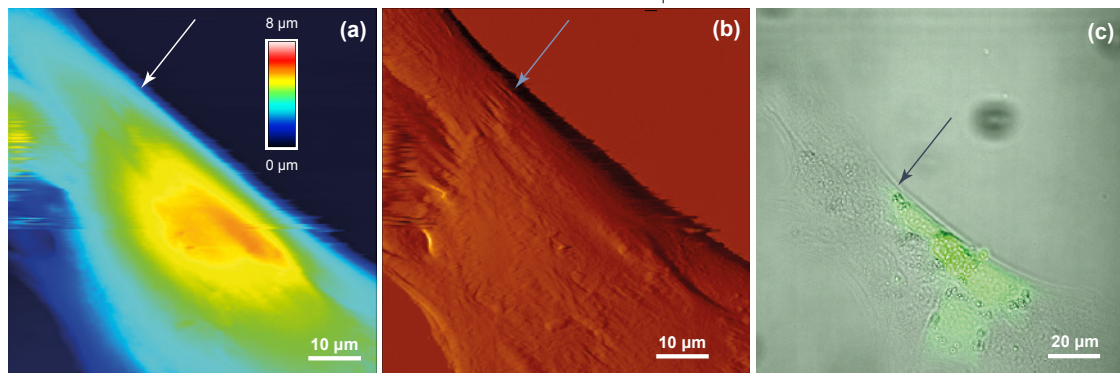


Figure 4.3: Live C2C12 myoblasts during fusion. Half of the cell population was stained with the cytosol marker CellTracker™ Green before seeding. The AFM images (height (a) and error signal (b)) show two cells in fusion where the membranes appear to be continuous. The corresponding CLSM image (c) shows that no exchange of cytosols had yet occurred (arrow at the same location as in (a) and (b)), hence at this stage no fusion pore had been formed. However, as the AFM detects the cell membrane supported by cytoskeleton, what this figure panel shows is a continuous cytoskeletal structure.

4.2.4 the basic functional unit of muscle tissue: the myofiber

C2C12 myoblasts were grown for 7 days in DM and afterwards fixed, permeabilized and stained for cadherin, actin filaments and nuclei. The samples were imaged with a CLSM.

In these samples several, both nascent and larger, myotubes could be observed. Figure 4.4(a) shows an example of a myotube where a branch indicates that the original nascent myotube has grown into a mature myofiber. Unlike the first stage of myogenesis where the cells had a flat shape, these tubes show, as expected, a tube like shape. The cross section in Figure 4.4(b) indicates that the tubular shape was supported by actin filaments at the periphery of the cytosol. The focus in Figure 4.4(b) was chosen at a position in the middle of the tube. No actin filaments were found traversing the cytosol. This indicates that the cell shape supported by actin filament rearrangements during the first stages of the fusion process remains to develop into the shape of a mature myotube.

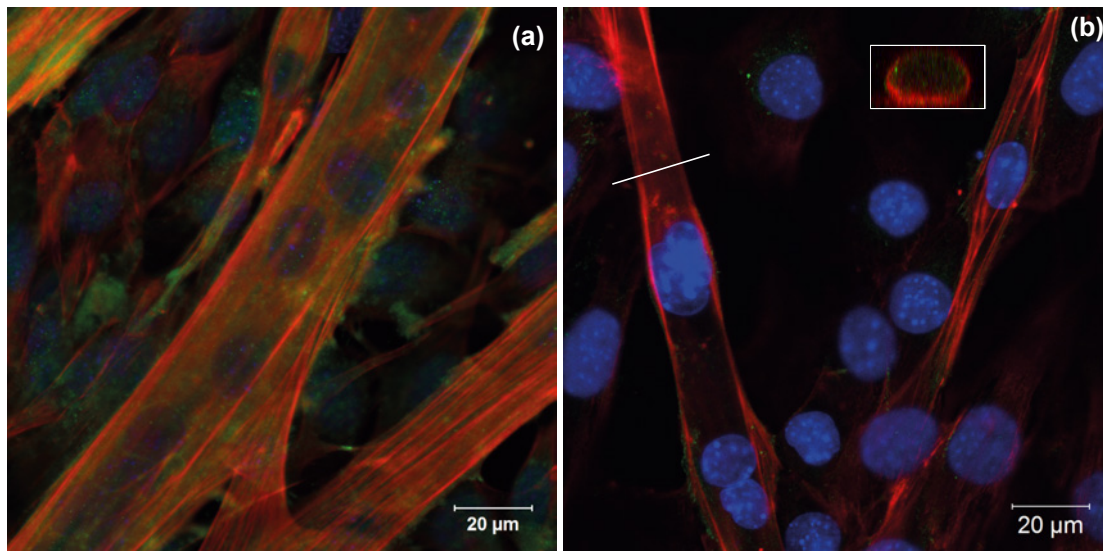


Figure 4.4: The final stage of myogenesis; the myotube. After 7 days of culture in DM, both nascent and mature myotubes could be observed. (a) shows an example of a mature myotube. The fact that it has several nuclei incorporated as well as being fused to another myotube through a branch shows that the original nascent myotubes have continued their fusion processes with other myotubes/myoblasts and grown to form a mature myotube. (b) displays a myotube with the focus in the middle of the tube. Actin filaments are seen only at the border of the tube. The cross section framed in white shows that cortical actin surrounds the cytosol but does not traverse the tube. Actin filaments red, cadherin green, nuclei blue.

4.2.5 fusion is a fast event

C2C12 myoblasts were grown for 3, 4 and 7 days in DM and afterwards fixed, permeabilized and stained for cadherin, actin filaments and nuclei. The samples were imaged with a CLSM. Myoblasts were divided into 4 different groups: "making contact", "in fusion process", "nuclei in myotubes" and "not differentiating". We defined a not differentiating myoblast as a cell not belonging to any of the three differentiation stages. There were

dividing cells observed, as well as lonely migrating ones. Nuclei were counted by eye in each picture and sorted into the different groups.

Figure 4.5 shows the percentage of myoblasts from all cells belonging to each group. At all time points, myoblasts making contact was the most represented group, proving that not all the cells making contact go further in the fusion process *in vitro*. After 3 and 4 days in culture we could see a very small number of myoblasts in fusion process, nuclei in myotubes and not differentiating myoblasts. After 7 days, the number of nuclei in myotubes had increased to 27% of all nuclei while myoblasts in fusion process or not differentiating were not found at all.

At each time point there were very few myoblasts involved in the fusion process in comparison with the number of cells making cell-cell contact. After 7 days of culture, 0% of the observed cells were engaged in the fusion process but, with 27% of the nuclei residing inside myotubes, the fusion event must have taken place to a large extent. A paired T-test ($\alpha = 0.05$) for each time point was performed in MATLAB in order to examine the differences between myoblasts in fusion process and nuclei in myotubes. At the given significance level the difference of the percentage of myoblasts in fusion and the percentage of nuclei in myotubes was not statistically significant for the batches cultured for 3 or 4 days. For 7 days however, the difference was significant. This is indicated in Figure 5 with an asterisk ($p < 0.05$). The percentage of nuclei in myotubes exceeded the percentage of myoblasts in fusion process at day 7 with statistical significance but the opposite was not observed at any time point. Therefore the total amount of captured nuclei in myotubes was larger than the total amount of recorded myotubes in fusion process for all time points.

We draw the conclusion that the reason why it is so difficult to record myoblasts during the fusion process is that the event is very fast in comparison with all other stages of differentiation. It has been reported that the fusion event including alignment takes 2.5 ± 0.5 hours [73]. Given the density of fusing myoblasts at day 4 and the measured amount of nuclei in myotubes at day 7, we have estimated that the fusion event, after alignment has been fully established, requires around 1 hour to be completed. For details on this calculation, please see materials and methods.

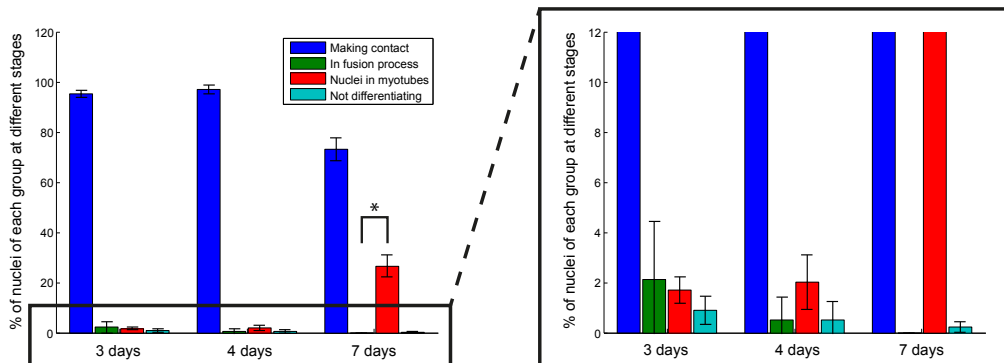


Figure 4.5: Statistical analysis of the occurrence of the different stages during myogenesis. The bars show the percentage of the total amount of cells belonging to a certain group after 3 days, 4 days and 7 days in differentiation medium. The data are shown as average values ± 1 standard deviation, $n = 3$ biological replicas. In total 260 images were analyzed. At all time points very few cells were engaged in the activity of fusion. However, after 7 days of culture 27% of the nuclei resided inside myotubes, hence the fusion event must have taken place to a large extent. This indicates that the fusion process is a fast event in comparison with the other stages of myogenesis and therefore rarely captured. Performing a paired T-test ($\alpha = 0.05$) of "In fusion process" and "Nuclei in myotubes" separately for all time points, showed that the null hypothesis could be rejected only for the measurements made after 7 days of culture.

4.2.6 proposed model of cadherin-actin complex function during fusion

Our results suggest that cytoskeletal rearrangements play an important role during myogenesis and, in particular, during the fusion process. In Figure 4.6 we propose a model that describes the sequence of events that takes place during muscle fusion. Actin filaments are marked in red, catenin complexes in blue and cadherin in green.

Figure 4.6(a) shows a schematic view of cell-cell contacts through adherens junctions at the interface between two myoblasts, as we observed in Figure 4.1. This is the first stage of muscle differentiation. Cadherins diffuse freely in the cell membrane until they find a partner from the adjacent cell membrane to attach to in a calcium dependent manner. Upon attachment, actin filaments assemble and adhere to the cadherins through a catenin complex. This way the actin cytoskeletons in two neighboring cells become linked together. This is in agreement with previous findings [8, 80].

As shown in cross section b in Figure 4.2(a), the cadherin-actin complex is found at the periphery of the cell to allow for and support a rounded cell shape at the fusion site. Here we propose a novel mechanism for the role of the adherens junction as a cytoskeletal

support during fusion. Cell shape is maintained by the cytoskeleton being linked to points of adhesion, may it be adhesion to the extracellular matrix or cell-cell adhesion. On a flat substrate, single cells without neighbors have nothing but the underlying surface onto which they can create anchor points and spread. Given that the actin cytoskeleton is contractile and mainly nucleates at the cell cortex as described in the introduction, a single cell in a 2D culture is forced to assume a flat shape with the exception of the nucleus that has a 3D shape internally maintained by the nuclear lamina. When cell-cell contacts are established, the anchor points for the associating actin filaments are not focal adhesions adhered to a rigid substrate but cadherin-based homophilic interactions between adjacent cells. The adherens junctions are motile within the lipid bilayers until associated with the actin cytoskeleton [97]. Since the adhering actin filaments will polymerize from the cell cortex, their internal tension forces will guide the cadherin complexes to the periphery of the cell. The complexes with actin filaments attached to the cortical network above the nucleus will end up at its level of height providing a tubular structure.

Figure 4.6(b) shows a schematic of this event. The grey arrows mark the directions of the tension forces in the actin filaments. The green arrows show the migration direction of the cadherin-actin complex guided to the periphery of the cell-cell contact area by these tension forces. In Figure 4.6(c) the cadherin-actin complexes are stable at their positions at the cortex of the cell, supporting a tubular structure. This way the two fusing myoblasts share a common cortical actin network surrounding the entire cell complex underneath the membranes. This cytoskeletal arrangement indeed resembles the one of clustering epithelial cells [357]. We assume that the fusion pore can open only after the cytoskeletal structure is formed, according to Figure 4.3. Figure 4.6(d) is based on the results showed in Figure 4.4. The cadherin-actin complexes are eventually disassembled and the tubular structure of the myotube will be maintained by a cortical actin network extending its filaments over the entire tube.

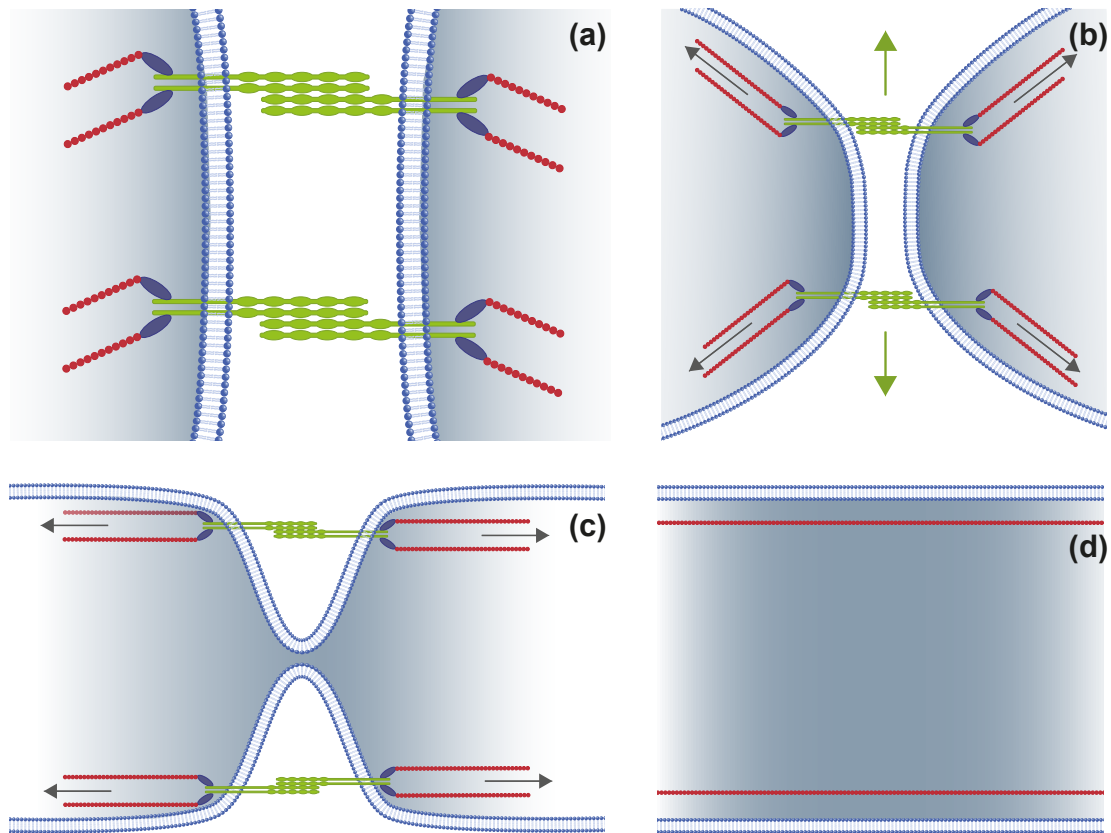


Figure 4.6: Model suggesting a mechanism behind the migration of adherens junctions during myoblast fusion. a, myoblasts making first cell-cell contacts through cadherins. Actin filaments associate. b, tension in the actin filaments (displayed by grey arrows) causes the cadherin-actin complex to travel (displayed by green arrows) to the periphery of the cells. c, here they form a rigid outer stabilizing network to allow for the fusion process to happen at the contact site. The fusion pore will open only after the tubular structure is formed. d, the cadherin-actin complexes eventually disassemble and a cortical actin network with long actin filaments protruding the entire tube encircles the cytosol of the formed myotube. Actin filaments are marked in red, catenin complexes in blue and cadherin in green.

4.3 Chapter Conclusions

In this chapter we have investigated rearrangements of the cadherin-actin complex in mouse myoblasts *in vitro* in a 2D culture during myogenesis. Our findings let us infer that the adherens junctions, established during initial cell-cell recognition and contact, might migrate within the cell membranes to form a tubular structure in the early stages of myoblast differentiation, resembling a mechanism previously described only for epithelial cells.

In addition, we have used a combined AFM CLSM setup to image a co-culture of live fusing myoblasts, half of them stained with CellTrackerTM Green. The results from these experiments indicate that the tubular cytoskeletal support established by the migration of the cadherin-actin complexes forms prior to the opening of the first fusion pore.

In order to establish whether the fusion process is a fast event in comparison with the other stages during myoblast differentiation, we did a statistical analysis based on approximately 4500 nuclei counted from 260 images of fixed and stained myoblast cultures at different development stages of myogenesis. The percentage of myoblasts found at the stage of fusion was significantly lower than that of myoblasts found at the stages of making contact, nuclei in myotubes or myoblasts not in the process of differentiation at almost all time points. Since the nuclei in the myotubes must have gone through a fusion process, we conclude that fusion is a very fast event in comparison with all other stages during myogenesis.

We have proposed a model to explain the mechanism of the migration of adherens junctions into a tubular structure during fusion. According to this model, actin filaments nucleate from the cortical actin in each cell to assemble at the newly paired cadherin couple. Internal tension forces along the filaments guide the established adherens junctions to the periphery of the cell causing a tubular shape. It remains for future studies to record the movements of the adherens junctions live as well as its disassembly after new actin filaments have protruded the cell bodies to provide the new cytoskeletal support.

Cell-cell Contact Forces Measured with Fluid Force Microscopy

Measuring cellular forces such as cell-ligand, cell-surface and cell-cell interactions with AFM spectroscopy is an emerging field. By recording the bending of the AFM tip as a function of the distance from the surface, a force-distance curve can be achieved. By using a bare AFM tip, the stiffness of a material, or a living cell can be probed. More sophisticated setups include a probe glued to the tip. This can be a ligand, a bead with ligands attached to it or even an entire cell. Cell-cell contact forces can be measured this way [359–365].

Yet, AFM force spectroscopy of cells presents obstacles. Drawbacks of cell-cell contact measurements are related to the adhesion of the probing cell. The adhesion time prior to measuring could be 30 minutes depending on the conditions [366]. In this time the cell may change properties. Furthermore, the cell cannot be released after probing, hence another preparation round is needed should the experiment require measurements by different probing cells. The Fluid Force Microscopy (FluidFMTM) technique, however, enables pick-up and release of micron sized objects within seconds, by applying suction to a hollow cantilever.

Chapter 1.1.3 elucidated the crucial importance of cadherin in myoblast fusion. Diffusive cadherin monomers are always abundant in the cell membrane to allow for cell-cell adhesion when the opportunity arises. In this work we show that myoblast-myoblast adhesion forces can be measured with FluidFMTM. Furthermore, our results indicate that force-time curves have a square root of time shape until equilibrium. This suggests that initial cell-cell contact is mediated by freely diffusing adhesion molecules. Finally, the result of the measurement data followed a Gaussian distribution which indicates that the

experimental errors probably are negligible in comparison to natural fluctuations of the binding process.

Another cell system where measurements of contact forces are highly relevant is the monocyte-endothelial monolayer interaction as a model for the early stages of extravasation of white cells through the wall of the blood vessel. *In vivo*, white blood cells circulating in the blood stream form weak adhesion to a vessel wall expressing specific adhesion molecules such as ICAM-1, VCAM-1 and E-selectin. These molecules are expressed as a response to endothelial interaction with inflammatory cytokines such as interleukins, IL-1 and IL-6, or tumor necrosis factor, TNF- α . The weak adhesion of the white blood cells in combination with the fluid force exerted by the blood stream causes rolling of these cells on the endothelial wall. Eventually the circulatory cells arrest on the wall and extravasate either in between two cells of the wall or through one endothelial cell [367–386]. Here we show that the FluidFMTM setup can measure forces of monocytes to a HUVEC monolayer undergoing inflammatory response.

5.1 Setup and Data Processing of FluidFMTM Cell-Cell Contact Measurements

5.1.1 cell sample preparation

myoblast monolayers

Round glass slides, 24 mm in diameter, thickness 1 (Menzel-Gläser), were sterilized by dipping them in pure ethanol and flaming it off. The glass slides were put into six-well-plates (surface area per well; 10 cm², TPP) with GM. No coating of the glass slides was necessary since myoblasts are very adhesive cells and the stiff hydrophilic surface provided a good growth environment. C2C12 myoblasts were seeded at a density 50000 cells/cm² in GM and let in the incubator to grow for two days. After one day, the samples were moved to new wells with fresh GM. After two days, the cells had formed continuous monolayers on top of the glass slides.

HUVEC monolayers

The HUVEC monolayers were prepared in the in the biolab of the Laboratory of Thermodynamics in Emerging Technologies under the supervision on Dr. Aldo Ferrari.

Round glass slides , 20 mm in diameter, thickness 1 (Menzel-Gläser), were sterilized with ethanol and afterwards washed with PBS and put into 12-well-plates (Falcon). The glass slides were coated with gelatin according to the following protocol: The glass slides were coated with sterile 1.5% gelatin (Merck, USA) in water and incubated at room temperature for 1 hour. Excess gelatin was removed and 2% glutaraldehyde (Sigma-Aldrich) solution in water was added for 15 minutes at room temperature in order to cross link the gelatin. The glutaraldehyde was replaced by 70% ethanol in PBS and the samples were left to incubate for 1 hour in room temperature. The samples were subsequently washed with sterile PBS 5x5 minutes and 2 mM glycine (Sigma-Aldrich) in PBS was added over night at room temperature. The samples were finally washed 5x5 minutes with PBS and stored at 4 °C until used.

HUVECs (Invitrogen Life Technologies) up to passage 7 were grown in HUVEC medium (200PRF supplemented with FBS 2% v/v, hydrocortisone 1 mg/ml, human epidermal growth factor 10 ng/ml, basic fibroblast growth factor 3 ng/ml and heparin 10 mg/ml (all reagents from Invitrogen Life Technologies)), trypsinized, centrifuged (7 min 800 rpm) and resuspended in HUVEC medium. The HUVECs were counted in a hemocytometer and seeded on the gelatin coated glass slides at a density of 45000 cells/cm². The HUVECS were let to grow in the incubator for 3 days in order to form monolayers and differentiate. Afterwards they were treated with TNF- α (Sigma-Aldrich) 10 ng/ml for 9 hours in order to induce inflammatory reaction.

Monocytes from human blood were isolated in the research group of Dr. Bernhard Winkler at the University hospital of Basel. They were transported in suspension in FACS buffer (PBS/0.5% BSA/5 mM EDTA) to the experiment directly after isolation. The monocytes were activated with 1 μ M N-formyl-methionine-leucine-phenylalanine (Sigma-Aldrich) for 1 hour and afterwards spinned down (5 minutes 800 rpm) and re-suspended in HUVEC medium. The activated monocytes in HUVEC medium were used directly for the force measurements.

5.1.2 FluidFMTM procedure

The setup and calibration of the FluidFMTM as well as the force measurements were done as described in Chapter 3.3.2. The monolayers were moved to a petri dish (60 mm in diameter) with GM for myoblasts, and with HUVEC medium for HUVECs. For the myoblast-myoblast force interaction measurements, C2C12 myoblasts were trypsinized, spun down (5 minutes 800 rpm) and resuspended in GM. These myoblasts in suspension were finally added on top of the myoblast monolayer at a density of 2500 cells/cm² directly before the force measurements. For the monocyte-HUVEC force interaction measurements, activated monocytes in HUVEC medium were added on top of the HUVEC monolayers at a density of 2500 cells/cm² directly before the measurements.

For myoblast-myoblast force interaction measurements, two experiments were conducted. The preparation conditions were identical for both but the measurements were conducted slightly differently. In experiment 1 there was a temperature drop from 37 °C to room temperature during the experiment. Three different locations were probed with the same myoblast adhered to the FluidFMTM tip by applying suction. Location 1 was affected by the temperature drop but locations 2-3 were measured in constant room temperature. At each location the cell-cell contact force was measured after the following interaction times: 0.09 s, 0.36 s, 0.81 s, 1.44 s, 2.25 s, 3.24 s, 4.41 s, 5.76 s, 7.29 s, 9 s, 10.89 s. These specific time points were chosen in order to spread the data evenly on a square root of time graph. For each time point approximately 20 repeated measurements were performed which generated nearly 700 graphs. In experiment 2 the temperature was kept constant at 37 °C and two locations were probed. For each location the cell-cell contact force was measured after the following interaction times: 0.09 s, 0.81 s, 2.25 s, 4.41 s, 7.29 s, 10.89 s, 15 s, 30 s, 60 s. This time frame was broader than in experiment 1. Each time point was measured with approximately 20 repeats giving a total of slightly more than 300 graphs.

5.1.3 processing of FluidFMTM data in MATLAB

The force curves from the FluidFMTM measurements were exported in the JPK software to txt files and further analyzed in MATLAB. In order to automate the readout process, a function was written to identify and return the approach, retract and position data found in the txt files as vectors. To simplify further analysis of the large amount of data generated,

a script was written where a struct, containing all retract and position vectors, was created for each experiment.

The retract curves were aligned so that $F=0$ at all positions above the contact point. This was done by subtracting a fitted first degree polynomial. From the fitted graphs, the cell-cell contact force was read out as the absolute value of the minimum force detected in the retract curve. The dissociation energy was calculated as the absolute value of the area below $F=0$ and above the retract curve. Figure 5.1 shows an example of a retract curve measured when a myoblast was separated from a myoblast monolayer. The contact force is encircled and the dissociation energy is represented by the green area. MATLAB was further used to plot graphs and histograms as well as performing t-tests.

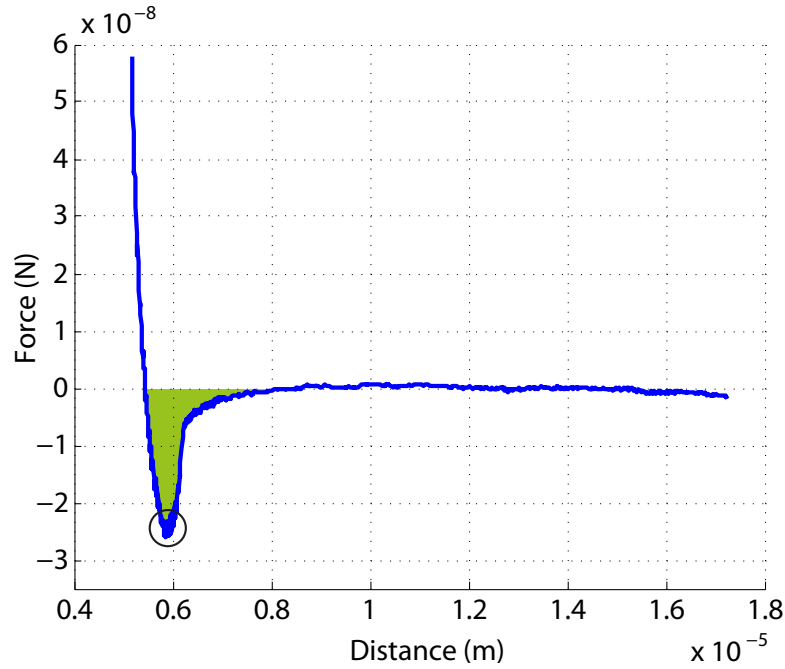


Figure 5.1: This figure shows an example of a retract curve measured when a myoblast was separated from a myoblast monolayer. The cell-cell contact force can be read out as the minimum value of this graph (encircled). The dissociation energy is represented by the green area below $F=0$ and above the graph.

5.2 Time Dependence of Initial Myoblast-Myoblast Contact Formation

5.2.1 measuring contact forces with FluidFMTM

Figure 5.2(a) shows the force distance curve for a myoblast-myoblast contact measurement. The black curve represents the approach while the blue curve represents the retract. Above the contact point, the approach and retract curves are overlapping as expected. At the contact point, however, the retract curve does not start where the approach curve ends but rather $0.5 \mu\text{m}$ below. The explanation for this is that cells are not stiff but rather viscoelastic. During the time the cells are let to be in contact they flatten, forcing the tip to go down in order to keep a constant force. The raw output data is given in mV. In order to translate that signal into Newtons, a calibration step is needed.

The original position of the approach and retract curves in Figure 5.2(a) was not aligned with $V=0$. Although perfectly overlapping, the two curves had not only an offset

but also a tilt. We explain both by the fact that the tip holder was home made and had to fit two different systems; the AFM machine and the FluidFMTM tip. Hence perfect alignment was not achieved. To solve this problem, we subtracted the same polynomial of first power from both curves. For the analysis of the entire experiments, only the retract curves were considered.

Figure 5.2(b) shows a myoblast monolayer with myoblasts put on top (rounded shapes). These rounded myoblasts did not have time to adhere rigidly to the underlying layer before one of them was picked up by the FluidFMTM tip by applying suction. A pair of sharp eyes can see that there are two circles at the tip of the cantilever. The inner circle is the hole of the cantilever (8 μm in this case) and the outer the rim of the adhered myoblast.

With this system the adhesion of the cell is immediate in contrast to conventional AFM measurements where an adhesion time of 30 minutes has to precede the measurement [365, 366]. By applying pressure, the adhered cell can be released from the tip and a new one can be picked up. This allows for instantaneous serial measurements of biological replicas within the same sample. However, with the given functionalization of the cantilever the release of the cell has to take place within a time frame of minutes after pick-up. A cell that stays longer starts to form its own adhesion sites to the cantilever. We even had an example of a myoblast that managed to crawl into the hole of the cantilever after 3 hours of continuous measurements.

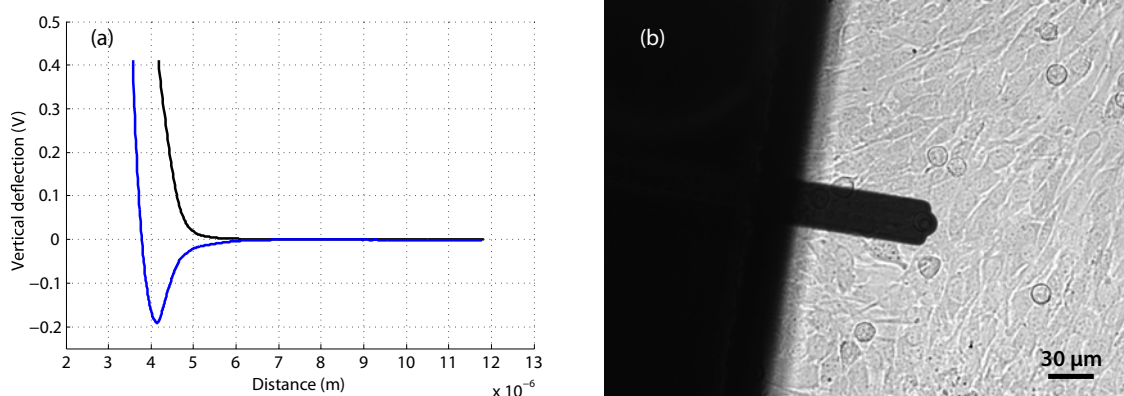


Figure 5.2: This figure shows a force distance curve from a contact force measurement of myoblasts (a) where the approach is coloured in black while the retract is blue. In (b) we see a myoblast monolayer with myoblasts on top. Their rounded shapes reveal that the myoblasts on top have not yet adhered to the underlying layer. On the tip of the cantilever a myoblast is seen. It has been picked up through suction.

5.2.2 initial myoblast-myoblast contact forces and dissociation energies increase linearly with the square root of time

contact forces and dissociation energies at one location

In a feasibility study, repeated force measurements were performed in room temperature up to a time frame of approximately 11 seconds, see Chapter 5.1.2. Figure 5.3 shows measured contact forces (a) and dissociation energies (b) as a function of time, at one location of a myoblast monolayer. The red dots display all the repeated measurements for each time point and the blue dots their mean value per time point with error bars denoting ± 1 standard deviation. The green graph is a fit to the first 4 time points in both Figure 5.3(a) and (b). The scale of the x-axis is square root of time to make comparison between data and fitted graph easier. As we can see in 5.3(a), the contact force increases linearly with the square root of time up until a time point where it appears to reach a constant value. In Figure 5.3(b) this deviation is not as clear. However, the error bars in Figure 5.3(b) are larger than in Figure 5.3(a) so the point of deviation may be hidden in the noise.

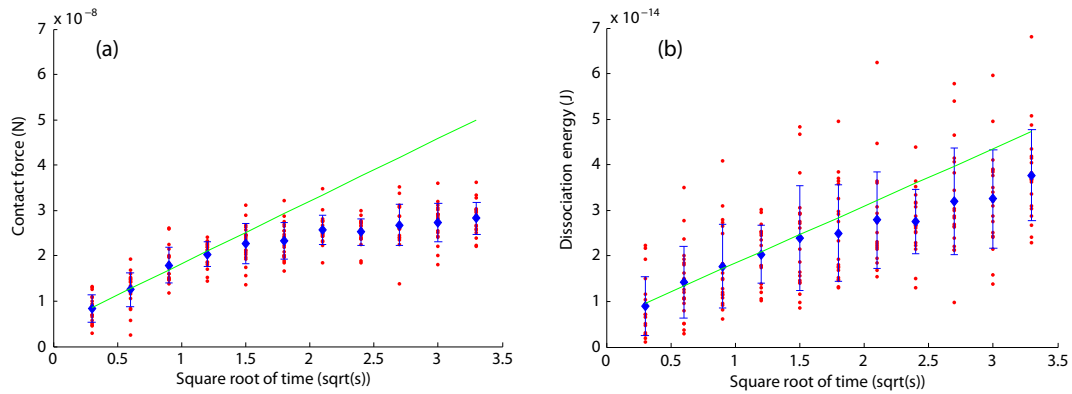


Figure 5.3: This figure shows measured contact forces (a) and dissociation energies (b) as a function of square root of time, at one location of a myoblast monolayer. The red dots display all the repeated measurements for each time point and the blue dots their mean value per time point with error bars denoting ± 1 standard deviation. The green graph is a square root of time curve, fit to the first 4 time points in both a and b

the experimental errors are probably negligible in comparison to natural fluctuations of the binding process

There was a theoretical possibility that the cells used for the measurements could change properties during the time course of the entire experiment. It would not be desirable

to record these changes as time dependent changes in cell-cell interaction. In order to exclude this outcome, a random collection of data points with respect to interaction time was measured. These data points were normalized to their own means and plotted in histograms. Figure 5.4 shows two histograms where all measurements from Figure 5.3 have been normalized to the mean of the time point to which they belong and collected in 20 bins of an evenly distributed size. Figure 5.4(a) corresponds to the force measurements from Figure 5.3(a) and the histogram in Figure 5.4(b) bins the energy measurements in Figure 5.3(b). In both Figure 5.4(a) and (b) all data fit in a single Gaussian curve. This indicates that the errors are of similar type and that probably no additional experimental errors were introduced.

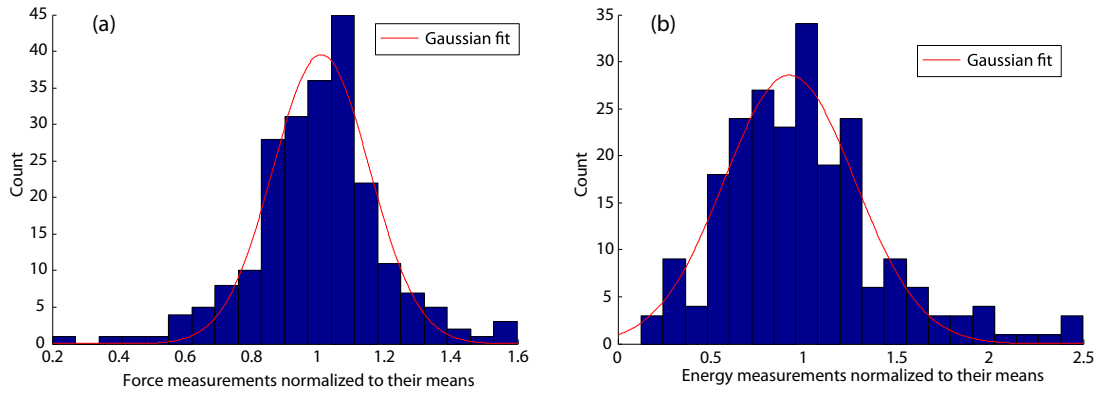


Figure 5.4: Two histograms are displayed where all measurements from Figure 5.3 have been normalized to the mean of the time point to which they belong and collected in 20 bins of an evenly distributed size. (a) corresponds to the force measurements from Figure 5.3(a) and the histogram in (b) bins the energy measurements in Figure 5.3(b). In both (a) and (b) the data has been fit to a Gaussian curve. It is visible that the data has a normal distribution.

contact forces and dissociation energies stabilize at a constant value with time

Two experiments were conducted as described in Chapter 5.1.2. Figure 5.5 shows the outcome where the error bars show ± 1 standard deviation and the green graphs are fitted to the first four points in each graph. In Figure 5.5(a) the mean values of the contact forces at the three different locations of experiment 1 are displayed by blue dots as a function of time. In (b) the blue dots denote the mean dissociation energies of experiment 1 while (c) displays the mean contact force of experiment 2 and (d) the mean dissociation energy of experiment 2. In (a) and (b) it is not clear whether the force and energy stabilize at a constant value. As a matter of fact, it rather appears that they don't. Both contact forces

and dissociation energies in Figure 5.5(a) and (b) follow a square root of time behavior, especially clearly for the first time points. Even if a deviation is visible, no point of steady state is. In order to clarify whether the square root of time increase of contact forces and dissociation energies indeed ceases at some point, experiment number 2 was conducted under controlled temperatures and longer adhesion times were probed. In both Figure 5.5(c) and (d) it is now clearly visible that the data follow a square root of time curve up until a certain time point where it stops to increase in order to remain at a sort of constant level.

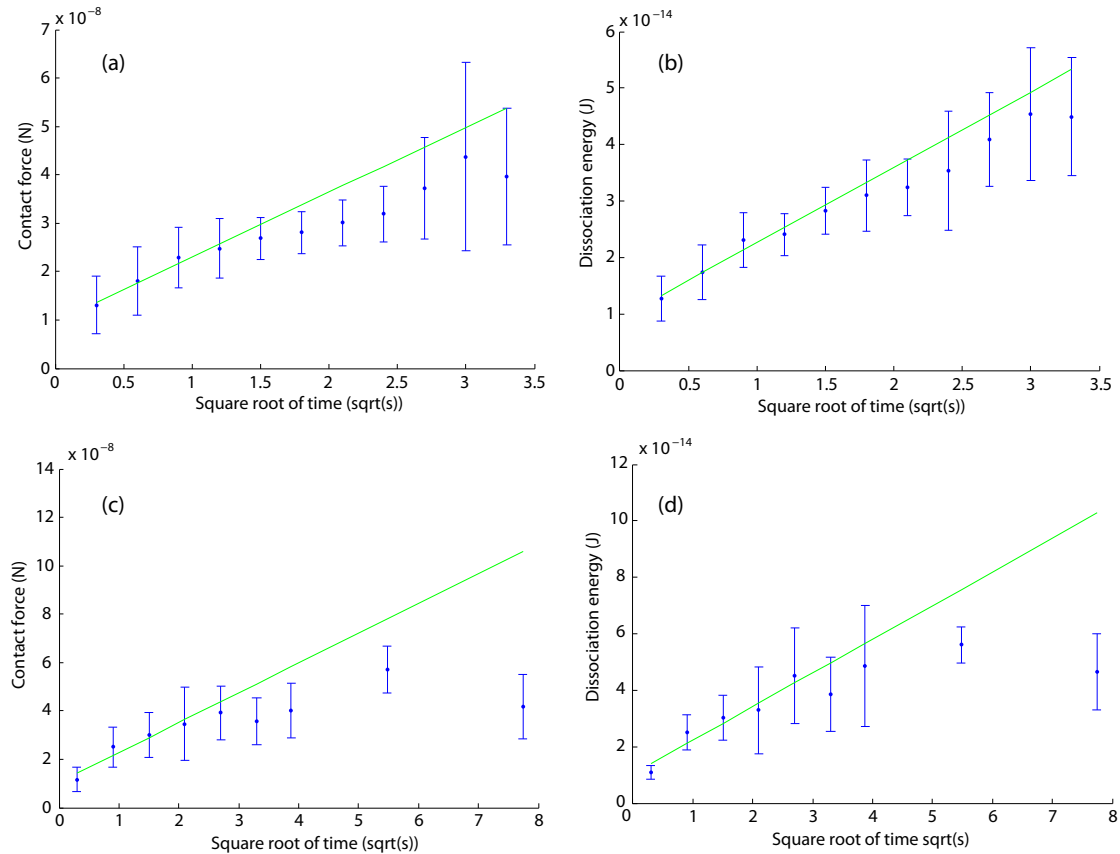


Figure 5.5: This figure shows the outcome of a short term and a long term experiment. In (a) the mean values of the contact forces at the three different locations of the short term experiment are displayed by blue dots as a function of time. In (b) the blue dots denote the mean dissociation energies of the same experiment while (c) displays the mean contact force of the long term experiment and (d) the its mean dissociation energies. The error bars are ± 1 standard deviation and the green graphs are square root of time curves, fitted to the first four data points in each graph.

5.2.3 monocyte adhesion to TNF- α treated HUVEC monolayers

An example of another cell system where force interactions are of crucial importance is the extravasation of white blood cells through the wall of the blood vessel. Here we show that the FluidFMTM setup can measure adhesion forces of monocytes to a HUVEC monolayer undergoing inflammatory response.

In Figure 5.6(a) we can see a TNF- α activated HUVEC monolayer with monocytes on top. Monocytes are not migrative cells and, therefore, remain round (about 10 μm in diameter) on top of the HUVEC monolayer. A few of the HUVEC cells have shapes that remind of those caused by blebbing. This occurred when the monolayer had been outside the incubator for more than one hour, most probably due to the fact that the pH was not controlled. The hole in the cantilever was in this case 4 μm in diameter and we can see a monocyte picked up by suction and situated under the hole. The major point of this picture is to show that monocytes could be picked up by suction after a longer time than in the case of myoblasts which indicates that neither monocyte migration nor extravasation took place. This has also been confirmed in samples left in the incubator under controlled temperature and pH (data not shown). It was to be expected since no fluid flow was present, a prerequisite for extravasation. Hence only initial monocyte-HUVEC interaction forces can be measured in this setup.

Figure 5.6(b) shows a retract curve from a force distance measurement of monocyte-HUVEC interaction (0.5 seconds). We experienced oscillations and, therefore, the curve has been smoothed in MATLAB. The measured force of 100 nN is ten fold higher than that for myoblast-myoblast although generated by half the interaction time. It is also 1000 times larger than reported values [368]. There are details that point in the direction that this number shouldn't be interpreted too literally. The calibration of the cantilever is based on a simulation made for all FluidFMTM cantilevers. There are, of course, individual differences which are not taken into account. The measurement experienced considerable magnitudes of oscillation (± 200 nN) which made the measurement inexact. The material point of this graph is not to extract any absolute numbers. What we can conclude from Figure 5.6(b) is that cell sizes and magnitudes of force interactions in a monocyte-HUVEC system are within ranges that can be measured by the FluidFMTM setup. This opens up the door for investigation and clarification of the force interactions taking place during the extravasation process under different conditions.

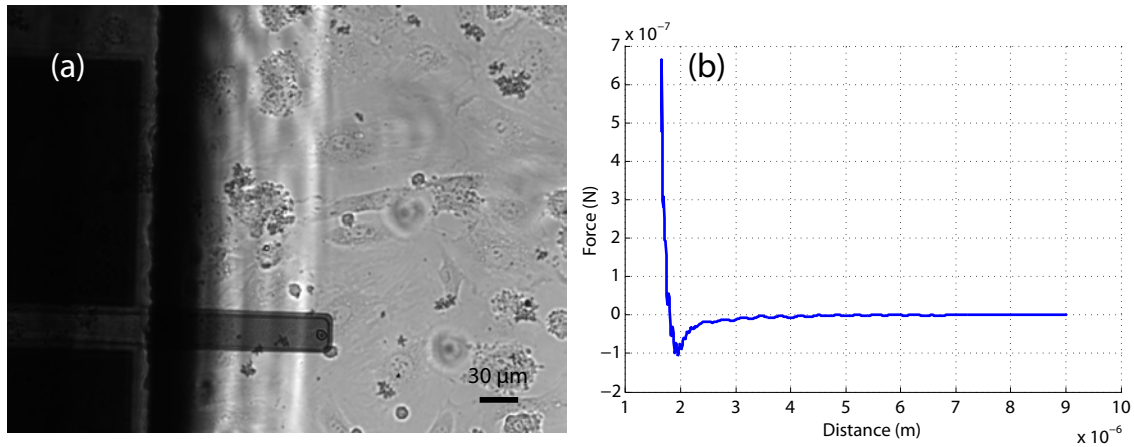


Figure 5.6: This figure shows an example of a measurement of monocyte-HUVEC force interaction. In (a) a monocyte has been picked up from a TNF- α activated HUVEC monolayer. (b) shows a graph from a force-distance measurement of monocyte-HUVEC interaction of 0.5 s.

5.2.4 initial myoblast-myoblast contact is mediated by freely diffusing adhesion molecules in the cell membranes

The displacement of a particle in Brownian motion is proportional to the square root of time [387]. This is what Einstein postulated and mathematically showed in one of 5 papers in a series called "Investigations on the Theory of the Brownian Movement" between 1905 and 1908. His equations concern the motion of only one particle. If the problem is extended to two bodies that interact with each other it can be solved by splitting it up in two independent single body problems. Moving on to three and more interacting bodies, no analytical solution can be derived for their motions except in special cases. The solution for such problems are simulated [388].

Now, imagine freely diffusing particles of two kinds on a surface. No interaction occurs between particles of the same population. But, when two particles of different constitution collide, they interact and cannot dissociate to further interact with other particles. This is the same situation as two cell membranes adhering to each other through interaction of antiparallel adhesion proteins. During the time before interaction with another protein, it is a fair approximation that each molecule behaves like an independent particle in brownian motion. Hence, the first part of the force-time interaction curve is expected to be proportional to the square root of time. With time, the two populations interact and get depleted. Thereby, the interaction is expected to approach a constant value. These are indeed the trends our results indicate. We draw the conclusion that initial myoblast-myoblast adhesion is mediated by freely diffusing adhesion molecules

in the cell membrane. Moreover, given the fact that cadherins are responsible for initial cell-cell contact, what we see here is the interaction behavior of cadherin in living cells.

There are, of course, questions associated with these data. Why does the dissociation energy deviate from the square root of time behavior later than the contact force? We could speculate that internal rearrangements in the adherens junctions lead to increasing dissociation energies although the amount of cadherin bonds remain the same, hence giving rise to the same force breaking the bonds. It could also be that the higher error bars in the energy dissociation graphs statistically do not allow us to conclude that the square root of time graph and the measured data do not belong to the same distribution until a later time point is reached. Although they in reality do deviate at the same time point as the force. However, we cannot be certain. We made around 700 measurements but even more measurements might bring clarification. By varying crucial parameters such as pH and temperature further information on the interaction kinetics would be elucidated.

5.3 Chapter Conclusions

In this chapter we have shown that we can probe myoblast-myoblast contact forces with the fluid force microcopy technology. The pick-up of a myoblast in suspension takes only a few seconds which allows for a simple experimental setup. The release is equally fast, but has to be carried out within a few minutes. Coating the tip with a non-fouling polymer did not prevent cell adhesion indefinitely. Future improvement of this coating would allow for more reproducible experiments.

Force measurements were carried out as a function of adhesion time. The time ranged from 0.1 seconds to 1 minute. We used MATLAB to calculate the adhesion forces and dissociation energies and saw that the forces and energies increased proportionally to the square root of time up until a certain time point when they stabilized at a constant force or energy. This time point was approximately 2 seconds for the contact force and around 5 seconds for the dissociation energy.

About 100 measurements from the recordings of the contact force and dissociation energy respectively, were plotted in one histogram each, with count on the y-axis and normalization to the mean of each individual time point on the x-axis. The plots could be fit to a Gaussian curve, which indicates that the experimental errors probably are negligible in comparison to natural fluctuations of the binding process.

An example of another cell system where force interaction is of crucial importance is the extravasation of white blood cells through the endothelial inner wall of blood vessels as a response to an inflammatory reaction. We have shown that we can measure the interaction between a monocyte (probe) and an endothelial monolayer with fluid force microscopy. It is a proof of principle that could open a new avenue of possibilities for further studies of the immune system and force interactions. However, the absolute value of the measurement should not be taken literally.

Based on the theory of Brownian motion, freely diffusing particles move a distance proportional to the square root of time. Adding the parameter that these particles stop moving upon interaction, the displacement should decay. Our graphs show an increase in both contact force and dissociation energy proportional to the square root of time up until a certain time point when the values stabilize. We suggest that the system we are studying is a system of freely diffusing adhesion molecules in the cell membranes. Moreover, these adhesion molecules must be cadherins since cadherin is responsible for initial cell-cell contact formation.

Calcium Mediated IGF-1 Expression as a Response to Stretch

Today there is a big interest in muscle related disorders, such as sarcopenia, the age-related decline in muscle mass that will inflict us all-if it hasn't already... As a result, viable methods for combating muscle wasting disorders are urgently being sought. But in order to achieve satisfactory results new therapies and technologies to enhance muscle regeneration have to be developed based on a better understanding of muscle development.

In Chapter 1, we were previously introduced to the mechanobiology of muscle development and the role of Stretch Activated calcium Channels (SACs) and IGF-1 splicing in this context. In short; Activated myoblasts first undergo many rounds of cell division. They may next withdraw from the cell cycle to fuse to form myotubes. Division and fusion are differentially modulated by mechanical stimuli transmitted to the cell's biosynthetic mechanisms via the actin-based cytoskeleton; Specifically, cyclic stretch promotes proliferation and inhibits differentiation. Additionally cyclic stretch induces up-regulation of MGF expression but inhibits IGF-1Ea expression. This stands to reason, as MGF has been found to promote proliferation and IGF1-Ea differentiation. Ramp stretch, on the other hand promotes both MGF and IGF-1Ea. The influx of calcium appears to be a prerequisite for both proliferation and differentiation of myoblasts to take place. Furthermore, this influx has been shown to be partially or fully mediated by SACs. We hypothesize that stretch induced up-regulation of MGF is mediated via calcium influx through SACs.

To test this hypothesis, we have put proliferating myoblasts under cyclic stretch in the presence of channel blockers; Streptomycin, nifedipine and BAPTA AM as an intracellular calcium chelator.

6.1 Preparation and Analysis of Myoblast Stretching Experiments

6.1.1 preparation of cell samples

plating cells on cell culture dishes

1 ml of GM per sample was put into round cell culture dishes (TCPS) with 35 mm in diameter (TPP). The dishes were next put into the cell incubator to heat up to 37 °C. C2C12 myoblasts were seeded in GM at a density of 4000 cells/cm² and put into the incubator.

plating cells on stretching compartments

PDMS (Sylgard 184) was thoroughly mixed at a weight ratio of 1:10 curing agent to polymer. The mixture was put in a vacuum chamber and degassed until no more bubbles could be seen. 10 ml was injected by a syringe into a home made mold. This mold was designed to replicate the dimensions of the commercially available stretching compartments from B-Bridge. After curing in 80 °C for four hours, the PDMS stretching compartment could be released from its mold.

Prior to cell seeding, the compartments were cleaned with 70% ethanol in order to remove non-cured polymer residues and then rinsed in ultrapure water and dried with a nitrogen gas jet. PDMS is a hydrophobic material and as cells grow better on hydrophilic surfaces the compartments were subsequently plasma treated at 5×10^{-2} mBar for 1 min at the highest power the machine could provide (see Chapter 3.3.3), in order to render the surface hydrophilic. 2 ml PBS per compartment was immediately added in order to impair hydrophobic recovery. The compartments were brought in this state into the cell culture hood where they were left under UV light for 30 minutes in order to be sterilized. After sterilization, 1 ml of FBS was added to each compartment for 2 hours in order to functionalize the surface with ECM proteins. The FBS was replaced with GM and compartments were put in the cell incubator to warm up to 37 °C. C2C12 myoblasts were seeded onto the surface of the compartment in GM at a density of 9000 cells/cm² and put into the incubator.

6.1.2 preparation of ion channel blockers

Stock solutions of all channel blockers were prepared by dissolving the agent directly in GM and sterile filtering the solution under the sterile cell culture hood (pore size 0.2 μm). The concentration was set to 10x of the working solution. The acidic stock solution of GdCl_3 was supplemented with NaOH in order to bring it back to physiological pH. BAPTA AM was first made up at 18 mM in Pluronic[®] and nifedipine at 10 mM in DMSO.

6.1.3 channel blocker test

C2C12 myoblasts were plated on TCPS dishes and one type of ion channel blocker was added to each dish after one day of culture. The tested ion channel blockers were: streptomycin (100 μM and 200 μM), ruthenium red (5 μM and 50 μM) and Gd^{3+} (100 μM). The cells were grown in DM for a total of 7 days and imaged each day with a phase contrast microscope, see Chapter 3.2.1 for details.

6.1.4 stretching C2C12 myoblasts

C2C12 myoblasts were plated on stretching compartments and kept in the incubator until the next day. 5 minutes before stretch commenced, one type of channel blocker was added per compartment except in the controls. For the static control with streptomycin, the cells were lysed 5 minutes after the addition of the agent. The working solution for streptomycin had a concentration of 100 μM , nifedipine 10 μM and BAPTA AM 18 μM . Compartments were put into the stretcher (see Chapter 3.3.3 for specifications) which in turn was put into the incubator. A saw tooth wave, 0.5 Hz 4% stretch amplitude, was applied for 2, 5, 10, 15, 30 and 60 minutes for different compartments. Immediately after stretch, the GM in the compartments was aspirated and samples lysed according to Chapter 3.2.3.

6.1.5 QRT-PCR analysis

QRT-PCR analysis was performed on the lysates acquired from the stretching. RNA was extracted according to Chapter 3.2.3 and cDNA subsequently synthesized according to Chapter 3.2.4. The QRT-PCR procedure was performed as described in Chapter 3.3.2.

6.2 Subjecting Myoblasts to Stretch and Channel Blockers

6.2.1 channel blockers and myotube formation

The ion channel blockers streptomycin (100 μM and 200 μM), ruthenium red (5 μM and 50 μM) and Gd^{3+} (100 μM) were tested on cultures of C2C12 myoblasts. The biggest effect in terms of myoblast fusion, was seen in the sample treated with 100 μM streptomycin. Figure 6.1(a) shows myoblasts grown in DM for 7 days. Some myotubes are visible indicating that this colony of cells has committed to myogenesis. Figure 6.1(b) shows cells from the same batch and split, grown under the same conditions but with the addition of 100 μM streptomycin on the second day. These myoblasts have formed large myotubes. Even fusion between myotubes has taken place. The result of this event is visible from the fact that single myotubes branch into two tubes.

For this batch and split, the addition of streptomycin seemed to make myoblasts more prone to fuse and to form myotubes than those in the control. However, later experiments also showed the opposite behaviour meaning that the myoblasts in the control fused to a larger extent than those treated with streptomycin. Apparently we could not assign the change in myoblast fusion to the addition of streptomycin. On the contrary we appeared to be looking at normal variations within different samples, channel blocker or no channel blocker. Not wanting to abandon this promising scenario without an answer, we decided to change our read-out system to a more precise one. We changed the approach to do QRT-PCR analysis of the proliferation stage of myoblasts during stretch under the influence of channel blockers.

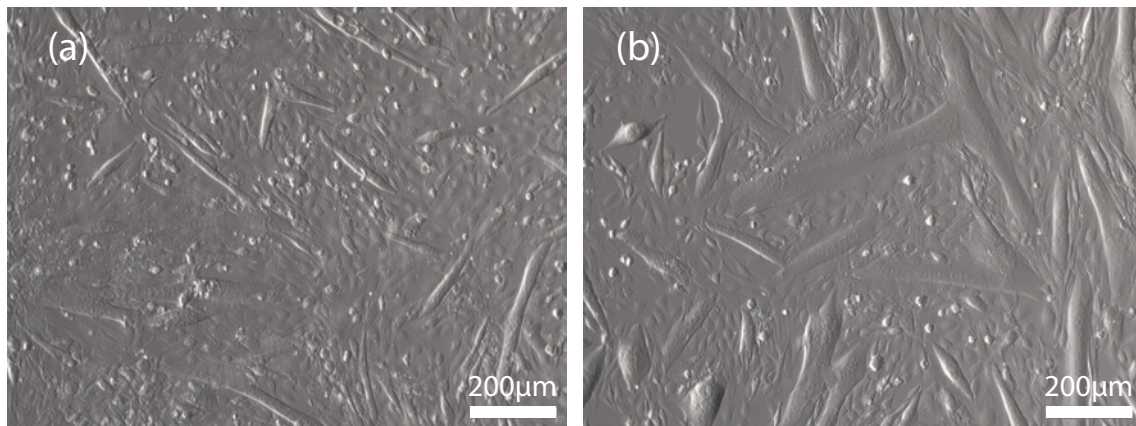


Figure 6.1: Myoblasts grown for 7 days in DM. (a) displays the control while (b) shows a sample where streptomycin was added on the second day. For this batch and split, the addition of streptomycin seemed to make myoblasts more prone to fuse and to form myotubes than those in the control. However, later experiments also showed the opposite behavior meaning that the myoblasts in the control fused to a larger extent than those treated with streptomycin.

6.2.2 stretch with streptomycin

varying the stretching time

Figure 6.2 displays the results of C2C12 myoblasts being stretched for 0, 2, 5, 10, 15, 30 and 60 minutes with and without streptomycin. The samples were lysed immediately after stretch, total RNA was extracted and cDNA synthesized and analyzed in a QRT-PCR for MGF and IGF-1Ea expression. The graphs show quantitation relative to static control for one biological and three technical replicates per time point. The error bars are ± 1 standard deviation. The controls show an elevation of MGF expression for 10, 15 and 30 minutes of stretch and with the peak at 15 minutes, Figure 6.2(a). The error bar at 15 minutes is rather large. In the same graph the MGF expression of streptomycin treated samples is plotted. These samples were subjected to the same stretching times as the controls. The stretch induced MGF expression peak we can see in the control seems to have been brought back to values comparable to the static control (100%). For the IGF-1Ea expression the control shows a peak at 10 minutes of stretch and the addition of streptomycin appears to cancel this effect as well, Figure 6.2(b). This indicates that a stretch induced increase of the expression of any isoform of IGF could be mediated by stretch activated calcium channels. Later on, however, these results turned out to be irreproducible.

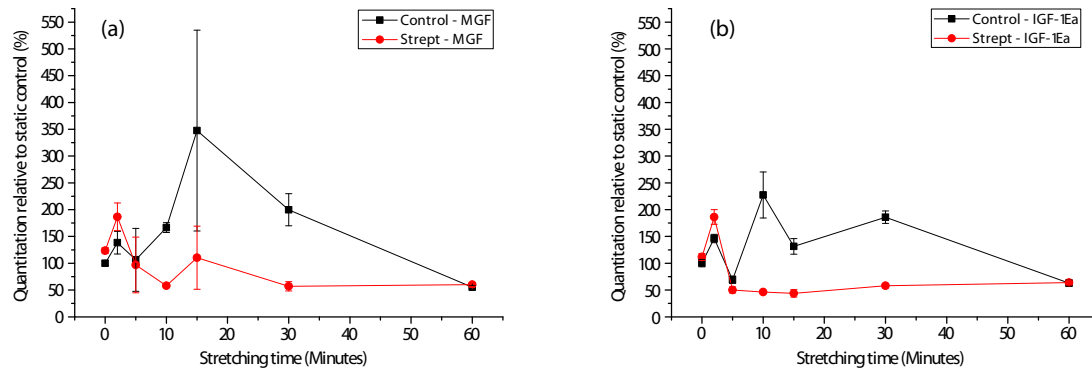


Figure 6.2: This figure displays the results of C2C12 myoblasts being stretched for 2-60 minutes with and without streptomycin. The samples were lysed immediately after stretch, total RNA was extracted and cDNA synthesized and analysed in a QRT-PCR for MGF and IGF-1Ea expression. The graphs show quantitation relative to static control for one biological and three technical replicates per time point. Later on, these results turned out to be irreproducible. The error bars are ± 1 standard deviation.

varying the incubation time

As Figure 6.2 indicated, stretching could increase the expression of both isoforms of IGF in C2C12 myoblasts, while cells subjected to the same mechanical environment but also with the addition of streptomycin did not appear to be affected by the stretch. In order to establish the time frame of the interaction between the streptomycin and the myoblasts, different incubation times were tested (0, 2, 5, 8, 10 and 15 min). The stretching time was 10 minutes at 0.5 Hz and 4% stretching amplitude. Figure 6.3 shows the quantitation of MGF and IGF-1Ea expression relative to static control as a response to incubation time of streptomycin for one biological and three technical replicates per time point. The error bars are ± 1 standard deviation. The incubation time ranged from 0-15 minutes. Streptomycin was always added at the designated amount of minutes before the stretch was stopped.

All incubation times except that of 10 minutes yielded a slight decrease in the expression of both isoforms. At 10 minutes there was a peak indicating that for this particular incubation time the streptomycin had a positive effect on the IGF expression. This is highly unlikely since neither 8 minutes nor 15 minutes incubation time yielded an increase in gene expression and the streptomycin is not expected to lose its functionality only to regain it 5 minutes later. Either this experiment had an outlier or we were observing natural variations between samples.

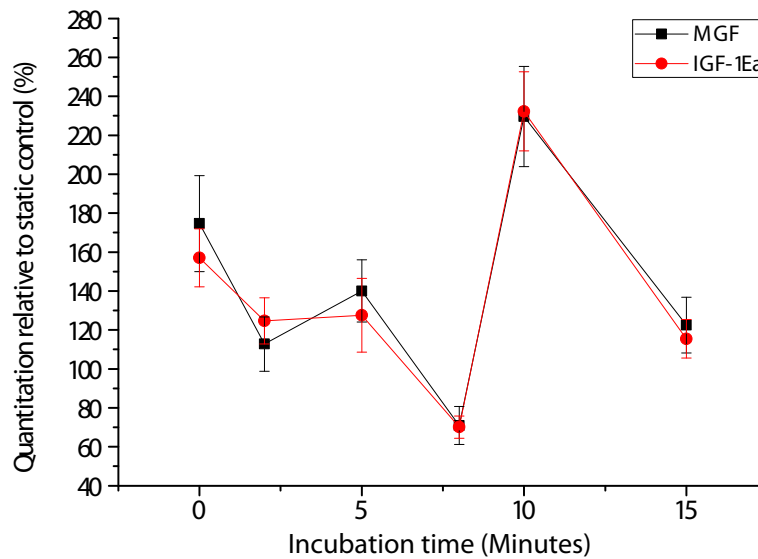


Figure 6.3: This figure shows the quantitation of MGF and IGF-1Ea expression relative to static control as a response to incubation time of streptomycin for one biological and three technical replicates per time point. The error bars are ± 1 standard deviation. The stretching time was 10 minutes at 0.5 Hz and 4% stretching amplitude while the incubation time ranged from 0-15 minutes. Streptomycin was always added at the designated amount of minutes before the stretch was stopped. These graphs show fluctuations rather than trends and are also inconsistent with the results displayed in Figure 6.2.

6.2.3 stretch with nifedipine

In Chapter 1.1.7 the function of streptomycin as an ion channel blocker was described. It turns out that streptomycin is not specific for stretch activated ion channels but also blocks voltage gated ion channels. In order to elucidate whether the absence of stretch induced increase in IGF expression could partially have been mediated by calcium influx through voltage gated ion channels, myoblasts were stretched with nifedipine, a specific voltage gated ion channel blocker. The same batch and split of myoblasts was used as in the experiment with streptomycin. Moreover, these experiments were performed at exactly the same time, which allowed for comparison with the same control.

Figure 6.4 shows the expression of MGF (a) and IGF-IEa (b) under stretching conditions with nifedipine versus without. The graphs show quantitation relative to static control for one biological and three technical replicates per time point. The error bars are ± 1 standard deviation. In difference to stretch with streptomycin, a small peak can be seen for stretching times up to 15 minutes for MGF and 10 minutes for IGF-1Ea. But these peaks are lower than the those of the controls. This result indicates that blockage

of calcium influx through voltage gated ion channels lowers the effect stretch has on IGF expression but not to the same extent as streptomycin does.

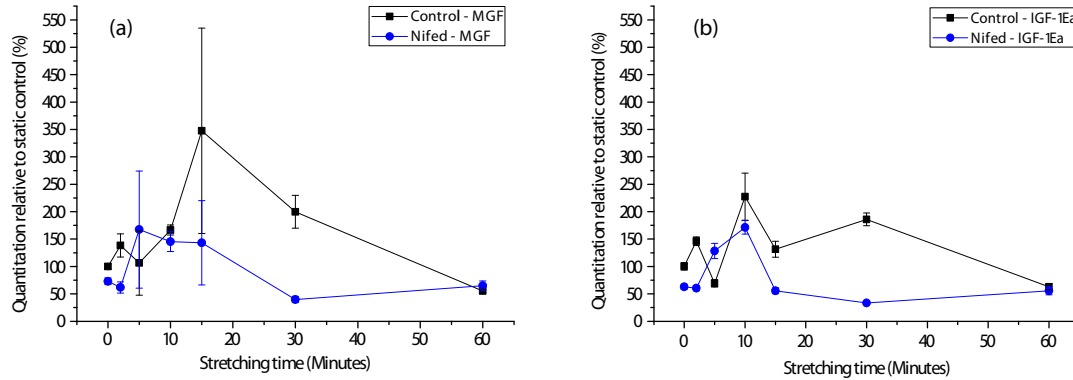


Figure 6.4: This figure shows the expression of MGF (a) and IGF-IEa (b) under stretching conditions with nifedipine versus without. The graphs show quantitation relative to static control for one biological and three technical replicates per time point. The error bars are ± 1 standard deviation. The control graphs are the same as the control data in Figure 6.2. Later, these graphs turned out to not be reproducible.

6.2.4 stretch with BAPTA AM

So far, our results have indicated that proliferating myoblasts increase their gene expression of the two isoforms of IGF when subjected to a specific time frame of stretch. It has also appeared plausible that this effect is inhibited by the presence of the ion channel blockers streptomycin and nifedipine, where blockage of stretch activated ion channels appeared to have the biggest effect. In order to target whether indeed calcium is the responsible second messenger for the stretch induced up-regulation of IGF expression, proliferating myoblasts were subjected to stretch in the presence of BAPTA AM. As described in Chapter 1.1.7, BAPTA AM is a cell-permeant chelator which is highly selective for calcium. The intra cellular calcium storages of cells treated with a proper amount of BAPTA AM are depleted. Incoming calcium will also be chelated.

Figure 6.5 shows the expression of MGF (a) and IGF-IEa (b) under stretching conditions in the presence of BAPTA AM versus without. The graphs show quantitation relative to the static control for one biological and three technical replicates per time point. The error bars are ± 1 standard deviation. Both isoforms appear to be expressed at a similar rate. In this experiment, in difference to earlier experiments, a 5 fold peak was recorded for both isoforms for cells stretched for 10 minutes. Previously, the peak was 2 to 3 fold

larger than static control. However, myoblasts treated with BAPTA AM only showed a slight elevation of the MGF and IGF-1Ea expression compared to control. Indeed, the stretch induced effect we see appears to be mediated by calcium. This is a promising indication but it also raises worries as the values recorded for the control experiments don't appear to be the same. The shapes of the control graphs in Figure 6.5 differ from those in Figure 6.2. Our error bars were large from the beginning and they represent the standard deviation of three technical replicates. At this point biological replicates were required to confirm that the results we saw were indeed significant.

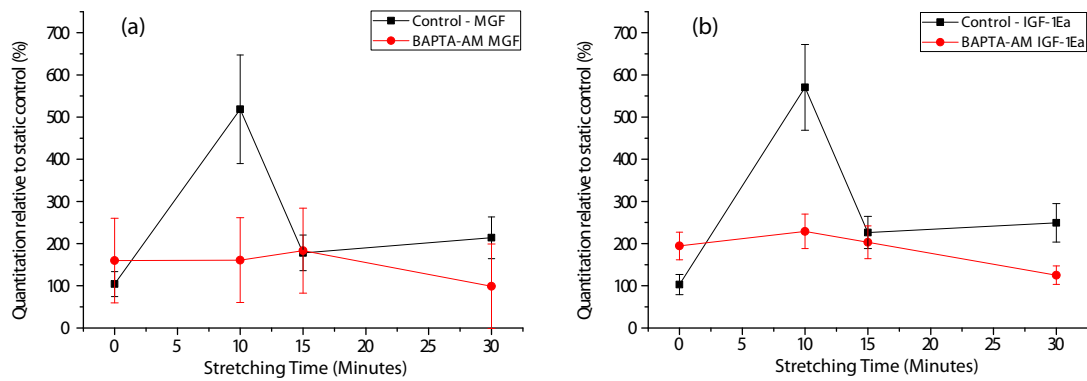


Figure 6.5: This figure shows the expression of MGF (a) and IGF-1Ea (b) under stretching conditions in the presence of BAPTA AM versus without. The graphs show quantitation relative to static control for one biological and three technical replicates per time point. The error bars are ± 1 standard deviation. The control data is inconsistent with control data from Figures 6.2, 6.3 and 6.4.

6.2.5 MGF expression as a response to stretch

In order to examine whether the results of the stretch induced IGF expression were significant, a set of experiments were conducted. The MGF expression was measured for several biological replicates at different stretching times. Figure 6.6 summarizes the MGF expression of myoblasts from different batches subjected to stretch without (black bars) and with streptomycin (red bars). 2 min: $n=1$; 5 min: $n=2$; 10 min: $n=10$ for the control and $n=9$ for the streptomycin treated; 15 min: $n=2$ for the control and $n=1$ for the streptomycin treated; 30 min: $n=3$ for the control and $n=2$ for the streptomycin treated; 60 min: $n=1$. Error bars display ± 1 standard deviation.

Two sample t-tests were performed in Origin (OriginLab) on the control group and the group of streptomycin treated samples, for time points 5, 10, 15 and 30 in order to test for significant differences between these two groups at each time point. Time points 2 and

60 did not make sense to test since $n=1$ for both of them. The null hypothesis could not be rejected for any of the tested time points. Therefore the control group belongs to the same distribution as the group of treated samples. One sample t-tests were performed in Origin for time points 5, 10, 15 and 30 on the control group and the treated group separately. The mean of all measurements within each group was subtracted from the same group. The null hypothesis could not be rejected for any of the groups. All time points belonged to the same distribution. These tests showed that neither the difference of the data at each time point between the two groups, nor the difference of the data compared to the mean within the groups are statistically significant.

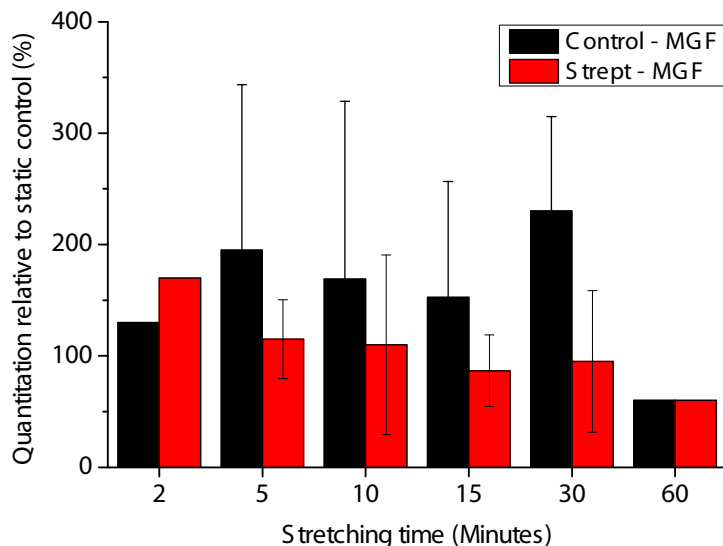


Figure 6.6: This figure summarizes the MGF expression of myoblasts from different batches subjected to stretch without (black bars) and with streptomycin (red bars). 2 min: $n=1$; 5 min: $n=2$; 10 min: $n=10$ for control and $n=9$ for treated; 15 min: $n=2$ for control and $n=1$ for treated; 30 min: $n=3$ for control and $n=2$ for treated; 60 min: $n=1$. Error bars display ± 1 standard deviation. One sample t-tests and two sample t-tests were performed in Origin. These tests showed that neither the difference of the data at each time point between the two groups, nor the difference of the data compared to the mean within the groups are statistically significant.

6.2.6 the non-trivial task of setting up a stretching experiment

The data of this chapter did not prove our hypothesis. Unfortunately, they did also not prove the opposite. What, at first, appeared to be promising results, turned out, at the end, to be outliers. Statistical analysis of the data in Figure 6.6 leads us to two conclusions. Firstly, the difference between MGF expression in proliferating myoblasts subjected to

cyclic stretch and myoblasts under the same conditions with the addition of streptomycin is not statistically significant. Regardless of stretching time. Secondly, neither of these groups showed a statistically significant difference from their own means for any time point. This is contradicting previous findings where cyclic stretch has been shown to promote MGF expression in proliferating myoblasts [102, 121, 203].

According to Figure 6.2, the IGF-1Ea expression was also up-regulated after cyclic stretch of proliferating myoblasts. This should not have been the case according to Cheema et al [121]. If not earlier, this would have been a good moment to start doubting the data. Instead, we were encouraged by them and continued our experiments. In retrospect, the proper way to start would have been to establish a protocol for stretching myoblasts where we see the same effects as those that have already been reported. With such a protocol in hand, new hypotheses can relatively easily be tested.

This is of course easier said than done. As Chapter 1.2.1 informs, there is no established protocol for stretching cells. Not a single research group uses the same parameters as another lab. However, they report similar results. As a reader you get the impression that no matter how you set up your experiment, you will see these clear trends. In reality, given the diversity of previous stretching set-ups, no matter how you set up your experiment you will face difficulties. Two outcomes reporting the same result are not the same if the set-ups are not identical.

Our major problem originated in the MGF expression itself. In absolute terms, it was low for all conditions. The threshold value was reached at cycle 30-35 which is to be compared with the housekeeping gene, GAPDH, which had reached its threshold already at the 18th-20th cycle. With low concentrations, the error bars are large. In Figure 6.6, 10 measurements are displayed at time point 10 minutes. The error bar is of the same size as the average measurement itself. The cell is a complicated system. There are hundreds of intracellular as well as extracellular processes taking place at the same time in order for a cell to stay alive. This means that even in the most perfectly designed *in vitro* environment, most parameters governing cell behavior will not be controlled. This often renders base lines with high error bars. In order to draw solid conclusions from a cell experiment the outcome must be very clear in terms of rigid statistics which, in the case of a wide spread base line, usually requires a drastic change in behavior as a response to the added stimulus or removed necessity. In addition to having a rather noisy baseline, we did not see any such drastic change in our experiments.

The area of mechanobiology has been recognized and established in only three decades. The field is intriguing and prompts further investigations to elucidate the signaling transduction taking place during myogenesis. Indeed, unraveling the mechanisms and effects of mechanotransduction is necessary for the complete understanding of cell behavior and development. The researched community rejoiced when the first version of the Flexercell[®] was introduced on the market in 1987. Only years later, the first performance tests were initiated. It turned out that the stretch was not homogeneous and that the strains stated were not correct. This led to an improved version in 1995. Apparently, already from the start, the need of an established stretching protocol was pronounced. The eagerness to accept the Flexercell[®] as the solution, blinded the research community and the device was used under false assumptions for years. An established protocol for stretching cells is still missing. Not only from the point of view of stretching paradigms, but also surface functionalization, cell age, culturing conditions, etc. We don't know why and how cells respond to certain stretch modalities. Consequently we cannot control the response. In my opinion, this is what has to be unraveled next. Until we have this knowledge, and can act accordingly, contributions to the field of mechanobiology will not succeed in putting all the puzzle pieces together.

6.3 Chapter Conclusions

In this chapter, we hypothesized that stretch induced up-regulation of MGF is mediated via calcium influx through stretch activated calcium channels (SACs). In order to test this hypothesis, proliferating myoblasts were subjected to cyclic stretch in the presence of ion channel blockers.

An ion blocker test was performed in static conditions, where the results indicated that streptomycin has an effect of promoting myoblast differentiation. Hence streptomycin was chosen for further studies. The stretching experiments were performed in a STREX instrument from B-Bridge inc and the results were analyzed in a Step-One-Plus PCR system from Applied Biosystems. Varying the stretching time indicated that a peak of MGF expression would appear at 10 minutes of stretch in samples grown without streptomycin. Samples subjected to stretch and streptomycin, however, seemed to be rescued from the stretch induced increase in MGF expression. These preliminary results were very promising. Also the IGF-1Ea expression increased with cyclic stretch. Although the increase was lower than in the case of MGF, this result contradicted previous findings

stating that the expression of IGF-1Ea should decrease upon cyclic stretch [121]. The stretch induced IGF-1Ea peak was decreased by addition of streptomycin. The next step consisted in varying the incubation time of streptomycin. In this experiment the result of a stretch induced MGF peak could not be reproduced. The expression of both isoforms at 15 minutes of incubation time in Figure 6.3 should be the same as time point 10 minutes in Figure 6.2.

Given that streptomycin also blocks voltage gated ion channels, we investigated the influence of these ion channels in our experimental setup, in order to see if we could exclude this possibility. Also Nifedipine provided a lower expression of both isoforms during stretch. These results indicated that voltage gated ion channels are important during proliferation. However, it does not exclude that SACs are activated in parallel. We additionally measured the IGF expression of the two isoforms when adding BAPTA AM, an intracellular calcium chelator. And indeed, the stretch induced MGF and IGF-1Ea increase was inhibited. This is to be expected. With all calcium inside the cell being immediately chelated, the influx also through SACs will not cause any signalling cascade.

The experiment with BAPTA AM showed for a second time that reproducibility of our results was a problem. Hence we performed several identical measurements of MGF expression from cultures subjected to stretch and streptomycin and to stretch alone. The result showed that no statistically significant difference could be measured and that we, in fact, had been working in the noise.

We finally conclude that, in order to properly test a hypothesis in the field of mechanobiology, an established stretching protocol is needed. Most research groups use different paradigms and growth conditions. The results are more or less coherent. However, coherent results coming from different setups cannot be interpreted as answers to the same scientific question.

Devices Designed to Stretch Cells in Culture and Single Cells

As presented in Chapter 1 there are several commercial and home made solutions for providing a desired cell stretching environment. In Chapter 6, a commercial cell stretcher (STREX, B-Bridge inc.) was used to stretch cells in culture. Most of the cell stretchers in use are based on mechanical actuation by a stepper motor. Mechanical stretching is reliable, but produces heat that often calls for complicated cooling systems, given the fact that the motor needs to operate in 37 °C in a humid environment. Additionally, fine tuning of the precise stretching area cannot be done easily.

Actuation with dielectric elastomers (DE) constitutes a promising platform for stretching cells. The stretch is in-plane and there are endless choices of frequency and strain settings making it possible to create any stretch paradigm one would like. The electrodes causing the stretch can be stamped onto the acrylic DE and are therefore possible to pattern. This way distinct stretching areas can be constructed. The generators can be stored outside of the incubator, eliminating the over heating problem.

Because of all of the above mentioned properties that these materials provide, we have investigated the possibility of engineering a cell stretcher based on electrically stretch-induced DE actuators (DEAs). The original idea was born in the Nanotechnology group, Department of Mechanical and Process Engineering, ETH Zurich. We have also brought the technique one step further and designed a single cell stretcher based on patterning of electrodes with ion implantation onto PDMS. The construction was done in collaboration with the Microsystems For Space Technologies Lab, EPFL, Neuchâtel.

7.1 Creation of Devices for Cell Stretching

7.1.1 creation of acrylic DEA

The creation of the acrylic DEA followed the protocol established Dr Manuel Aschwan- den and Raoul Enning in the Nanotechnology group, department of mechanical and process engineering, ETH Zurich.

Circular frames were cut out from 3 mm and 6 mm thick PMMA sheets. These frames were paired two and two, 3 and 6 mm, and clamped around a DE membrane connected to zinc coated copper band electrodes, with the thicker frame on top. The construction was fixed with four screws and finally spin coated with PDMS (Sylgard 184, 1:10 weight ratio curing agent:polymer) at 5000 rpm for 2 minutes. The setup was put in 60 °C for 4 hours. Figure 7.1(a) shows the finalized stretching compartment with GM inside. In the middle, stacked electrodes in the DE membrane are visible as a black elongated area. It is on this area that stretch takes place as a response to applied voltage. The white arrows display the stretch direction which, due to geometry, is uni-axial.

The preparation of the DE membrane consisted of several steps: 1. A double-sticky scotch tape (VHB, acrylic DE) was pre-stretched 300% bi-axially and carbon black powder was contact printed with a 5x40 mm PDMS stamp on the bottom and top side to form electrodes. 2) These electrodes were elongated by gluing stripes of zinc coated copper band and, finally, the scotch tape was glued to the bottom PMMA frame. 3) Another double-sticky scotch tape was pre-stretched bi-axially 300% and glued on top. 4) A third carbon black electrode was stamped on top and elongated by zinc coated copper band. 5) A protective upper layer of Montageband Transparent, 3M, (VHB acrylic DE) was pre-stretched bi-axially 300% and glued on top. 6) The two grounded zinc coated copper band electrodes were glued together for easier handling. The two electrodes seen in Figure 7.1(a) are therefore grounded and active respectively. Figure 7.1(b) shows a schematic picture of a cross section of the DE membrane. The white sheets symbolize the acrylic polymer and the black lines carbon black electrodes. The uppermost layer of spin coated PDMS protects the underlying construction from the ionic medium on top as well as provides a surface chemistry that allows for coating with ECM proteins in order to enable cell attachment.

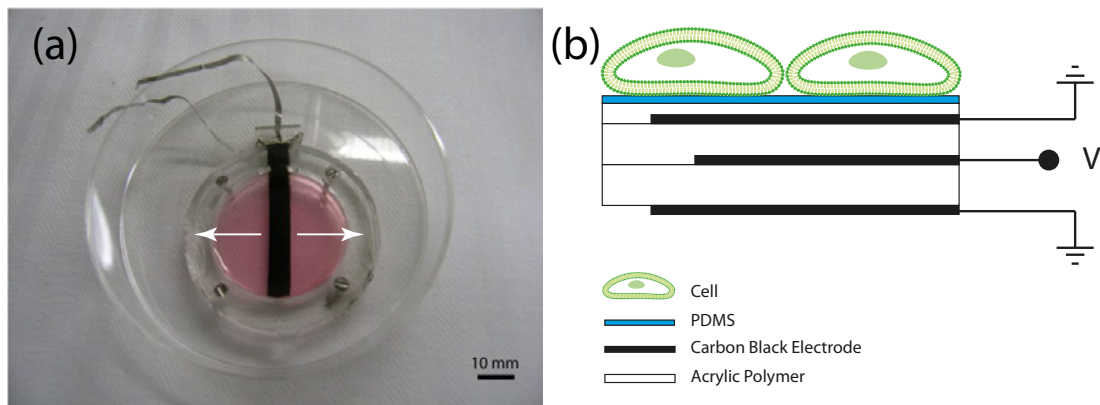


Figure 7.1: This figure shows the finalized stretching compartment with GM inside, (a). In the middle, stacked electrodes in the DE membrane are visible as a black elongated area. It is on this area that stretch takes place as a response to applied voltage. The white arrows display the stretch direction, which due to geometry, is uni-axial. (b) shows a schematic picture of a cross section of the DE membrane. The white sheets symbolizes the acrylic polymer and the black lines carbon black electrodes. The uppermost layer of spin coated PDMS protects the underlying construction from the ionic medium on top. It also provides a surface chemistry that allows for coating with ECM proteins in order to enable cell attachment. This design was developed in the Nanotechnology group, department of mechanical and process engineering, ETH Zurich

7.1.2 creation of single cell stretcher

photolithography

Photolithography was used in order to produce a master for a replica molding step that finally would cast 100 μm wide grooves into PDMS (Sylgard 184). The design of the mask was created in AutoCAD 2002. The masks were printed on foil using a 16000 dpi photoplotter (MIVA Technologies GmbH, Germany).

A two inch silicon wafer was cleaned by spin coating 2-propanol 10 s: 600 rpm and 1 min: 1500 rpm. Afterwards, a spin coating step with a negative photoresist followed (SU-8 GM 1070, Gersteltec Sarl, Switzerland): 10 s: 600 rpm and 1 min: 800 rpm which should give around 100 μm high structures. The wafer was let to relax 30 minutes and afterwards soft baked at 65 $^{\circ}\text{C}$ for 15 minutes followed by a temperature increase (2 $^{\circ}\text{C}/\text{min}$) to 95 $^{\circ}\text{C}$ at which the wafer was kept for 1 hour. After being cooled down to room temperature, the wafer was covered with the mask, slid into the mask aligner (Karl Suss MJB3, Karl Suss, Garching, Germany) and exposed for 40 s. Hard baking was done at 65 $^{\circ}\text{C}$ for 10 minutes to be followed by a temperature increase (2 $^{\circ}\text{C}/\text{min}$) to 95 $^{\circ}\text{C}$ at which the wafer was kept for 30 minutes. Development was done with the provided

developer for 1 minute. A final rinse with 2-propanol was done before the last baking: 135 °C for 2 hours.

replica moulding

PDMS (Sylgard 184) was mixed at a weight ratio of 1:10 curing agent:polymer, degassed and poured on top of the silicon master in order to create grooves with replica moulding. The PDMS was put at 80 °C for 4 hours to cure. The reason why PDMS Sylgard 184 was chosen and not any other PDMS was because it is rather stiff and thereby suits the purpose of stabilizing the underlying layer.

fabrication procedure

The fabrication of the single cell stretcher was done in the Microsystems For Space Technologies Lab, EPFL, Neuchâtel by Samin Akbari. First, gold was sputtered on the PDMS replica. A thin membrane of PDMS (Sylgard 186) was produced on polyamid. Gold ion implantation of elongated electrodes and gold contacts was done on the membrane. Oxygen plasma was used to bind the membrane to the PDMS replica. Finally, the top layer of the membrane was sputtered with gold ions and electrical wires were connected. The reason why Sylgard 186 was chosen is because it is slightly softer than Sylgard 184 and therefore more suitable for the ion implantation. Due to its lower young's modulus it also responds with a higher strain to the same voltage input.

7.1.3 cell culture

acrylic DEAs

Acrylic DEAs were sterilized with Pen Strep and washed with PBS. With PBS still inside the compartment, the actuators were put under UV light in the sterile cell culture hood for 40 minutes in order for a second sterilization step to take place which also provided slight hydrophilization of the surface. To plasma treat the compartments would have lead to a stiffening and cracking of the PDMS membrane which, in turn, would have caused a short circuit in the membrane. After the UV treatment, the PDMS surface of the DEAs was functionalized with either PLL or fibronectin, dependent on the application,

for 20 minutes. 2 ml of GM was put into each DEA and they were subsequently put in the incubator to heat up to physiological pH. C2C12 myoblasts were seeded according to the protocol in Chapter 3.2.1 at densities dependent on the application.

myoblasts on single cell stretcher models

Electrodes were implanted into PDMS (Sylgard 186) membranes by gold ion sputtering. The membranes were attached on a PDMS (Sylgard 184) piece with oxygen plasma. This part was done in the Microsystems For Space Technologies Lab, EPFL, Neuchâtel by Dr. Samuel Rochet. The PDMS piece had holes ($100\ \mu\text{m} \times 200\ \mu\text{m}$) created by replica moulding according to Chapter 7.1.2.

Samples were cleaned with Pen Strep and washed 2 times with PBS. In order to functionalize the membrane, pure FBS was added for 3 hours and afterwards aspirated to be replaced with GM. The samples were put into the incubator to heat up to physiological temperatures. C2C12 myoblasts were seeded according to Chapter 3.2.1 at a density of $2000\ \text{cells}/\text{cm}^2$. Pictures were taken after two days in culture.

7.2 Design and Performance of DEA Cell Stretchers

7.2.1 characterizaton of acrylic DEA

strain response to input voltage

Before the DEAs were used, their strain response to input voltage was tested in dry conditions. Figure 7.2 shows a graph summarizing the strain output from 20 individual actuators. The error bars display ± 1 standard deviation. There were individual differences, but the trend of the graph is clear. From 0 kV to 2.7 kV the strain response had a nonlinear behavior from 0 to 4% strain, but from 2.7 kV to 4 kV it appeared linear (4%-15% strain). After one night of stretch in wet conditions in the incubator the strain decreased to around 1% at 4 kV for all actuators.

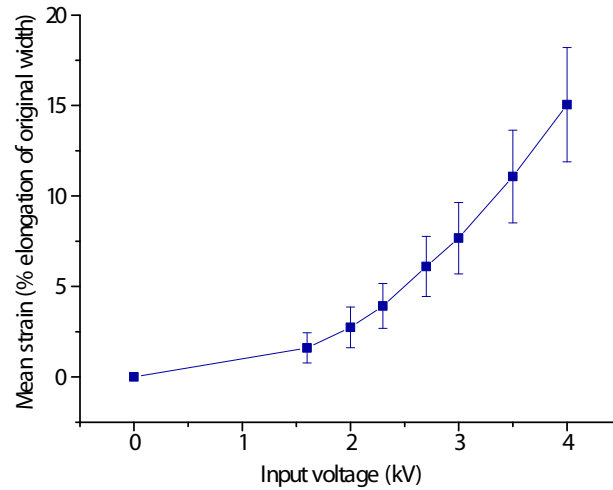


Figure 7.2: DEA strain output as a response to voltage input. Mean strain values (% elongation of original electrode width) are displayed. Error bars show ± 1 standard deviation. $n=20$

electric field at the cell culture surface

Figure 7.3 shows a schematic picture of the electric field distribution in the DEA designed as displayed in Figure 7.1(b). The active electrode is surrounded by two slightly larger grounded electrodes, one on top and one the bottom. This design traps the electric field between the grounded electrodes as in Faraday's cage. This implies that the cells on top should experience close to zero electric field.

The potential in a typical actuator was measured at a distance of $2.5 \mu\text{m}$ above the PDMS surface in dry conditions with Kelvin force microscopy (KFM) by Raoul Enning in the Nanotechnology group, department of mechanical engineering, ETH Zurich. For a DEA with an active electrode sandwiched between two grounded electrodes (Figure 7.1(b)) a potential of 400 mV was measured as a response to 3.5 kV input voltage. In comparison, a two-electrode model with the active electrode on top had a potential of 1 kV close to the PDMS surface as a response to 1.5 kV input voltage. With ionic cell culture medium in the compartment, ions will - in theory - arrange in such a way that an electric field of the magnitude 400 mV should cancel out.

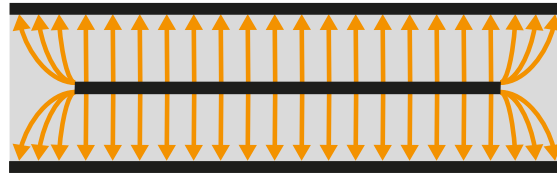


Figure 7.3: Overview of the electric field distribution with the working electrode sandwiched between two grounded electrodes. This distribution is generated by the design showed in Figure 7.1(b). The electric field is trapped by the grounded electrodes with the same principle as Faraday's cage. With this design, the cells are expected to experience no, or a very small, electric field. This design was developed in the Nanotechnology group, department of mechanical and process engineering, ETH Zurich

7.2.2 myoblast behaviour when subjected to stretch in acrylic DEA

In order to create stretch induced myoblast alignment, the PDMS surface of acrylic DEAs were functionalized with $0.05 \mu\text{g/ml}$ fibronectin, put only on top of the electrode area, that is the stretching area, in order to make cells preferentially grow there. Myoblasts were plated at a density of 6000 cells/cm^2 according to the protocol in Chapter 7.1.3. The cells were left to adhere for 3.5 hours and afterwards a 0.05 Hz cyclic stretch was applied at 3.5 kV which corresponded to a strain of 15%. Initial survival outside the carbon black electrode was poor in comparison with on top of the electrode. After 4 days in culture the entire actuator surfaces were covered with cells that had migrated out from the electrode area. Figure 7.4(a) shows alignment of myoblasts after one day of stretch. At this time point the strain was down to 1%. The cells have oriented their major axis perpendicular to the stretch direction. Possibly in order to achieve as little disturbance as possible from the stretching substrate.

The beginning of detachment of a myoblast cell sheet was observed in the same samples after 4 days of stretching, Figure 7.4(b). What we can see is a sheet that has stopped detaching and cells migrating out to the empty space. It is not clear if this detachment was induced by stretch or by spontaneous detachment due to low cell-substrate adhesion and strong cell-cell connections. The detachment started at the edges of the compartment, outside of the stretching area, where there are practically no disturbances. But we cannot exclude that the stretch may have played a role since it adds movements to the center of the confluent cell sheet. This can be compared to spontaneous detachment in acrylic DEAs which we induced by functionalizing the entire PDMS surface with PLL, a polymer to which cells adhere weakly. Cells were seeded at a density of $150000 \text{ cells/cm}^2$. After two hours in the incubator the cell sheet detached spontaneously.

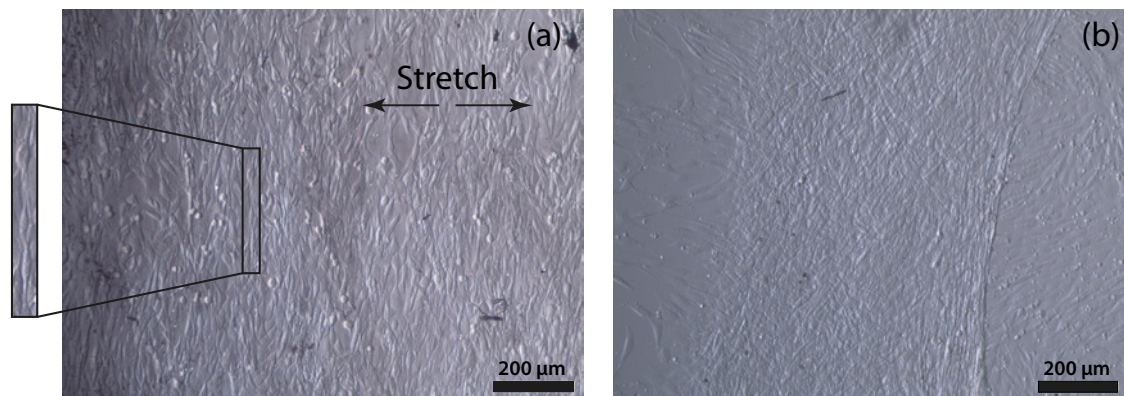


Figure 7.4: Alignment of myoblasts after one night of stretch in the EAP actuator, (a). The cells have oriented their major axis perpendicular to the stretch direction. Possibly in order to achieve as little disturbance as possible from the stretching substrate. (b) shows the beginning of the detachment of a cell sheet.

In the work with the acrylic DEA, it became clear that there were a few characteristics that needed to be optimized in order to have a reliable cell stretcher. Long term cell culture tests showed that myotubes didn't form in these stretchers. The cells would preferentially adhere to the electrode area even if the functionalization of the PDMS surface was homogeneous. The stretch amplitude was hard to control due to stretch loss with time and individual behaviors of DEAs. An additional problem that frequently appeared was that the membrane would rip up from the bottom, possibly because of a local weakness and stress due to the pre-stretch of the membrane.

7.2.3 Single Cell Stretcher

construction of single cell stretcher

The creation of the single cell stretcher was done in collaboration with the Microsystems For Space Technologies Lab, EPFL, Neuchâtel. This lab has developed a technique for patterning electrodes with ion implantation in PDMS. Showing excellent conductivity properties during stretch, these electrodes perform very well in DEAs, see Chapter 1.2.2.

The basic idea of the single cell stretcher is to create a surface that is compatible for cell growth and with several stretching areas, each of the size of one cell, distributed over the surface. In between these areas, the surface should be static. Patterning ECM proteins on chosen spots and isolating these spots by surrounding them with a non-fouling polymer, such as PLL-g-PEG, should trap single cells to stay on a particular spot, may it be a stretching or non-stretching one.

Figure 7.5 shows the theoretical design of the single cell stretcher (not to scale). The upper picture is a drawing of a cross section. On top are two stacked PDMS membranes. The lower one of these two has a gold electrode implanted on the bottom. This electrode is active and patterned in stripes. The PDMS membrane on top has also a gold electrode implanted underneath. This electrode is grounded and covers the entire surface area. The thick blue area is solid PDMS which will not be affected by the force ranges exerted by the stretching squares in the membrane. The white squares show the cross section of two grooves. The part of the membrane suspended over these grooves will be free to stretch. On the very bottom there is another grounded electrode which can be made of any convenient material since it will not stretch. This electrode should also cover the entire area. This way the active electrode is sandwiched between two grounded ones and, therefore, the electric field at the level of the cells will be minimal. The top view shows the stretch direction of the areas where a patterned electrode crosses the grooves. Only cells growing exactly on these areas will experience stretch.

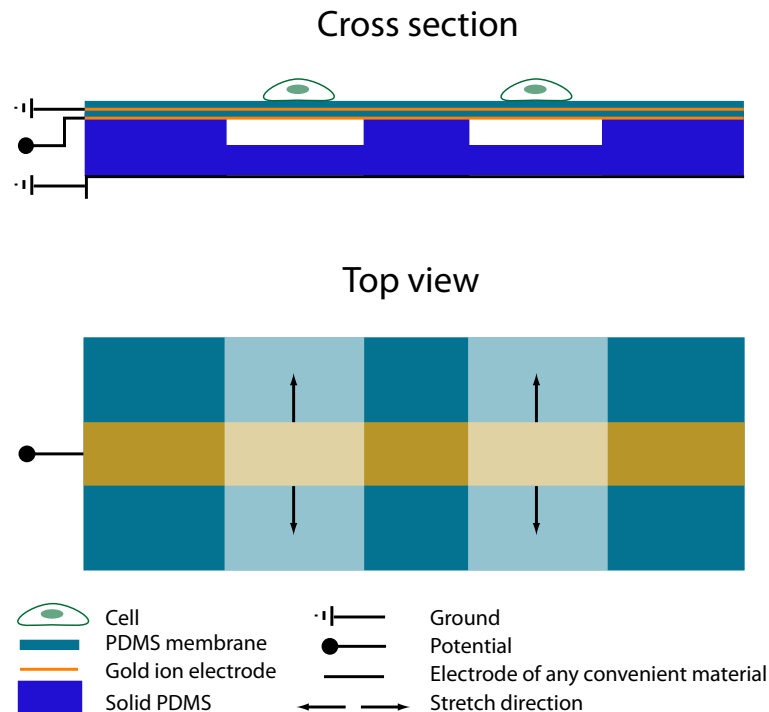


Figure 7.5: Schematic drawing of the design of the single cell stretcher. Only cells grown on top of the area where grooves and active electrodes meet will be subjected to stretch.

Figure 7.6 shows a prototype of the single cell stretcher assembled by Samin Akbari, Microsystems For Space Technologies Lab, EPFL, Neuchâtel. In Figure 7.6(a) we see an explanatory drawing of the two samples displayed in Figure 7.6(b) and in Figure 7.6(c). The gold contacts can be individually connected which allows for different stretch paradigms at different areas of the membrane. In Figure 7.6(c) the actuator also has a covering sheet of gold implanted on top. The PDMS membranes with implanted electrodes were made of PDMS Sylgard 186 while the replica molded bulk with grooves was made of PDMS Sylgard 184.

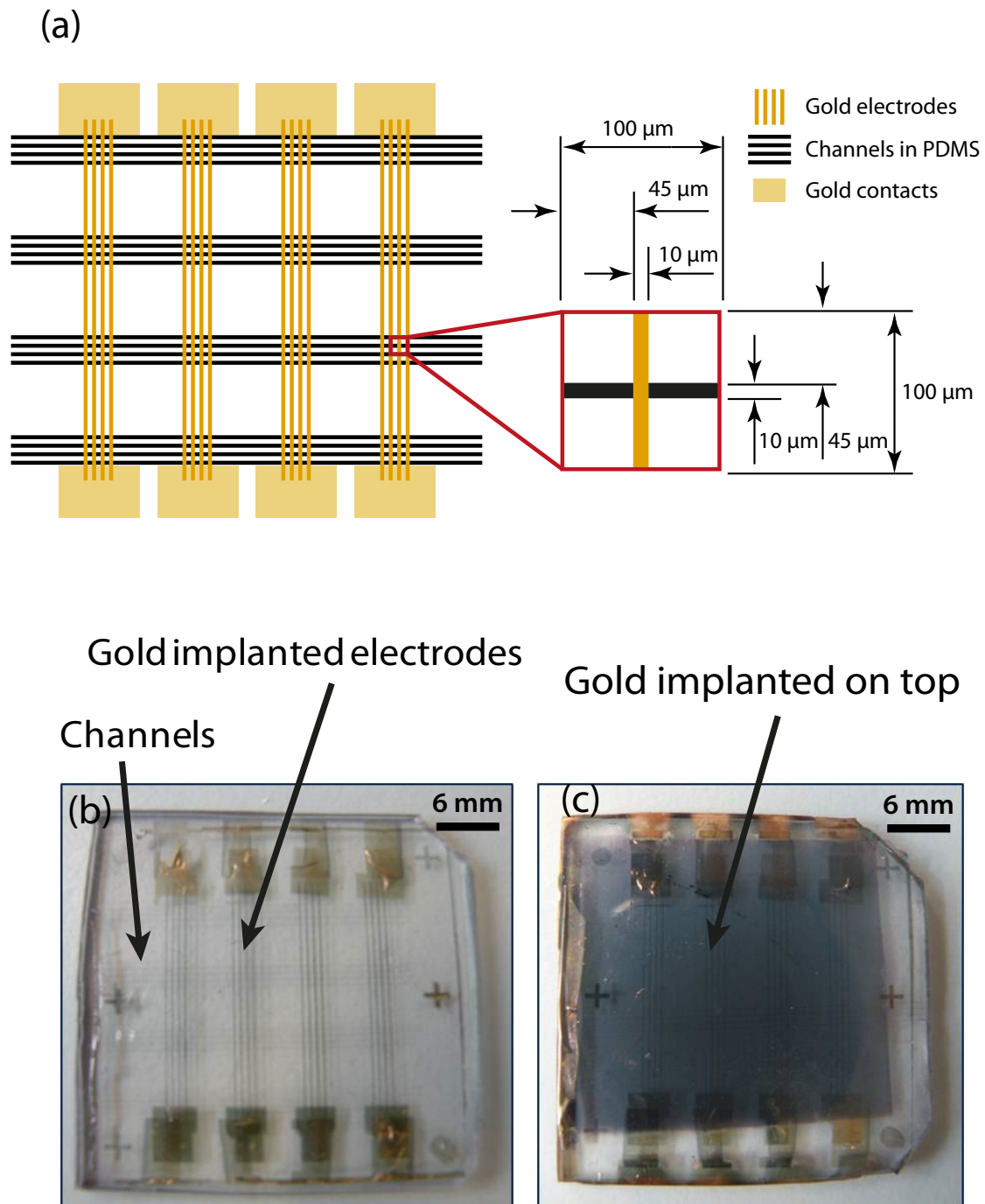


Figure 7.6: This figure shows a prototype of the single cell stretcher. (a) shows an explanatory drawing of the two samples displayed in (b) and in (c). The gold contacts can be individually connected which allows for different stretch paradigms at different areas of the membrane. In (c) the actuator also has a covering sheet of gold implanted on top. The design and construction of this prototype were done in the Microsystems For Space Technologies Lab, EPFL, Neuchâtel

Figure 7.7 shows a micrograph of the prototype of the single cell stretcher in action in dry conditions. It is clear that a deformation of the membrane takes place only at the cross section of the channels and the patterned lines of gold electrodes. When the prototype was tested in wet conditions, problems with electrical break downs occurred, most probably due to cracks in the PDMS membrane that allowed ionic solution to enter.

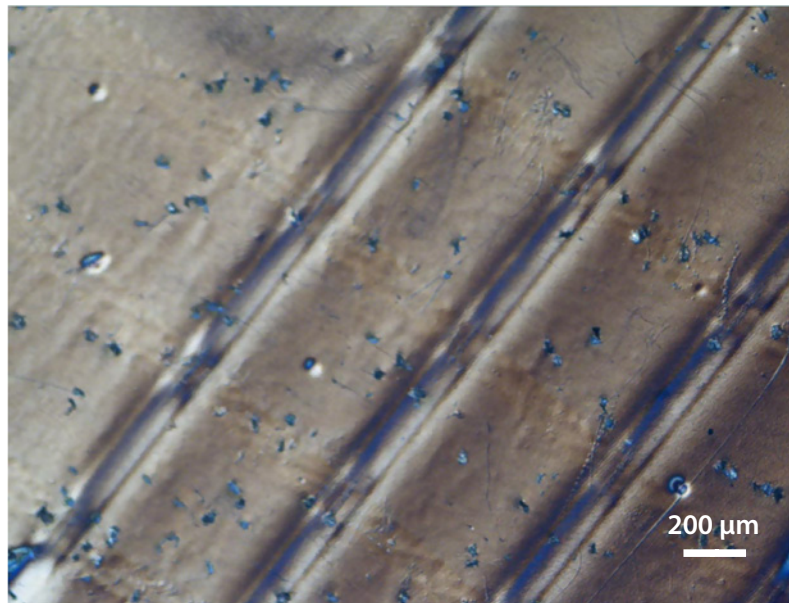


Figure 7.7: A prototype of the single cell stretcher in action. Where the gold electrodes cross the grooves, stretch occurs. The prototype was constructed in the Microsystems For Space Technologies Lab, EPFL, Neuchâtel

myoblasts on single cell stretcher models

In order to test the biocompatibility of the single cell stretcher, a simple prototype was produced. Figure 7.8 shows a PDMS membrane (Sylgard 186) with gold implanted electrodes on top, adhered to PDMS (Sylgard 184) with replica molded holes. The myoblasts preferentially grow on top of the electrodes, showing that even in the case of exposed gold, the stretcher does not exhibit cytotoxicity. The reason why cells prefer the gold is most probably because it is hydrophilic and also slightly stiffer. The cells also grow on top of the membrane suspended over holes, which shows that they should not experience adhesion problems on the stretching areas.

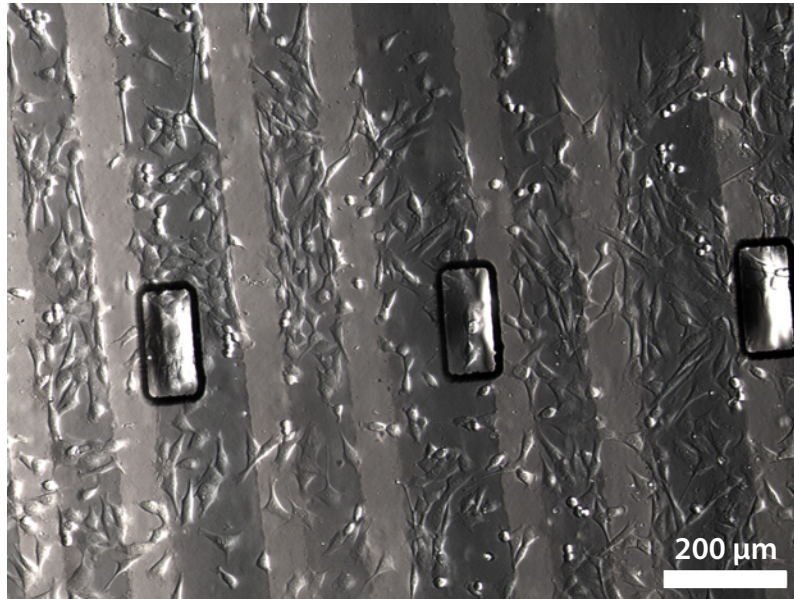


Figure 7.8: C2C12 myoblasts grown on a Sylgard 186 membrane with implanted gold electrodes. The PDMS membrane is suspended over holes. The myoblasts preferentially grow on top of the electrodes, showing that even in the case of exposed gold, the stretcher does not exhibit cytotoxicity. The cells also grow on top of the membrane suspended over holes, which shows that they should not experience adhesion problems on the stretching areas.

7.2.4 advantages and disadvantages of DEAs

To use actuation of dielectric elastomers as a platform to stretch cells is a new concept. The idea is brilliant. The system is highly tunable in terms of stretching paradigms and stretching areas. The stretching is in-plane and exact, and reproducible in dry conditions. Additionally, PDMS is a biocompatible elastomer that allows for cell growth and can easily be spin coated on top of any other DE used for actuation. As our results show for the acrylic DE, we had good cell growth on top of the stretching electrode. We achieved alignment by stretching and partial cell sheet detachment.

A closer look at the alignment causes confusion though. There is an electric field of 400 mV with a certain directionality present at the cell surface in dry conditions. According to previous findings, cells align guided by the direction of an electric field in a calcium dependent manner [150]. We cannot exclude that the 400 mV measured at the cell surface does not additionally guide the cells to align, although with an ionic solution on top, this field should be very close to 0. Anyway, the stretch plays a crucial role too. We saw in the STREX (data not shown) that alignment occurred as a response to stretch. However, for experiments aiming at revealing Ca^{2+} dependent behavior as a response to stretch, the possible influence of an electric field becomes problematic.

In dry air and at macroscopic scales, the acrylic DE has proved to stretch with precision and reproducibly. In wet conditions however, the scenario turned out to be different. Adding an ionic liquid solution on top of the polymers and putting the entire device in a warm, humidified incubator created two problems that had not been seen before: The strain amplitude decreased from 20% to less than 1% over night, and in more than 50% of the cases the stretching membrane started to rip up from the bottom. Additionally, preferential cell adhesion on top of the electrode and not on the sides showed that the surface properties were not homogeneous, although intended to be so. Finally and most unexpectedly, myotube formation was never observed in these stretchers. Trials were made to figure out what inhibited the fusion. By adding the materials used in for the actuator one by one in petri dishes with cells, we were hoping to find the problematic material. Carbon black for instance has been reported to alter material properties and cell behavior [389–394]. No single piece of material involved in the fabrication of the actuators affected the myotube formation in the tests. It could be that a combination of materials was responsible. It was time, however, to move on to a different solution.

Changing the material became a natural step in the process of improving the stretcher and the choice fell upon PDMS. PDMS does not only allow for cell growth, it also has a stronger resistance against humidity and temperature as described in Chapter 1.2.2. The Microsystems For Space Technologies Lab, EPFL, Neuchâtel, has developed a refined method for patterning electrodes on PDMS with ion implantation. We decided to use this patterning possibility for something new and designed a single cell stretcher. The single cell stretcher was constructed by them and functioned well in dry conditions. It has been further developed since then [395–397], but the adaptation for wet conditions still remains.

7.3 Chapter Conclusions

The aim of the work presented here was to create cell stretchers based on actuation of DEs. DEs are materials that deform upon applying a voltage over two sandwiching electrodes. They have been used in so called artificial muscle (not to be confused with the biological tissue) and their in-plane stretching as well as their tunable stretching area offered an opportunity to use them for cell stretching.

The Nanotechnology group, Department of Mechanical and Process Engineering, ETH Zurich started the project of designing and constructing a DEA, based on an acrylic

polymer. The area on top of the electrode constituted the active stretching area. Due to the pre-stretch of the material, no buckling occurred and the stretching was in-plane. The strain response to input signal ranged from 0 to 15% on average for input voltages from 0 to 4 kV. Despite of the high input voltage, thanks to the design mimicking a Faraday's cage, only 400 mV was measured close to the surface in dry conditions. With an ionic solution on top, that field should be neutralized by ion arrangement.

Myoblasts were able to adhere and proliferate on top of these actuators. They appeared to have a preference towards growing on the electrode. We explain this effect by the fact that the area on top of the electrode was slightly stiffer than the surrounding surface area. We observed alignment and partial detachment of a myoblast cell sheet in these actuators upon stretch over night. However, as we may have a small electric field at the cell surface, the alignment may have been an effect of both electric and mechanic stimulation. The acrylic DEA presented a few problems: no myotube formation, inhomogeneous surface functionalization, stretch loss with time, different response in different stretchers and ripping up from the bottom. This motivated us to change material to a silicone based elastomer.

A single cell stretcher was designed with several stretching areas in one actuator. Each area of a proper size for one cell. The material was PDMS and the electrodes consisted of metal ions implanted into the PDMS surface. The construction was done in the Microsystems For Space Technologies Lab, EPFL, Neuchâtel. Preliminary results showed that cell could grow on the stretcher. Actuation, however has only been achieved in dry conditions. The adaptation for wet conditions is yet to be done.

Myoblast Cell Sheet Engineering Using Ion-induced dissolution of Polyelectrolyte Multilayers¹

Cell sheet engineering is an emerging technology which has proved to be very successful in clinical trials. Instead of using a scaffold to construct a 3D tissue, a sheet of cells is harvested and used as it is, or stacked with more cell sheets to create more advanced constructs. The core technology of cell sheet engineering is the harvesting platform which should provide cell attachment and growth in the first stages and later cell sheet detachment. Up to date, the most used platform is the polymer poly(N-isopropylacrylamide) (PNIPAAm), see Chapter 1.3. Polyelectrolyte multilayers (PEMs), with their tunable mechanical and chemical properties, have proven, however, to also constitute a useful platform for cell sheet engineering.

Clinical trials have shown that myoblast cell sheets can heal cardiomyopathy [293–298]. This encourages further development of platforms that can produce myoblast cell sheets. In this work we have, for the first time, used the dissolution of PEMs with hexacyanoferrat(II) (FC) for the purpose of cell sheet engineering. FC is an FDA approved agent that you can find in your daily salt. Addition of FC to a PEM system built up from alternate deposition of hyaluronic acid (HA) and Poly(L-lysine) (PLL), will cause dissolution. The PLL has a higher affinity to FC than to the polyanions. Thereby less PLL is available in the multilayer, hence the ratio PLL/HA changes and dissolution starts within the first minute.

¹Parts of this chapter was published in *Biomaterials* as R. Zahn, E. Thomasson, O. Guillaume-Gentil, J. Vörös and T. Zambelli, Ion-induced cell sheet detachment from standard cell culture surfaces coated with polyelectrolytes. Reprinted with permission from *Biomaterials* 33 (2012) 3421-3427. Copyright 2012 American Chemical Society.

8.1 Construction of a PEM Platform for Cell Sheet Engineering

8.1.1 PEM assembly and fibronectin adsorption

Glass slides were cleaned by 15 minutes sonication in isopropanol (Sigma-Aldrich) followed by another 15 minutes sonication in ultrapure water. The glass slides were subsequently rinsed in ultrapure water, blow-dried under a stream of nitrogen and oxygen plasma cleaned for 2 minutes. Cell culture dishes (Iwaki) were already cleaned and sterilized by the company and therefore no further cleaning procedures were performed except for 2 minutes of oxygen plasma cleaning.

PEI-(HA/PLL)₁₀ was built-up on both glass slides and cell culture dishes by using a custom-made spraying system based on the Lego Mindstorms NXT robotic kit (LEGO Group). This spraying system has been previously described by Guillaume-Gentil *et al.* [322]. Each layer, starting with PEI, was adsorbed by spraying polymer solution for 5 s, incubating for 15 s and finally rinsing away of the remaining polymer solution by spraying HEPES 2 buffer for 15 s. The spraying system alternated between HA and PLL until 10 double layers had been assembled. The PEI-(HA/PLL)₁₀ multilayers were crosslinked for 12 hours at 4 °C in an EDC/NHS solution (400 mM N-(3 dimethylaminopropyl)-N0-ethylcarbodiimide hydrochloride (Sigma-Aldrich) and 100 mM and N-hydrosulfosuccinimide in HEPES 2 buffer (Sigma-Aldrich)). A similar procedure has previously been described by Richert *et al.* [316].

After the crosslinking step, a second block of native (HA/PLL)_n (n=0,2,3 and 5) was adsorbed on top. Each layer was deposited by immersing the substrate in a polymer solution for 5 minutes and afterwards rinsing three times with HEPES 2 buffer. By alternating polyanions and polycations, the native PEM block was built up to the requested amount of double layers. Prior to cell seeding, the native PEM block was coated with fibronectin from bovine plasma (Sigma-Aldrich) (50 µg/ml in HEPES 2 buffer) for 45 minutes at room temperature. Afterwards, the substrates were sterilized for 30 minutes in 1000 units/ml of streptomycin.

8.1.2 cell culture and cell sheet harvesting

Sterilized PEM substrates were washed once with GM and put into the incubator with GM inside in order to stabilize pH and temperature. GM was removed from the PEM substrate and C2C12 myoblasts were seeded on top at a density of 200000 cells/cm² in GM and left in the incubator for 2 days. During this time, the development of the cell sheet was observed with a phase-contrast microscope once per day. Figure 8.1(a) shows a schematic picture of the PEM build-up with fibronectin adsorbed and cells on top. The grey area on the bottom is the solid substrate, in this case glass or polystyrene. The blue area with white crosses represents the crosslinked block while the light blue line on top is the native PEM block. The green irregular structure represents the final layer of fibronectin and the orange squares represent cells.

After two days of incubation time, the cell sheets were subjected to 5 mM FC and followed live using a phase-contrast microscope. Figure 8.1(b) shows the schematic design of FC (marked as black dots) dissolving the native PEM block and thereby forcing a release of an intact cell sheet.

8.1.3 viability test

A live dead cell viability assay was performed according to the protocol provided by the supplier. The stained cell sheet was immediately imaged with CLSM. Filter settings to image calcein (excitation 494 and emission 517 nm) and Ethidium homodimer-1 (excitation 528 and emission 617 nm) were used in two separate channels respectively. Calcein AM, green, is enzymatically converted by esterase activity in live cells to emit fluorescent light. Ethidium homodimer-1, red, only enters physically ruptured cell membranes, a property of dead cells. Its fluorescent activity is enhanced by binding to nucleic acids, making it detectable only inside dead cells.

8.1.4 reattachment of the harvested cell sheet

Reattachment of the harvested cell sheet was performed by moving the sheet to a new cell culture dish with fresh GM. The cell sheet was carefully unfolded with two pairs of tweezers and, while keeping the sheet in an unfolded state, all GM but a thin layer was removed in order not to let the cell sheet dry out. Thereby the unfolded cell sheet was

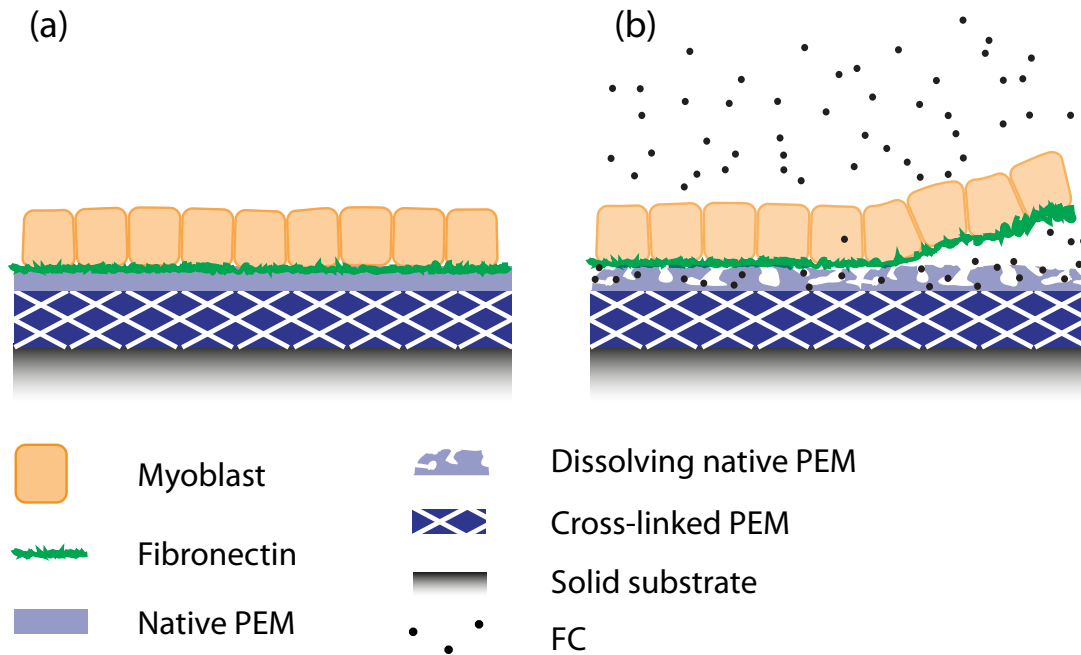


Figure 8.1: (a) shows a schematic picture of the PEM build-up with fibronectin adsorbed and cells on top. The grey area on the bottom is the solid substrate, in this case glass or polystyrene. The blue area with white crosses represents the crosslinked block while the light blue line on top is the native PEM block. The green irregular structure represents the final layer of fibronectin and the orange squares cells. (b) shows the schematic design FC (marked as black dots) dissolving the native PEM block and thereby forcing the release of an intact cell sheet.

forced to stick to the bottom of the dish. The sample was put in the incubator for 5 minutes to allow for adhesion. Afterwards, the dish was filled with GM and the sheet was left over night to grow. The day after, pictures were taken with a phase contrast microscope.

8.1.5 QCM setup

QCX 301 gold crystals (Q-Sense AB) were cleaned by immersion in a 2% (w/w) sodium dodecyl sulfate (Sigma-Aldrich) solution for 30 minutes. The crystals were further rinsed in ultrapure water, dried under a stream of nitrogen gas and finally UV/ozone cleaned for 30 minutes. The QCM-D experiment was performed at 25 °C and injected solution (0.5 ml) already temperature equilibrated. The gold crystals were mounted in the chambers of the QCM-D and a solution of 50 $\mu\text{g/ml}$ fibronectin was injected. After 45 minutes of adsorption, the flow cells were rinsed with HEPES 2 and left in this buffer for 2 minutes. On top of the fibronectin layer, PLL-(HA/PLL)_n (n=2,5) was built up. The adsorp-

tion step of the polymers lasted 5 minutes and was followed by a 2-minute rinsing step with HEPES 2. After the build-up of the PEMs was achieved, 10 mM FC was injected and left in the flow cell to incubate for 30 minutes. The measurement was completed with a final rinse with HEPES 2 for 2 minutes.

8.2 Harvesting of a Viable Cell Sheet by Dissolution of PEMs

8.2.1 dissolution of (HA/PLL)_n with FC leaves no residues behind

When creating a cell sheet, it is not only desirable that the sheet remains attached to its ECM but also that there are no residues from other materials left. Since we used PEMs as a platform for cell sheet engineering, having no residues is particularly critical. Both HA and PLL turn out to be cytotoxic [398–400]. In order to investigate the dissolution process of PEMs at a molecular level, we assembled an "up-side down" construct in the QCM. For details of the build-up, please see Chapter 8.1.5. Figure 8.2 shows the results of the build-up and the dissolution. The data are mean values of three technical replicas and the error bars display ± 1 standard deviation. Two PEMs of different thickness were used, $n=2$ (black) and $n=5$ (red striped), to resemble the substrates used for the cell sheet engineering. (A) shows the measured frequency change upon adhesion of a fibronectin monolayer. Upon build-up of the PEMs, the frequency change increased more for the thicker PEM, which was expected, (B). (C) displays the frequency measured after adding FC and rinsing. Comparing the frequency differentials in (A) and (C), we see exactly the same number (-60 Hz). This brought us to two important observations: Firstly, the fibronectin monolayer stays at the surface and, secondly, the PEMs are dissolved completely. We can conclude that the FC treatment breaks the bonds between fibronectin and PEMs, does not affect the fibronectin monolayer and dissolves the PEMs completely so that no residues are left behind. The dissolution of the PEMs was also fast. The FC was left in the flow cell for 30 minutes but according to the QCM output (data not shown) the dissolution of the PEMs was complete already after 2 minutes.

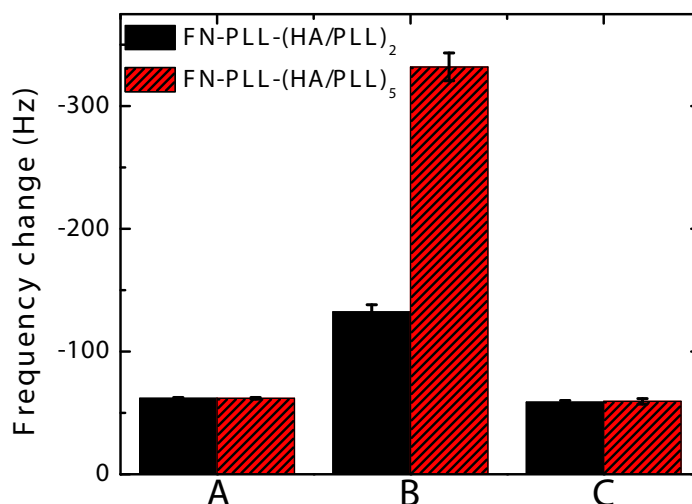


Figure 8.2: This figure shows the QCM measurements during build-up and dissolution of FN-PLL-(HA/PLL)_n, n=2,5. The data are mean values of three technical replicas and the error bars display ± 1 standard deviation. (A) shows the measured frequency change upon adhesion of a fibronectin monolayer. Upon build-up of the PEMs the frequency change increased more for the thicker PEM, which was expected, (B). (C) displays the frequency measured after adding FC and rinsing.

8.2.2 detachment of myoblast cell sheet by dissolution of PEMs

Glass substrates and polystyrene dishes were coated with a crosslinked block of PEI-(HA/PLL)₁₀, several layers of native HA/PLL and finally with a monolayer of fibronectin and C2C12 myoblasts were seeded at a density of 200000 cells/cm² according to the description in Chapter 8.1.1. Myoblasts adhered and grew well on constructs with native PEMs, made up of 0, 2 and 3 HA/PLL layers. For n=5 the adhesion was impaired and no intact sheet was formed. Cells in general adhere better to stiff substrates. The softer the substrate, the more rounded the shape turns out [308], which was observed for n=5.

The cell sheets were subjected to 5 mM FC diluted in GM on day 2 of culture. For n=0, no attachment was observed. This shows that a crosslinked PEM block is not affected by addition of FC. For n=2,3 and 5, however, full detachment was observed within 2-5 minutes. No cells were left behind, which means that no holes were created in the sheet. Visual inspection confirmed that the sheet didn't tear but that the cell-cell contacts remained intact. Figure 8.3 shows the detachment of a myoblast cell sheet upon being

subjected to 5 mM FC. The substrate (polystyrene) was coated with PEI-(HA/PLL)₁₀-xlink-(HA/PLL)₂-FN. The time indicated in the upper left corner of each picture in the panel denotes the time elapsed since addition of FC. The sheet starts to come off at the edges of the dish and folds into the middle. Although FDA approved, FC was added overnight to a confluent layer of myoblasts on tissue culture polystyrene without coating to test the viability of the cells. The cells were trypsinized and viability measured with a trypan blue assay in the cell countess. The viability was above 90% which is the same as the viabilities seen in confluent myoblast monolayers without FC treatment (data not shown). The growth and detachment of the myoblast monolayer did not seem to be affected at all by the choice of underlying substrate. Glass and polystyrene gave the same results.

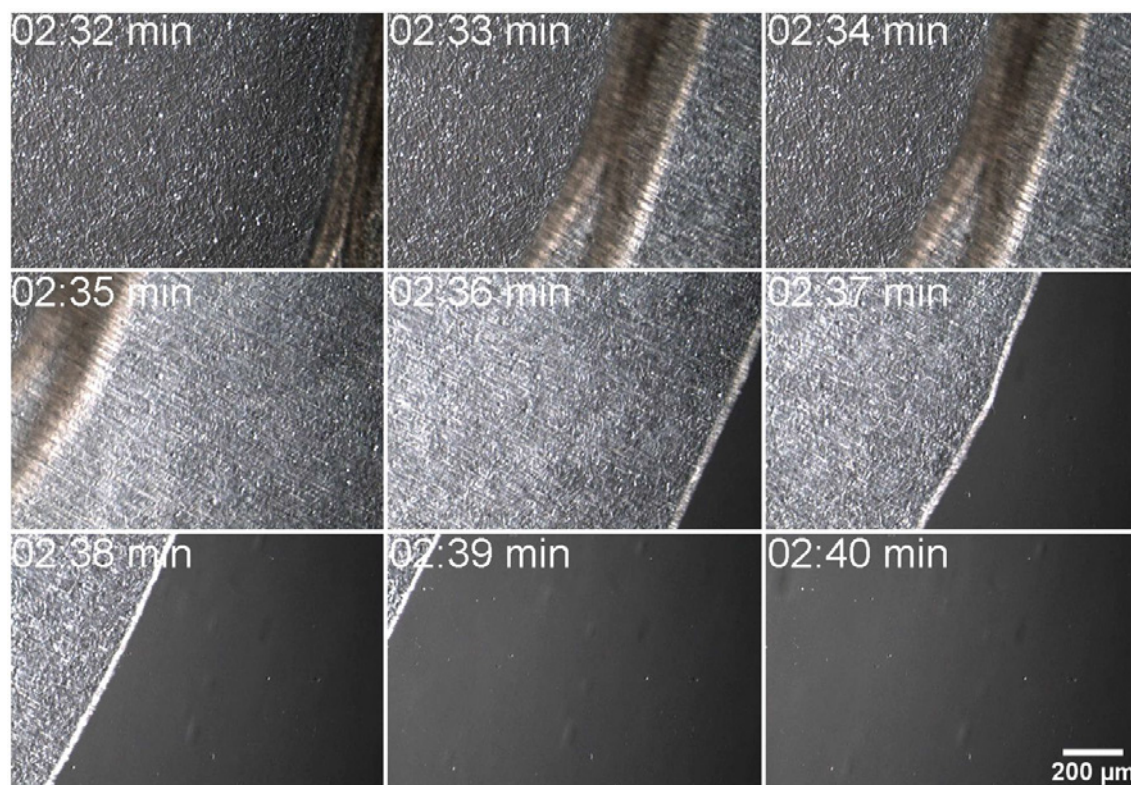


Figure 8.3: This figure shows the detachment of a myoblast cell sheet upon being subjected to 5 mM FC. The substrate (polystyrene) was coated with PEI-(HA/PLL)₁₀-xlink-(HA/PLL)₂-FN. The time indicated in the upper left corner of each picture in the panel denotes the time elapsed since addition of FC. The sheet starts to come off at the edges of the dish and folds into the middle.

8.2.3 myoblast migration and differentiation in a reattached cell sheet

The detached myoblast cell sheet shrank to roughly 1/10 of its original size. This can be seen in Figure 8.4(a) where the sheet, before detachment, spanned all the way to the edge of a dish with the same size. This shrinkage was caused by intracellular contraction forces generated by the cytoskeletons of the cells in the sheet. Figure 8.4(a) shows the reattachment of a harvested myoblast cell sheet only 10 minutes after reattachment. However, the sheet adhered already after 5 minutes on the dish. After 1 day of culture, it was observed that myoblasts had started to migrate out of the sheet onto the empty TCPS, Figure 8.4(b). Indeed the limited space in the shrunk cell sheet was not physiological and the cells migrated in a direction where they could find more space. Figure 8.4(c) shows a reattached cell sheet after 2 days in culture. Nascent myotubes are visible (encircled) which would have been too early, had these cells been cultured under normal conditions, especially given the fact that GM and not DM was used. The cell-cell contacts obviously inhibited the cell cycle and pushed the myoblasts into differentiation. As a comparison, no myotubes were seen in the middle of the cell sheet which indicates that an area with less space constrains is favourable for myoblast fusion.

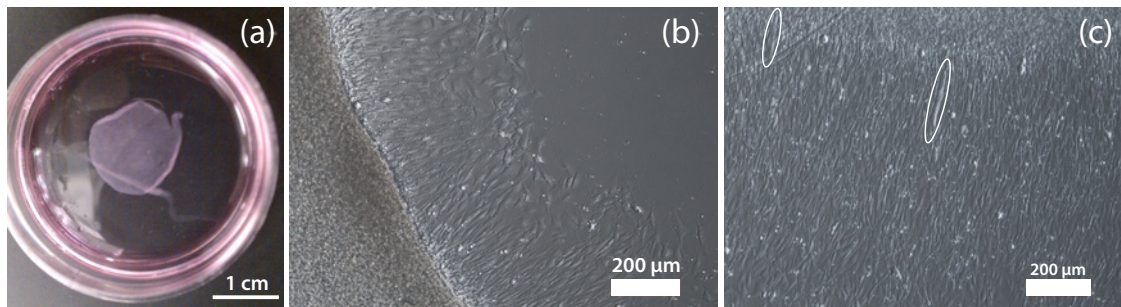


Figure 8.4: This figure shows reattachment of a harvested myoblast cell sheet (a), migration of myoblasts from a reattached cell sheet after one day of culture (b) and nascent myotube formation in the area outside the sheet after two days of culture (c).

8.2.4 viability of the harvested cell sheet

A live dead cell viability assay was performed on a newly detached myoblast cell sheet. Figure 8.5 shows the result. The sheet had mainly alive cells (green) with only a few dead cells (red) visible as single isolated spots. This shows that the cell sheet was perfectly healthy directly after harvesting.

The migration of myoblasts out from the cell sheet (Figure 8.4) indicates that the sheet is alive also after reattachment. A live dead cell staining assay was performed on a reattached cell sheet after three days (data not shown) and the survival was good in the middle of the sheet where the myoblasts were constrained to a small space.

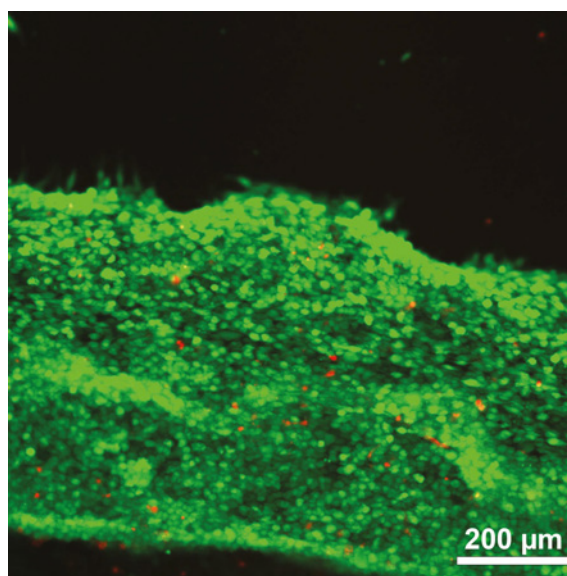


Figure 8.5: A live dead cell viability assay was performed on a newly detached myoblast cell sheet. The sheet had mainly alive cells (green) with only a few dead cells (red) visible as single isolated spots. This shows that the cell sheet was perfectly healthy directly after harvesting.

8.2.5 why does it work?

In cell sheet engineering, the critical point is to design a substrate that allows for cell attachment and growth in the initial stages and that later induces cell sheet detachment, preferably on demand. Up until now, the design of this platform has included polymers that undergo some sort of conformational changes upon altering of the environment. In the case of temperature responsive polymers, the individual molecules reshape to extended brushes due to the hydrophilization of side groups as a response to a lowering of the temperature. In the case of electrochemical dissolution of PEMs, the entire construct dissolves as a response to a pH change induced by the potential.

In this work we have presented an alternative method to dissolve PEMs on demand, for cell sheet engineering. We built up a construct consisting of two blocks of PEMs. The lower block was cross-linked, and the upper consisted of native PEMs. Native PEMs assembled on glass, for example, tend to form droplets up until a certain amount of layers

have been deposited, when the droplets coalesce into a continuous film. The critical number of layers for this event vary depending on the setup [401, 402]. However, the more layers deposited, the softer the surface becomes. For our system (HA/PLL), the PEMs provided a surface that was already too soft for cell attachment before a continuous film had been achieved. As cell attachment on the underlying glass was not desirable, a continuous film was necessary. Hence, the two-block system. Cross-linked PEMs have a higher Young's modulus than native PEMs, and it is more than high enough to provide good cell attachment [315, 403]. The native PEM block formed a continuous film on top of the cross-linked block. Only 2 deposited layers were enough to induce cell sheet detachment by chemical dissolution. With such few layers, the stiffness of the substrate is high enough to allow for cell adhesion and growth.

As mentioned in the beginning of this chapter, FC dissolves certain PEM constructs through interaction with the cations. In our case, PLL had higher affinity to the FC than to the anions (HA). When interacting with the FC, less PLL became available for the anion interaction. Through depletion of the cations, the PEM construct dissolved. Not all PEM constructs dissolve upon exposure to FC, it depends on the type of anion present. For example for poly(glutamic acid) (PGA) the dissolution is only partial. Cross-linked PEMs don't dissolve at all.

The mechanics of the detachment of a cell sheet were better understood when the spontaneous detachment platform was developed. By growing cells on a PEM substrate with a stiffness so high that cell adhesion and growth was promoted but still low enough, so that the sheet would detach once formed, the conclusion was drawn that cell sheet detachment takes place once the cell-cell adhesion forces are stronger than the detachment forces of the cell-substrate adhesion cites [308]. We further conclude that the detachment process always starts from the edges. This is not because the PEM starts dissolving there or polymer brushes start extending there, since conformational changes of the polymers take place everywhere at the same time. The sheet starts to detach at the edge because, only there, neighbors are missing on one side. If the attachment sites to the substrate disappear but all sides are fixed through cell-cell contacts, the cell will stay in place. However, if one side is free which is the case at the edge, the cell will start to detach from that side. The next row of cells will now have one side without attached neighbors and thereby also come off. Eventually, the entire sheet will come off by domino effect.

8.3 Chapter Conclusions

In this chapter, we have presented a novel method for harvesting myoblast cell sheets by chemically dissolving PEMs. Our platform consisted of a two-block system. A lower cross-linked PEM block and an upper native PEM block. The native PEMs were coated with fibronectin. This design provided a continuous PEM film on which cell adhesion and growth was possible.

An upside-down build-up of this PEM system in the QCM-D, excluding the cross-linked block, showed that the addition of FC dissolved the PEMs fully, but the fibronectin remained on the surface. This means that the bonds between the fibronectin layer and the PEM layer break upon dissolution. Hence, no PEM residues are left at the cell sheet after detachment, but the ECM remains attached. This is of key importance for the functionality of the cell sheet.

We further showed that addition of FC to the system indeed caused cell sheet detachment. Already for only two bilayers, the substrate attachment was impaired and the sheet detached within 2-5 minutes, upon dissolution. The detached myoblast cell sheet shrank to roughly 1/10 of its original size, due to intracellular contraction forces. This shrunk sheet was reattached in a tissue culture dish. After one day of culture, myoblasts had migrated out from the space constrained sheet to the unpopulated areas of the dish. After two days, nascent myotubes were visible. The contact inhibition provided by the high confluence in the cell sheet pushed the myoblasts into the path of differentiation. As proved already by the fact that cells migrated after reattachment, the sheet was viable after detachment. A viability test showed that, with only a few exceptions, all cells in the sheet were alive directly after harvesting.

We finally conclude that mechanisms behind the success of cell sheet engineering in general and of our system in particular, are both cell and material derived. The detachment of any cell sheet is successful because the cells at the edge lack neighbors in one direction. The dissolution of the native PEM block in our particular setup is successful because PLL has higher affinity to FC than to HA. The cell attachment on a continuous PEM film was achievable because of the property of native PEMs to form a continuous layer instead of droplets on top of cross-linked PEMs. These mechanisms together allowed for successful engineering of a myoblast cell sheet.

Conclusions and Outlook

Our bodies consist of many different organs, specified by their functions and the cell types they are built up from. The loss of an organ can imply everything from minimal changes in life quality to death. Life without a spleen will cause lower resistance to infections and life with one kidney will impair sports performance while life without a liver implies immediate death. As far as skeletal muscle is concerned, the consequences for the body may vary. Loosing functionality in legs and arms changes life significantly while impaired performance of the diaphragm may be fatal. Sarcopenia and muscular dystrophy are two examples of diseases that cause muscle loss and in the latter case early death. In order to combat such disorders, new therapies and technologies to enhance muscle regeneration have to be developed based on a better understanding of muscle development. In this thesis we present research on the development of muscle, myogenesis, from three different perspectives; fundamental, engineering and applied.

The first of the result chapters (Chapter 4) suggests new functions of adherens junctions during myoblast fusion. Three stages of myogenesis were captured with CLSM in fixed and stained cultures. These stages were; 1) first cell-cell contact, 2) fusion and 3) mature myotubes. Live myoblasts were also imaged with a combined AFM CLSM setup. Our findings let us infer that an actin based tubular cytoskeletal support is shared with the two fusing cells through adherens junctions before the fusion pore opens up. Statistical analysis further suggests that fusion is a fast event in comparison with the other stages. We finally proposed a model by which mechanism such a cytoskeletal rearrangement could take place.

Next, we focused on the first of these stages; myoblast-myoblast contact formation (Chapter 5). The profile of the force-time dependence was probed with fluid force mi-

croscopy instantly upon myoblast-myoblast contact. The results suggest that first cell-cell contact is mediated by adhesion proteins that diffuse freely in the cell membranes until they collide and interact with another adhesion protein, in order to contribute to the establishment of the contact. The contact force and dissociation energy both increased linearly with the square root of time at first and then stabilized at a sort of constant value. Figure 9.1 shows the time scales at which major events during myogenesis take place. The time line is based on results from Chapter 4 and Chapter 5.

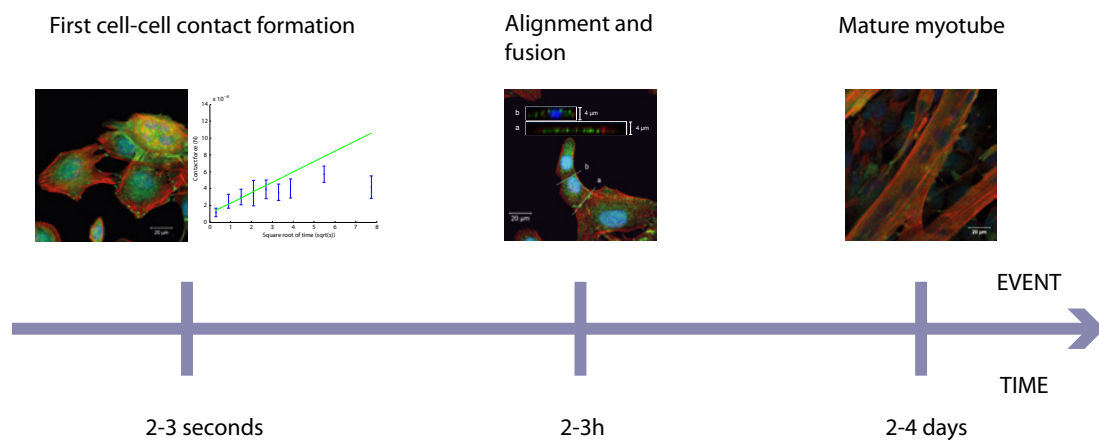


Figure 9.1: The major events during myogenesis take place at different time scales. According to our results in Chapter 4-5 initial cell-cell contacts are established within around 4 seconds after the cells are brought in contact. The alignment and fusion processes require 2-3 hours to finalize. However this process is not necessarily initiated immediately after cell-cell contacts are established. Some cell couples may choose instant alignment and fusion, others can wait up to days. Once a nascent myotube is formed, it grows and reaches size and functionality of a myofiber, or mature myotube, within 2-4 days.

In Chapter 6 we studied mechanotransduction of proliferating myoblasts under stretching conditions. We hypothesized that stretch induced up-regulation of MGF is mediated via calcium influx through stretch activated calcium channels (SACs). We tested this hypothesis by adding SAC blocker, voltage gated calcium channel blocker and intracellular calcium chelator to myoblast cultures subjected to cyclic stretch. We analyzed the gene expression with real-time PCR. The first results indicated a peak in MGF expression for 10 minutes of stretch. However, the peak did not appear in the culture additionally exposed to streptomycin, a SAC blocker. Further investigation of these very promising results showed that there was a large variability in the underlying mechanism due to the low abundance of MGF in the samples.

In order to study cells under stretching conditions, it is a must to have a tool for subjecting the cells to precisely defined mechanical stimuli. In Chapter 6 we presented

two approaches for stretching cells with actuation of DEAs. The first stretcher was based on an acrylic DE and was designed to stretch colonies of cells. Tests showed that myoblasts aligned as a response to stretch. Also partial stretch-induced cell detachment was achieved. The second stretcher used ion implantation of gold particles into PDMS membranes. This fine-tuned technique allowed us to pattern electrodes such, that single cells could be stretched.

Applying the gained knowledge is the eventual goal of all fundamental science. Few applications of knowledge in cell behavior have made as big difference for human health as those of tissue engineering. Within this class of applications, one type has showed outstandingly successful results in clinical trials; cell sheet engineering. In Chapter 8 we showed the results of a new cell sheet engineering platform consisting of a PEM construct. The construct consisted of two blocks; the bottom one had cross-linked PEMs which contributed to mechanical stability, while the top one consisted of native PEMs which dissolved upon addition of FC. The dissolution induced the cell sheet detachment. We could harvest viable myoblast cell sheets. Additional tests showed that our platform did not leave any polymer residues behind on the sheet, but the ECM remained.

The research presented in this thesis implied many challenges. These challenges are summarized in more detail in the result chapters. Some problems we could solve within the given time frame and others we had to leave for future talents to disentangle.

The study of the role of adherens junctions during myoblast fusion would certainly profit from an AFM-CLSM imaging of an entire fusion event in live myoblasts. A great deal of effort and time was invested in capturing time-lapse images of such an event. A co-culture of myoblasts transfected with cytosolic m-Cherry and eGFP respectively was monitored live. However, phototoxicity of the reporter dye in the transfected cells didn't allow for fusion to take place. This could be doable using another dye. Further investigation could include myoblasts expressing fluorescent actin and cadherin. Then it would be established exactly how the adherens junctions move in the cell membranes.

Probing of initial myoblast-myoblast contact with FluidFMTM can be extended to a larger study. By varying temperature and pH of the cell medium a larger picture of the mechanism behind cell-cell contact formation would emerge. The study would certainly profit from a future setup where the stiffness of the tips can be measured individually. Only then, absolute values of the contact forces and dissociation energies can be extracted.

The study of mechanotransduction requires establishment of a number of protocols before proceeding to testing further hypotheses. As mentioned already in Chapter 6, there

is no exact consensus between different research groups on what stretch paradigms we should use to see certain cell behavior. Several reviews summarize the current and past results of cell stretching. However, comparison becomes meaningless in most cases since the cells are not grown under equal conditions. Research of mechanobiology is only in its cradle. Once basic protocols and understanding have been established, we will see a take off of this scientific field.

Stretching cells by electrical actuation of DEAs is an intriguing approach. With a successful device it is very possible that stretching protocols will converge to a few that work reliably. However, before we are there, a couple of problems have to be solved first. The DEs are not allowed to change properties in wet conditions. Electrical breakdowns, ripping of the material and stretch loss are unacceptable consequences of putting these materials in contact with an ionic solution. Additionally, it must be proven that no electric field is present at the cell surface.

Cell sheet engineering by ion dissolution of PEMs turned out to be very successful. Given the homogeneity of the dissolution over the surface, this method could potentially also be used for gentle single cell harvesting, as opposed to the rather aggressive detachment enzymatic activity that, for example, trypsin presents. This method could be developed into stacking sheets for future 3D stretching of myoblasts at different stages of myogenesis.

References

- [1] Vogel, V. and Sheetz, M. Local force and geometry sensing regulate cell functions. *Nature Reviews Molecular Cell Biology*, **7**(4), 265–275, 2006.
- [2] Mullins, R. D. Cytoskeletal Mechanisms for Breaking Cellular Symmetry. *Cold Spring Harbor Perspectives in Biology*, **2**(1), 2010.
- [3] Peyton, S. R., Ghajar, C. M., Khatiwala, C. B. and Putnam, A. J. The emergence of ECM mechanics and cytoskeletal tension as important regulators of cell function. *Cell Biochemistry and Biophysics*, **47**(2), 300–320, 2007.
- [4] Chargé, S. B. P. and Rudnicki, M. A. Cellular and Molecular Regulation of Muscle Regeneration. *Physiological Reviews*, **84**(1), 209–238, 2004.
- [5] Bassel-Duby, R. and Olson, E. N. Signaling Pathways in Skeletal Muscle Remodeling. *Annual Review of Biochemistry*, **75**(1), 19–37, 2006.
- [6] Kee, A. J., Gunning, P. W. and Hardeman, E. C. Diverse roles of the actin cytoskeleton in striated muscle. *Journal of Muscle Research and Cell Motility*, **30**(5-6), 187–197, 2009.
- [7] Bottinelli, R. and Reggiani, C. Human skeletal muscle fibres: molecular and functional diversity. *Progress in Biophysics and Molecular Biology*, **73**(2–4), 195–262, 2000.
- [8] Alberts, B., Bray, D. and Lewis, J. *Molecular Biology of the Cell*. Taylor & Francis, New York, New York, 2002.
- [9] Pollard, T. D., Earnshaw, W. C. and Lippincott-Schwartz, J. *Cell Biology*. Saunders, Suite, Philadelphia, 2007.
- [10] Anderson, J. E. The satellite cell as a companion in skeletal muscle plasticity: currency, conveyance, clue, connector and colander. *Journal of Experimental Biology*, **209**(12), 2276–2292, 2006.
- [11] Grove, B. K. Muscle differentiation and the origin of muscle fiber diversity. *Critical reviews in neurobiology*, **4**(3), 201–234, 1989.
- [12] Abmayr, S. M. and Pavlath, G. K. Myoblast fusion: lessons from flies and mice. *Development*, **139**(4), 641–656, 2012.

- [13] Mauro, A. Satellite Cell of Skeletal Muscle Fibers. *The Journal of Biophysical and Biochemical Cytology*, **9**(2), 493–495, 1961.
- [14] Hawke, T. J. and Garry, D. J. Myogenic satellite cells: physiology to molecular biology. *Journal of Applied Physiology*, **91**(2), 534–551, 2001.
- [15] Luo, D., Renault, V. M. and Rando, T. A. The regulation of Notch signaling in muscle stem cell activation and postnatal myogenesis. *Seminars in Cell & Developmental Biology*, **16**(4-5), 612–622, 2005.
- [16] Chen, J. C. and Goldhamer, D. J. Skeletal muscle stem cells. *Reproductive biology and endocrinology : RB&E*, **1**, 101, 2003.
- [17] Tedesco, F. S., Dellavalle, A., Diaz-Manera, J., Messina, G. and Cossu, G. Repairing skeletal muscle: regenerative potential of skeletal muscle stem cells. *Journal of Clinical Investigation*, **120**(1), 11–19, 2010.
- [18] Muntz, L. Cellular and biochemical aspects of muscle differentiation. *Comparative Biochemistry and Physiology Part B: Comparative Biochemistry*, **97**(2), 215–225, 1990.
- [19] Buckingham, M., Bajard, L., Chang, T., Daubas, P., Hadchouel, J., Meilhac, S., Montarras, D., Rocancourt, D. and Relaix, F. The formation of skeletal muscle: from somite to limb. *Journal of Anatomy*, **202**(1), 59–68, 2003.
- [20] Leonid, V. C., Michael, M. K., Avinoam, O. and Podbilewicz, B. Chapter 9 - Eukaryotic Cell–Cell Fusion Families. In *Current Topics in Membranes*, volume 68, pages 209–234. Academic Press, 2011.
- [21] Inestrosa, N. C. Differentiation of Skeletal Muscle Cells in Culture. *Cell Structure and Function*, **7**(2), 91–109, 1982.
- [22] Curci, R., Battistelli, M., Burattini, S., D’Emilio, A., Ferri, P., Lattanzi, D., Ciuffoli, S., Ambrogini, P., Cuppini, R. and Falcieri, E. Surface and inner cell behaviour along skeletal muscle cell in vitro differentiation. *Micron*, **39**(7), 843–851, 2008.
- [23] Buckingham, M. Myogenic progenitor cells and skeletal myogenesis in vertebrates. *Current Opinion in Genetics & Development*, **16**(5), 525–532, 2006.
- [24] Abmayr, S. M., Balagopalan, L., Galletta, B. J. and Hong, S.-J. Cell and molecular biology of myoblast fusion. In Jeon, K. W., editor, *International Review of Cytology*, volume 225, pages 33–89. Academic Press, 2003.
- [25] Wakelam, M. J. The fusion of myoblasts. *Biochemical Journal*, **228**(1), 1–12, 1985.
- [26] Knoblauch, A., Will, C., Goncharenko, G., Ludwig, S. and Wixler, V. The binding of Mss4 to α -integrin subunits regulates matrix metalloproteinase activation and fibronectin remodeling. *The FASEB Journal*, **21**(2), 497–510, 2007.
- [27] Engler, A. J., Sen, S., Sweeney, H. L. and Discher, D. E. Matrix Elasticity Directs Stem Cell Lineage Specification. *Cell*, **126**(4), 677–689, 2006.
- [28] von der Mark, K. and Ocalan, M. Antagonistic effects of laminin and fibronectin on the expression of the myogenic phenotype. *Differentiation; research in biological diversity*, **40**(2), 150–157, 1989.
- [29] Maione, R. and Amati, P. Interdependence between muscle differentiation and cell-cycle control. *Biochimica et Biophysica Acta (BBA) - Reviews on Cancer*, **1332**(1), M19–M30, 1997.

-
- [30] Li, L. and Olson, E. N. Regulation of muscle cell growth and differentiation by the MyoD family of helix-loop-helix proteins. *Advances in cancer research*, **58**, 95–119, 1992.
 - [31] De Falco, G., Comes, F. and Simone, C. pRb: Master of differentiation. Coupling irreversible cell cycle withdrawal with induction of muscle-specification transcription. *Oncogene*, **25**(38), 5244–5249, 2006.
 - [32] Pownall, M. E., Gustafsson, M. K. and Emerson, C. P. Myogenic regulatory factors and the specification of muscle progenitors in vertebrate embryos. *Annual Review of Cell and Developmental Biology*, **18**, 747–783, 2002.
 - [33] Bach, L. A., Salemi, R. and Leeding, K. S. Roles of insulin-like growth factor (IGF) receptors and IGF-binding proteins in IGF-II-induced proliferation and differentiation of L6A1 rat myoblasts. *Endocrinology*, **136**(11), 5061–5069, 1995.
 - [34] Gawlitta, D., Boonen, K. J. M., Oomens, C. W. J., Baaijens, F. P. T. and Bouten, C. V. C. The influence of serum-free culture conditions on skeletal muscle differentiation in a tissue-engineered model. *Tissue Engineering Part A*, **14**(1), 161–171, 2008.
 - [35] Lawson, M. A. and Purslow, P. P. Differentiation of myoblasts in serum-free media: Effects of modified media are cell line-specific. *Cells Tissues Organs*, **167**(2-3), 130–137, 2000.
 - [36] Griffin, C. A., Apponi, L. H., Long, K. K. and Pavlath, G. K. Chemokine expression and control of muscle cell migration during myogenesis. *J Cell Sci*, **123**(18), 3052–3060, 2010.
 - [37] Ruiz-Gómez, M., Coutts, N., Price, A., Taylor, M. V. and Bate, M. Drosophila Dumbfounded: A Myoblast Attractant Essential for Fusion. *Cell*, **102**(2), 189–198, 2000.
 - [38] Strükelberg, M., Bonengel, B., Moda, L. M., Hertenstein, A., Couet, H. G. d., Ramos, R. G. P. and Fischbach, K.-F. *rst* and its paralogue *kirre* act redundantly during embryonic muscle development in Drosophila. *Development*, **128**(21), 4229–4239, 2001.
 - [39] Artero, R. D., Castanon, I. and Baylies, M. K. The immunoglobulin-like protein Hibris functions as a dose-dependent regulator of myoblast fusion and is differentially controlled by Ras and Notch signaling. *Development*, **128**(21), 4251–4264, 2001.
 - [40] Bour, B. A., Chakravarti, M., West, J. M. and Abmayr, S. M. Drosophila SNS, a member of the immunoglobulin superfamily that is essential for myoblast fusion. *Genes & Development*, **14**(12), 1498–1511, 2000.
 - [41] Taylor, M. V. Muscle Differentiation: How Two Cells Become One. *Current Biology*, **12**(6), R224–R228, 2002.
 - [42] Larsson, L. I., Bjerregaard, B. and Talts, J. F. Cell fusions in mammals. *Histochemistry and Cell Biology*, **129**(5), 551–561, 2008.
 - [43] Chen, E. H., Grote, E., Mohler, W. and Vignery, A. Cell–cell fusion. *Febs Letters*, **581**(11), 2181–2193, 2007.
 - [44] Jahn, R., Lang, T. and Südhof, T. C. Membrane Fusion. *Cell*, **112**(4), 519–533, 2003.
 - [45] Kwang, W. J., Shinn-Thomas, J. H. and Mohler, W. A. Chapter five - New Insights into the Mechanisms and Roles of Cell–Cell Fusion. In *International Review of Cell and Molecular Biology*, volume 289, pages 149–209. Academic Press, 2011.

- [46] Jeremic, A., Kelly, M., Cho, S.-J., Stromer, M. H. and Jena, B. P. Reconstituted Fusion Pore. *Biophysical Journal*, **85**(3), 2035–2043, 2003.
- [47] Baylies, M. K. and Michelson, A. M. Invertebrate myogenesis: looking back to the future of muscle development. *Current Opinion in Genetics & Development*, **11**(4), 431–439, 2001.
- [48] Gildor, B., Massarwa, R., Shilo, B.-Z. and Schejter, E. D. The SCAR and WASp nucleation-promoting factors act sequentially to mediate *Drosophila* myoblast fusion. *EMBO reports*, **10**(9), 1043–1050, 2009.
- [49] Richardson, B., Beckett, K. and Baylies, M. Visualizing new dimensions in *Drosophila* myoblast fusion. *BioEssays*, **30**(5), 423–431, 2008.
- [50] Sens, K. L., Zhang, S., Jin, P., Duan, R., Zhang, G., Luo, F., Parachini, L. and Chen, E. H. An invasive podosome-like structure promotes fusion pore formation during myoblast fusion. *The Journal of Cell Biology*, **191**(5), 1013–1027, 2010.
- [51] Haralalka, S., Shelton, C., Cartwright, H. N., Katzfey, E., Janzen, E. and Abmayr, S. M. Asymmetric Mbc, active Rac1 and F-actin foci in the fusion-competent myoblasts during myoblast fusion in *Drosophila*. *Development*, **138**(8), 1551–1562, 2011.
- [52] Önel, S.-F. and Renkawitz-Pohl, R. FuRMAS: triggering myoblast fusion in *Drosophila*. *Developmental Dynamics*, **238**(6), 1513–1525, 2009.
- [53] Haralalka, S. and Abmayr, S. M. Myoblast fusion in *Drosophila*. *Experimental Cell Research*, **316**(18), 3007–3013, 2010.
- [54] Horsley, V. and Pavlath, G. K. Forming a Multinucleated Cell: Molecules That Regulate Myoblast Fusion. *Cells Tissues Organs*, **176**(1-3), 67–78, 2004.
- [55] Rochlin, K., Yu, S., Roy, S. and Baylies, M. K. Myoblast fusion: When it takes more to make one. *Developmental Biology*, **341**(1), 66–83, 2010.
- [56] Pavlath, G. K. Spatial and functional restriction of regulatory molecules during mammalian myoblast fusion. *Experimental Cell Research*, **316**(18), 3067–3072, 2010.
- [57] Nishiyama, T., Kii, I. and Kudo, A. Inactivation of Rho/ROCK Signaling Is Crucial for the Nuclear Accumulation of FKHR and Myoblast Fusion. *Journal of Biological Chemistry*, **279**(45), 47311–47319, 2004.
- [58] Cossu, G. and Borello, U. Wnt signaling and the activation of myogenesis in mammals. *Embo Journal*, **18**(24), 6867–6872, 1999.
- [59] Sun, D., Li, H. and Zolkiewska, A. The role of Delta-like 1 shedding in muscle cell self-renewal and differentiation. *Journal of Cell Science*, **121**(22), 3815–3823, 2008.
- [60] Knight, J. and Kothary, R. The myogenic kinome: protein kinases critical to mammalian skeletal myogenesis. *Skeletal Muscle*, **1**(1), 29, 2011.
- [61] Forcales, S. V. and Puri, P. L. Signaling to the chromatin during skeletal myogenesis: Novel targets for pharmacological modulation of gene expression. *Seminars in Cell & Developmental Biology*, **16**(4-5), 596–611, 2005.
- [62] Mitin, N., Ramocki, M. B., Konieczny, S. F. and Taparowsky, E. J. Ras regulation of skeletal muscle differentiation and gene expression. In *Regulators and Effectors of Small Gtpases, Pt G*, volume 333 of *Methods in Enzymology*, pages 232–247. 2001.

-
- [63] Vasyutina, E., Martarelli, B., Brakebusch, C., Wende, H. and Birchmeier, C. The small G-proteins Rac1 and Cdc42 are essential for myoblast fusion in the mouse. *Proceedings of the National Academy of Sciences*, **106**(22), 8935–8940, 2009.
 - [64] Bryan, B. A., Li, D., Wu, X. and Liu, M. The Rho family of small GTPases: crucial regulators of skeletal myogenesis. *Cellular and Molecular Life Sciences*, **62**(14), 1547–1555, 2005.
 - [65] Fortier, M., Comunale, F., Kucharczak, J., Blangy, A., Charrasse, S. and Gauthier-Rouvière, C. RhoE controls myoblast alignment prior fusion through RhoA and ROCK. *Cell Death & Differentiation*, **15**(8), 1221–1231, 2008.
 - [66] Abramovici, H. and Gee, S. H. Morphological changes and spatial regulation of diacylglycerol kinase- ζ , syntrophins, and Rac1 during myoblast fusion. *Cell Motility and the Cytoskeleton*, **64**(7), 549–567, 2007.
 - [67] Sordella, R., Jiang, W., Chen, G. C., Curto, M. and Settleman, J. Modulation of rho GTPase signaling regulates a switch between adipogenesis and myogenesis. *Cell*, **113**(2), 147–158, 2003.
 - [68] Pollard, H. B., Burns, A. L. and Rojas, E. Synexin (annexin VII): a cytosolic calcium-binding protein which promotes membrane fusion and forms calcium channels in artificial bilayer and natural membranes. *The Journal of membrane biology*, **117**(2), 101–112, 1990.
 - [69] Clemen, C. S., Hofmann, A., Zamparelli, C. and Noegel, A. A. Expression and localisation of annexin VII (synexin) isoforms in differentiating myoblasts. *Journal of Muscle Research and Cell Motility*, **20**(7), 669–679, 1999.
 - [70] Selbert, S., Fischer, P., Pongratz, D., Stewart, M. and Noegel, A. A. Expression and localization of annexin VII (synexin) in muscle cells. *Journal of Cell Science*, **108**(1), 85–95, 1995.
 - [71] Duan, R. and Gallagher, P. J. Dependence of myoblast fusion on a cortical actin wall and nonmuscle myosin IIA. *Developmental Biology*, **325**(2), 374–385, 2009.
 - [72] Lipton, B. H. and Konigsberg, I. R. A Fine-Structural Analysis of the Fusion of Myogenic Cells. *The Journal of Cell Biology*, **53**(2), 348–364, 1972.
 - [73] Nowak, S. J., Nahirney, P. C., Hadjantonakis, A.-K. and Baylies, M. K. Nap1-mediated actin remodeling is essential for mammalian myoblast fusion. *Journal of Cell Science*, **122**(18), 3282–3293, 2009.
 - [74] Städler, B., Blättler, T. M. and Franco-Obregón, A. Time-lapse imaging of In Vitro myogenesis using atomic force microscopy. *Journal of Microscopy*, **237**(1), 63–69, 2010.
 - [75] Kim, S.-J., Kim, S., Shin, H. and Uhm, C.-S. Intercellular interaction observed by atomic force microscopy. *Ultramicroscopy*, **108**(10), 1148–1151, 2008.
 - [76] Knudsen, K. A. and Horwitz, A. F. Tandem Events in Myoblast Fusion. *Developmental Biology*, **58**(2), 328–338, 1977.
 - [77] Mikami, T., Koyama, S., Yabuta, Y. and Kitagawa, H. Chondroitin Sulfate Is a Crucial Determinant for Skeletal Muscle Development/Regeneration and Improvement of Muscular Dystrophies. *Journal of Biological Chemistry*, **287**(46), 38531–38542, 2012.
 - [78] Farmawati, A., Kitajima, Y., Nedachi, T., Sato, M., Kanzaki, M. and Nagatomi, R. Characterization of contraction-induced IL-6 up-regulation using contractile C2C12 myotubes. *Endocrine Journal*, **advpub**, 2012.

- [79] Rodriguez, J., Vernus, B., Toubiana, M., Jublanc, E., Tintignac, L., Leibovitch, S. and Bonniieu, A. Myostatin inactivation increases myotube size through regulation of translational initiation machinery. *Journal of Cellular Biochemistry*, **112**(12), 3531–3542, 2011.
- [80] Angst, B., Marozzi, C. and Magee, A. The cadherin superfamily: diversity in form and function. *Journal of Cell Science*, **114**(4), 629–641, 2001.
- [81] Koch, A. W., Bozic, D., Pertz, O. and Engel, J. Homophilic adhesion by cadherins. *Current Opinion in Structural Biology*, **9**(2), 275–281, 1999.
- [82] Pokutta, S. and Weis, W. I. Structure and Mechanism of Cadherins and Catenins in Cell-Cell Contacts. *Annual Review of Cell and Developmental Biology*, **23**(1), 237–261, 2007.
- [83] Yap, A. S., Brieher, W. M. and Gumbiner, B. M. Molecular and Functional Analysis of Cadherin-Based Adherens Junctions. *Annual Review of Cell and Developmental Biology*, **13**(1), 119–146, 1997.
- [84] Niessen, C. M., Leckband, D. and Yap, A. S. Tissue Organization by Cadherin Adhesion Molecules: Dynamic Molecular and Cellular Mechanisms of Morphogenetic Regulation. *Physiological Reviews*, **91**(2), 691–731, 2011.
- [85] Cifuentes-Diaz, C., Nicolet, M. and Mège, R. M. Cell adhesion and development of skeletal muscle. *Comptes rendus des séances de la Société de biologie et de ses filiales*, **188**(5-6), 505–525, 1994.
- [86] Krauss, R. S. Regulation of promyogenic signal transduction by cell–cell contact and adhesion. *Experimental Cell Research*, **316**(18), 3042–3049, 2010.
- [87] Mège, R., Goudou, D., Diaz, C., Nicolet, M., Garcia, L., Geraud, G. and Rieger, F. N-cadherin and N-CAM in myoblast fusion: compared localisation and effect of blockade by peptides and antibodies. *Journal of Cell Science*, **103**(4), 897–906, 1992.
- [88] Charrasse, S., Meriane, M., Comunale, F., Blangy, A. and Gauthier-Rouvière, C. N-cadherin-dependent cell–cell contact regulates Rho GTPases and β -catenin localization in mouse C2C12 myoblasts. *The Journal of Cell Biology*, **158**(5), 953–965, 2002.
- [89] Matsuda, T., Takahashi, K., Nariai, T., Ito, T., Takatani, T., Fujio, Y. and Azuma, J. N-cadherin-mediated cell adhesion determines the plasticity for cell alignment in response to mechanical stretch in cultured cardiomyocytes. *Biochemical and Biophysical Research Communications*, **326**(1), 228–232, 2005.
- [90] Moore, R. and Walsh, F. The cell adhesion molecule M-cadherin is specifically expressed in developing and regenerating, but not denervated skeletal muscle. *Development*, **117**(4), 1409–1420, 1993.
- [91] Kaufmann, U., Martin, B., Link, D., Witt, K., Zeitler, R., Reinhard, S. and Starzinski-Powitz, A. M-cadherin and its sisters in development of striated muscle. *Cell and Tissue Research*, **296**(1), 191–198, 1999.
- [92] Kaufmann, U., Kirsch, J., Irintchev, A., Wernig, A. and Starzinski-Powitz, A. The M-cadherin catenin complex interacts with microtubules in skeletal muscle cells: implications for the fusion of myoblasts. *Journal of Cell Science*, **112**(1), 55–68, 1999.
- [93] Zeschnigk, M., Kozian, D., Kuch, C., Schmoll, M. and Starzinski-Powitz, A. Involvement of M-cadherin in terminal differentiation of skeletal muscle cells. *Journal of Cell Science*, **108**(9), 2973–2981, 1995.

-
- [94] Hollnagel, A., Grund, C., Franke, W. W. and Arnold, H.-H. The Cell Adhesion Molecule M-Cadherin Is Not Essential for Muscle Development and Regeneration. *Molecular and Cellular Biology*, **22**(13), 4760–4770, 2002.
 - [95] Charrasse, S., Comunale, F., Fortier, M., Portales-Casamar, E., Debant, A. and Gauthier-Rouvière, C. M-Cadherin Activates Rac1 GTPase through the Rho-GEF Trio during Myoblast Fusion. *Molecular Biology of the Cell*, **18**(5), 1734–1743, 2007.
 - [96] Sako, Y., Nagafuchi, A., Tsukita, S., Takeichi, M. and Kusumi, A. Cytoplasmic Regulation of the Movement of E-Cadherin on the Free Cell Surface as Studied by Optical Tweezers and Single Particle Tracking: Corralling and Tethering by the Membrane Skeleton. *The Journal of Cell Biology*, **140**(5), 1227–1240, 1998.
 - [97] Comunale, F., Causeret, M., Favard, C., Cau, J., Taulet, N., Charrasse, S. and Gauthier-rouvière, C. Rac1 and RhoA GTPases have antagonistic functions during N-cadherin-dependent cell-cell contact formation in C2C12 myoblasts. *Biology of the Cell*, **99**(9), 503–517, 2007.
 - [98] Delanoë-Ayari, H., Al Kurdi, R., Vallade, M., Gulino-Debrac, D. and Riveline, D. Membrane and acto-myosin tension promote clustering of adhesion proteins. *Proceedings of the National Academy of Sciences of the United States of America*, **101**(8), 2229–2234, 2004.
 - [99] Naumanen, P., Lappalainen, P. and Hotulainen, P. Mechanisms of actin stress fibre assembly. *Journal of Microscopy*, **231**(3), 446–454, 2008.
 - [100] Kim, S., Shilagardi, K., Zhang, S., Hong, S. N., Sens, K. L., Bo, J., Gonzalez, G. A. and Chen, E. H. A Critical Function for the Actin Cytoskeleton in Targeted Exocytosis of Prefusion Vesicles during Myoblast Fusion. *Developmental Cell*, **12**(4), 571–586, 2007.
 - [101] Peckham, M. Engineering a multi-nucleated myotube, the role of the actin cytoskeleton. *Journal of Microscopy*, **231**(3), 486–493, 2008.
 - [102] Formigli, L., Meacci, E., Sassoli, C., Squecco, R., Nosi, D., Chellini, F., Naro, F., Francini, F. and Zecchi-Orlandini, S. Cytoskeleton/stretch-activated ion channel interaction regulates myogenic differentiation of skeletal myoblasts. *Journal of Cellular Physiology*, **211**(2), 296–306, 2007.
 - [103] Frystyk, J., Freda, P. and Clemmons, D. R. The current status of IGF-I assays – A 2009 update. *Growth Hormone & IGF Research*, **20**(1), 8–18, 2010.
 - [104] Daughaday, W. H. A personal history of the origin of the somatomedin hypothesis and recent challenges to its validity. *Perspectives in biology and medicine*, **32**(2), 194–211, 1989.
 - [105] Van den Brande, J. A Personal View on the Early History of the Insulin-Like Growth Factors. *Hormone Research*, **51**(Suppl. 3), 149–175, 1999.
 - [106] Daftary, S. S. and Gore, A. C. IGF-I in the Brain as a Regulator of Reproductive Neuroendocrine Function. *Experimental Biology and Medicine*, **230**(5), 292–306, 2005.
 - [107] Goldspink, G., Wessner, B. and Bachl, N. Growth factors, muscle function and doping. *Current Opinion in Pharmacology*, **8**(3), 352–357, 2008.
 - [108] Goldspink, G. and Yang, S. Y. The Splicing of the IGF-I Gene to Yield Different Muscle Growth Factors. In *Advances in Genetics*, volume 52, pages 23–49. Academic Press, 2004.
 - [109] Hill, M. and Goldspink, G. Expression and splicing of the insulin-like growth factor gene in rodent muscle is associated with muscle satellite (stem) cell activation following local tissue damage. *The Journal of Physiology*, **549**(2), 409–418, 2003.

- [110] Milasincic, D. J., Pilch, P. F. and Farmer, S. R. Role of Cell-Adhesion in the IGF-1 and BFGF Signaling Pathways During the Growth and Differentiation of C2C12 Myoblasts. *Molecular Biology of the Cell*, **6**, 2230–2230, 1995.
- [111] Barton, E. R., DeMeo, J. and Lei, H. The insulin-like growth factor (IGF)-I E-peptides are required for isoform-specific gene expression and muscle hypertrophy after local IGF-I production. *J Appl Physiol*, **108**(5), 1069–1076, 2010.
- [112] Yang, S. Y., Alnaqeeb, M., Simpson, H. and Goldspink, G. Cloning and characterization of an IGF-1 isoform expressed in skeletal muscle subjected to stretch. *Journal of Muscle Research and Cell Motility*, **17**(4), 487–495, 1996.
- [113] McKoy, G., Ashley, W., Mander, J., Yang, S. Y., Williams, N., Russell, B. and Goldspink, G. Expression of insulin growth factor-1 splice variants and structural genes in rabbit skeletal muscle induced by stretch and stimulation. *Journal of Physiology-London*, **516**(2), 583–592, 1999.
- [114] Philippou, A., Papageorgiou, E., Bogdanis, G., Halapas, A., Sourla, A., Maridaki, M., Pissimissis, N. and Koutsilieris, M. Expression of IGF-1 Isoforms after Exercise-induced Muscle Damage in Humans: Characterization of the MGF E Peptide Actions In Vitro. *In Vivo*, **23**(4), 567–575, 2009.
- [115] Hameed, M., Orrell, R. W., Cobbold, M., Goldspink, G. and Harridge, S. D. R. Expression of IGF-I splice variants in young and old human skeletal muscle after high resistance exercise. *The Journal of Physiology*, **547**(1), 247–254, 2003.
- [116] Yang, S. Y. and Goldspink, G. Different roles of the IGF-I Ec peptide (MGF) and mature IGF-I in myoblast proliferation and differentiation. *FEBS Letters*, **522**(1–3), 156–160, 2002.
- [117] Qin, L.-L., Li, X.-K., Xu, J., Mo, D.-L., Tong, X., Pan, Z.-C., Li, J.-Q., Chen, Y.-S., Zhang, Z., Wang, C. and Long, Q.-M. Mechano growth factor (MGF) promotes proliferation and inhibits differentiation of porcine satellite cells (PSCs) by down-regulation of key myogenic transcriptional factors. *Molecular and Cellular Biochemistry*, **370**(1–2), 221–230, 2012.
- [118] Dai, Z., Wu, F., Yeung, E. W. and Li, Y. IGF-IEc expression, regulation and biological function in different tissues. *Growth Hormone & IGF Research*, **20**(4), 275–281, 2010.
- [119] Mills, P., Lafreniere, J. F., Benabdallah, B. F., El Fahime, E. M. and Tremblay, J. P. A new pro-migratory activity on human myogenic precursor cells for a synthetic peptide within the E domain of the mechano growth factor. *Experimental Cell Research*, **313**(3), 527–537, 2007.
- [120] Velloso, C. P. and Harridge, S. D. R. Insulin-like growth factor-I E peptides: implications for ageing skeletal muscle. *Scandinavian Journal of Medicine & Science in Sports*, **20**(1), 20–27, 2010.
- [121] Cheema, U., Brown, R., Mudera, V., Yang, S. Y., McGrouther, G. and Goldspink, G. Mechanical signals and IGF-I gene splicing in vitro in relation to development of skeletal muscle. *Journal of Cellular Physiology*, **202**(1), 67–75, 2005.
- [122] Yoshiko, Y., Hirao, K. and Maeda, N. Differentiation in C2C12 myoblasts depends on the expression of endogenous IGFs and not serum depletion. *American Journal of Physiology-Cell Physiology*, **283**(4), C1278–C1286, 2002.
- [123] Palmer, R. M., Thompson, M. G., Knott, R. M., Campbell, G. P., Thom, A. and Morrison, K. S. Insulin and insulin-like growth factor-I responsiveness and signalling mechanisms in C2C12 satellite cells: Effect of differentiation and fusion. *Biochimica Et Biophysica Acta-Molecular Cell Research*, **1355**(2), 167–176, 1997.

-
- [124] Stewart, C. E. and Pell, J. M. Point: Igf Is the Major Physiological Regulator of Muscle Mass. *Journal of Applied Physiology*, **108**(6), 1820–1821, 2010.
 - [125] Flueck, M. and Goldspink, G. Counterpoint: Igf Is Not the Major Physiological Regulator of Muscle Mass. *Journal of Applied Physiology*, **108**(6), 1821–1823, 2010.
 - [126] Stewart, C. E. and Pell, J. M. Rebuttal from Stewart and Pell. *Journal of Applied Physiology*, **108**(6), 1823–1824, 2010.
 - [127] Flueck, M. and Goldspink, G. Rebuttal from Flueck and Goldspink. *Journal of Applied Physiology*, **108**(6), 1824–1824, 2010.
 - [128] Stewart, C. E. and Pell, J. M. Last Word on Point:Counterpoint: IGF is the major physiological regulator of muscle mass. *Journal of Applied Physiology*, **108**(6), 1832–1832, 2010.
 - [129] Spangenburg, E. E., Phillips, S. M., Yang, S. Y., Musaro, A., Shenkman, B. S., Kachaeva, E., Turtikova, O., Leinsoo, T., Lysenko, E., Baar, K., Hamilton, D. L., Philp, A., Barton, E. R., Svensson, J., Loughna, P. T., Harridge, S. D. R., Shavlakadze, T., Grounds, M. D., Vinciguerra, M., Hede, M., Rosenthal, N., Esser, K. A., Song, Y.-H. and Ameredes, B. T. Comments on Point:Counterpoint: IGF is/is not the major physiological regulator of muscle mass. *Journal of Applied Physiology*, **108**(6), 1825–1831, 2010.
 - [130] Ringer, S. A further Contribution regarding the influence of the different Constituents of the Blood on the Contraction of the Heart. *The Journal of Physiology*, **4**(1), 29–42, 1883.
 - [131] Clapham, D. E. Calcium Signaling. *Cell*, **131**(6), 1047–1058, 2007.
 - [132] Berridge, M. J. Elementary and global aspects of calcium signalling. *Journal of Experimental Biology*, **200**(2), 315–319, 1997.
 - [133] Arruda, A. P., Nigro, M., Oliveira, G. M. and de Meis, L. Thermogenic activity of Ca²⁺-ATPase from skeletal muscle heavy sarcoplasmic reticulum: The role of ryanodine Ca²⁺ channel. *Biochimica Et Biophysica Acta-Biomembranes*, **1768**(6), 1498–1505, 2007.
 - [134] Bennett, D. L., Cheek, T. R., Berridge, M. J., Smedt, H. D., Parys, J. B., Missiaen, L. and Bootman, M. D. Expression and Function of Ryanodine Receptors in Nonexcitable Cells. *Journal of Biological Chemistry*, **271**(11), 6356–6362, 1996.
 - [135] Furuichi, T. and Mikoshiba, K. Inositol 1,4,5-Trisphosphate Receptor-Mediated Ca²⁺ Signaling in the Brain. *Journal of Neurochemistry*, **64**(3), 953–960, 1995.
 - [136] Bootman, M. D., Collins, T. J., Peppiatt, C. M., Prothero, L. S., MacKenzie, L., De Smet, P., Travers, M., Tovey, S. C., Seo, J. T., Berridge, M. J., Ciccolini, F. and Lipp, P. Calcium signalling—an overview. *Seminars in Cell & Developmental Biology*, **12**(1), 3–10, 2001.
 - [137] Berridge, M. J., Lipp, P. and Bootman, M. D. The versatility and universality of calcium signalling. *Nature Reviews Molecular Cell Biology*, **1**(1), 11–21, 2000.
 - [138] Berridge, M. J., Bootman, M. D. and Roderick, H. L. Calcium signalling: dynamics, homeostasis and remodelling. *Nature Reviews Molecular Cell Biology*, **4**(7), 517–529, 2003.
 - [139] Przybylski, R., Szigeti, V., Davidheiser, S. and Kirby, A. Calcium regulation of skeletal myogenesis. II. Extracellular and cell surface effects. *Cell Calcium*, **15**(2), 132–142, 1994.
 - [140] Capiod, T. Cell proliferation, calcium influx and calcium channels. *Biochimie*, **93**(12), 2075–2079, 2011.

- [141] Stiber, J. A. and Rosenberg, P. B. The role of store-operated calcium influx in skeletal muscle signaling. *Cell Calcium*, **49**(5), 341–349, 2011.
- [142] David, J. D. and Higginbotham, C.-A. Fusion of chick embryo skeletal myoblasts: Interactions of prostaglandin E1, adenosine 3':5' monophosphate, and calcium influx. *Developmental Biology*, **82**(2), 308–316, 1981.
- [143] Gutierrez-Martin, Y., Martin-Romero, F. J. and Henao, F. Store-operated calcium entry in differentiated C2C12 skeletal muscle cells. *Biochimica et Biophysica Acta (BBA) - Biomembranes*, **1711**(1), 33–40, 2005.
- [144] Lorenzon, P., Giovannelli, A., Ragozzino, D., Eusebi, F. and Ruzzier, F. Spontaneous and repetitive calcium transients in C2C12 mouse myotubes during in vitro myogenesis. *European Journal of Neuroscience*, **9**(4), 800–808, 1997.
- [145] Brandt, P. and Vanaman, T. C. Splicing of the Muscle-Specific Plasma Membrane Ca²⁺-ATPase Isoform PMCA1c Is Associated with Cell Fusion in C2 Myocytes. *Journal of Neurochemistry*, **62**(2), 799–802, 1994.
- [146] Allen, D. G. Skeletal muscle function: Role of ionic changes in fatigue, damage and disease. *Clinical and Experimental Pharmacology and Physiology*, **31**(8), 485–493, 2004.
- [147] Constantin, B., Cognard, C. and Raymond, G. Myoblast fusion requires cytosolic calcium elevation but not activation of voltage-dependent calcium channels. *Cell Calcium*, **19**(5), 365–374, 1996.
- [148] Constantin, B., Cognard, C. and Raymond, G. Myoblast Fusion Is Not a Prerequisite for the Appearance of Calcium Current, Calcium Release, and Contraction in Rat Skeletal Muscle Cells Developing in Culture. *Experimental Cell Research*, **217**(2), 497–505, 1995.
- [149] Kim, J., Adachi, T., Saiuchi, M. and Asada, A. Differentiation of Quail Myoblasts Transformed with a Temperature Sensitive Mutant of Rous Sarcoma Virus. II. Relationship of Myoblast Fusion with Calcium and Temperature. *Cell Structure and Function*, **17**(4), 249–255, 1992.
- [150] Onuma, E. K. and Hui, S. W. Electric field-directed cell shape changes, displacement, and cytoskeletal reorganization are calcium dependent. *The Journal of Cell Biology*, **106**(6), 2067–2075, 1988.
- [151] Pabelick, C. M., Prakash, Y. S., Kannan, M. S. and Sieck, G. C. Spatial and temporal aspects of calcium sparks in porcine tracheal smooth muscle cells. *American Journal of Physiology-Lung Cellular and Molecular Physiology*, **277**(5), L1018–L1025, 1999.
- [152] Bezanilla, F. The Voltage Sensor in Voltage-Dependent Ion Channels. *Physiological Reviews*, **80**(2), 555–592, 2000.
- [153] Catterall, W. A., Cestèle, S., Yarov-Yarovoy, V., Yu, F. H., Konoki, K. and Scheuer, T. Voltage-gated ion channels and gating modifier toxins. *Toxicon*, **49**(2), 124–141, 2007.
- [154] Zhorov, B. S. and Tikhonov, D. B. Potassium, sodium, calcium and glutamate-gated channels: pore architecture and ligand action. *Journal of Neurochemistry*, **88**(4), 782–799, 2004.
- [155] Cottrell, G. A. The first peptide-gated ion channel. *Journal of Experimental Biology*, **200**(18), 2377–2386, 1997.
- [156] Volpe, P., Salviati, G. and Chu, A. Calcium-gated calcium channels in sarcoplasmic reticulum of rabbit skinned skeletal muscle fibers. *The Journal of General Physiology*, **87**(2), 289–303, 1986.
- [157] Sachs, F. Stretch-Activated Ion Channels: What Are They? *Physiology*, **25**(1), 50–56, 2010.

-
- [158] Yoshimura, K. and Sokabe, M. Mechanosensitivity of ion channels based on protein-lipid interactions. *Journal of the Royal Society, Interface / the Royal Society*, **7 Suppl 3**, S307–320, 2010.
 - [159] Li, X. T., Dyachenko, V., Zuzarte, M., Putzke, C., Preisig-Müller, R., Isenberg, G. and Daut, J. The stretch-activated potassium channel TREK-1 in rat cardiac ventricular muscle. *Cardiovascular Research*, **69**(1), 86–97, 2006.
 - [160] McBride, T. A., Stockert, B. W., Gorin, F. A. and Carlsen, R. C. Stretch-activated ion channels contribute to membrane depolarization after eccentric contractions. *Journal of Applied Physiology*, **88**(1), 91–101, 2000.
 - [161] Franco, A. and Lansman, J. B. Calcium entry through stretch-inactivated ion channels in mdx myotubes. , *Published online: 12 April 1990*; | doi:10.1038/344670a0, **344**(6267), 670–673, 1990.
 - [162] Guharay, F. and Sachs, F. Stretch-activated single ion channel currents in tissue-cultured embryonic chick skeletal muscle. *The Journal of Physiology*, **352**, 685–701, 1984.
 - [163] Gottlieb, P. A. and Sachs, F. Cell biology: The sensation of stretch. *Nature*, **483**(7388), 163–164, 2012.
 - [164] Franco, A. and Lansman, J. B. Stretch-sensitive channels in developing muscle cells from a mouse cell line. *The Journal of Physiology*, **427**(1), 361–380, 1990.
 - [165] Wedhas, N., Klamut, H. J., Dogra, C., Srivastava, A. K., Mohan, S. and Kumar, A. Inhibition of mechanosensitive cation channels inhibits myogenic differentiation by suppressing the expression of myogenic regulatory factors and caspase-3 activity. *The FASEB Journal*, **19**(14), 1986–1997, 2005.
 - [166] Vandebrouck, C., Duport, G., Cognard, C. and Raymond, G. Cationic channels in normal and dystrophic human myotubes. *Neuromuscular Disorders*, **11**(1), 72–79, 2001.
 - [167] Yeung, E. W., Whitehead, N. P., Suchyna, T. M., Gottlieb, P. A., Sachs, F. and Allen, D. G. Effects of stretch-activated channel blockers on $[Ca^{2+}]_i$ and muscle damage in the mdx mouse. *Journal of Physiology-London*, **562**(2), 367–380, 2005.
 - [168] Hua, S. Z., Gottlieb, P. A., Heo, J. and Sachs, F. A Mechanosensitive Ion Channel Regulating Cell Volume. *American Journal of Physiology - Cell Physiology*, **73**(2), 195–262, 2010.
 - [169] Bowman, C. L., Gottlieb, P. A., Suchyna, T. M., Murphy, Y. K. and Sachs, F. Mechanosensitive Ion Channels and the Peptide Inhibitor GsMTx-4: History, Properties, Mechanisms and Pharmacology. *Toxicon : official journal of the International Society on Toxinology*, **49**(2), 249–270, 2007.
 - [170] Yang, X. C. and Sachs, F. Block of stretch-activated ion channels in *Xenopus* oocytes by gadolinium and calcium ions. *Science (New York, N.Y.)*, **243**(4894 Pt 1), 1068–1071, 1989.
 - [171] Hamill, O. P. and McBride, D. W. The pharmacology of mechanogated membrane ion channels. *Pharmacological Reviews*, **48**(2), 231–252, 1996.
 - [172] Sokabe, M., Hasegawa, N. and Yamamori, K. Blockers and Activators for Stretch-Activated Ion Channels of Chick Skeletal Muscles. *Annals of the New York Academy of Sciences*, **707**(1), 417–420, 1993.
 - [173] Chung, S. C., McDonald, T. V. and Gardner, P. Inhibition by SK&F 96365 of Ca^{2+} current, IL-2 production and activation in T lymphocytes. *British Journal of Pharmacology*, **113**(3), 861–868, 1994.

- [174] Haverstick, D. M., Heady, T. N., Macdonald, T. L. and Gray, L. S. Inhibition of Human Prostate Cancer Proliferation in Vitro and in a Mouse Model by a Compound Synthesized to Block Ca²⁺ Entry. *Cancer Research*, **60**(4), 1002–1008, 2000.
- [175] Nel, A. E., Dirienzo, W., Stefanini, G. F., Wooten, M. W., Canonica, G. W., Lattanze, G. R., Stevenson, H. C., Miller, P., Fudenberg, H. H. and Galbraith, R. M. Inhibition of T3 mediated T-cell proliferation by Ca²⁺-channel blockers and inhibitors of Ca²⁺/phospholipid-dependent kinase. *Scandinavian journal of immunology*, **24**(3), 283–290, 1986.
- [176] Panner, A. and Wurster, R. D. T-type calcium channels and tumor proliferation. *Cell Calcium*, **40**(2), 253–259, 2006.
- [177] Taylor, J. M. and Simpson, R. U. Inhibition of Cancer Cell Growth by Calcium Channel Antagonists in the Athymic Mouse. *Cancer Research*, **52**(9), 2413–2418, 1992.
- [178] Taylor, J. T., Huang, L., Pottle, J. E., Liu, K., Yang, Y., Zeng, X., Keyser, B. M., Agrawal, K. C., Hansen, J. B. and Li, M. Selective blockade of T-type Ca²⁺ channels suppresses human breast cancer cell proliferation. *Cancer Letters*, **267**(1), 116–124, 2008.
- [179] Enfissi, A., Prigent, S., Colosetti, P. and Capiod, T. The blocking of capacitative calcium entry by 2-aminoethyl diphenylborate (2-APB) and carboxyamidotriazole (CAI) inhibits proliferation in Hep G2 and Huh-7 human hepatoma cells. *Cell Calcium*, **36**(6), 459–467, 2004.
- [180] Spangenburg, E. E., Bowles, D. K. and Booth, F. W. Insulin-Like Growth Factor-Induced Transcriptional Activity of the Skeletal α -Actin Gene Is Regulated by Signaling Mechanisms Linked to Voltage-Gated Calcium Channels during Myoblast Differentiation. *Endocrinology*, **145**(4), 2054–2063, 2004.
- [181] Lorenzon, P., Grohovaz, F. and Ruzzier, F. Voltage- and ligand-gated ryanodine receptors are functionally separated in developing C2C12 mouse myotubes. *The Journal of Physiology*, **525**(2), 499–507, 2000.
- [182] Shen, Q. W., Zhu, M. J., Tong, J., Ren, J. and Du, M. Ca²⁺/calmodulin-dependent protein kinase kinase is involved in AMP-activated protein kinase activation by α -lipoic acid in C2C12 myotubes. *American Journal of Physiology - Cell Physiology*, **293**(4), C1395–C1403, 2007.
- [183] Chen, C. S., Tan, J. and Tien, J. Mechanotransduction at Cell-Matrix and Cell-Cell Contacts. *Annual Review of Biomedical Engineering*, **6**(1), 275–302, 2004.
- [184] Johnson, A. W. *Mechanobiology of cell-cell and cell-matrix interactions*. Springer Science+Business Media, New York, 2011.
- [185] Riemer, T. L. and Tung, L. Stretch-induced excitation and action potential changes of single cardiac cells. *Progress in Biophysics & Molecular Biology*, **82**(1-3), 97–110, 2003.
- [186] Wang, J. H.-C., Yang, G. and Li, Z. Controlling Cell Responses to Cyclic Mechanical Stretching. *Annals of Biomedical Engineering*, **33**(3), 337–342, 2005.
- [187] Silbert, O., Wang, Y., Maciejewski, B. S., Lee, H.-S., Shaw, S. K. and Sanchez-Esteban, J. Roles of RhoA and Rac1 on actin remodeling and cell alignment and differentiation in fetal type II epithelial cells exposed to cyclic mechanical stretch. *Experimental lung research*, **34**(10), 663–680, 2008.
- [188] Su, F. C., Wu, C. C. and Chien, S. Review: Roles of Microenvironment and Mechanical Forces in Cell and Tissue Remodeling. *Journal of Medical and Biological Engineering*, **31**(4), 233–244, 2011.

-
- [189] Park, J. S., Huang, N. F., Kurpinski, K. T., Patel, S., Hsu, S. and Li, S. Mechanobiology of mesenchymal stem cells and their use in cardiovascular repair. *Frontiers in Bioscience*, **12**, 5098–5116, 2007.
 - [190] Mammoto, T. and Ingber, D. E. Mechanical control of tissue and organ development. *Development*, **137**(9), 1407–1420, 2010.
 - [191] Iribe, G., Ward, C. W., Camelliti, P., Bollensdorff, C., Mason, F., Burton, R. A. B., Garny, A., Morphew, M. K., Hoenger, A., Lederer, W. J. and Kohl, P. Axial Stretch of Rat Single Ventricular Cardiomyocytes Causes an Acute and Transient Increase in Ca²⁺ Spark Rate. *Circ Res*, **104**(6), 787–795, 2009.
 - [192] Frey, J. W., Farley, E. E., O’Neil, T. K., Burkholder, T. J. and Hornberger, T. A. Evidence that Mechanosensors with Distinct Biomechanical Properties Allow for Specificity in Mechanotransduction. *Biophysical Journal*, **97**(1), 347–356, 2009.
 - [193] Liu, B., Kim, T. J. and Wang, Y. Live cell imaging of mechanotransduction. *Journal of The Royal Society Interface*, **7**(Suppl_3), S365–S375, 2010.
 - [194] Loesberg, W. A., Walboomers, X. F., van Loon, J. and Jansen, J. A. The effect of combined cyclic mechanical stretching and microgrooved surface topography on the behavior of fibroblasts. *Journal of Biomedical Materials Research Part A*, **75A**(3), 723–732, 2005.
 - [195] Jakkaraju, S., Zhe, X. N. and Schuger, L. Role of stretch in activation of smooth muscle cell lineage. *Trends in Cardiovascular Medicine*, **13**(8), 330–335, 2003.
 - [196] Kaunas, R., Nguyen, P., Usami, S. and Chien, S. Cooperative effects of Rho and mechanical stretch on stress fiber organization. *Proceedings of the National Academy of Sciences of the United States of America*, **102**(44), 15895–15900, 2005.
 - [197] Wang, J. H.-C. and Thampatty, B. P. An Introductory Review of Cell Mechanobiology. *Biomechanics and Modeling in Mechanobiology*, **5**(1), 1–16, 2006.
 - [198] Grossi, A., Karlsson, A. H. and Lawson, M. A. Mechanical stimulation of C2C12 cells increases m-calpain expression, focal adhesion plaque protein degradation. *Cell Biology International*, **32**(6), 615–622, 2008.
 - [199] Burkholder, T. J. Mechanotransduction in skeletal muscle. *Frontiers in bioscience : a journal and virtual library*, **12**, 174–191, 2007.
 - [200] Grossi, A., Yadav, K. and Lawson, M. A. Mechanical stimulation increases proliferation, differentiation and protein expression in culture: Stimulation effects are substrate dependent. *Journal of Biomechanics*, **40**(15), 3354–3362, 2007.
 - [201] Simpson, D. G., Carver, W., Borg, T. K. and Terracio, L. Role of Mechanical Stimulation in the Establishment and Maintenance of Muscle Cell Differentiation. In Gordon, R., editor, *International Review of Cytology*, volume 150, pages 69–94. Academic Press, 1994.
 - [202] Allen, D. G., Whitehead, N. P. and Yeung, E. W. Mechanisms of stretch-induced muscle damage in normal and dystrophic muscle: role of ionic changes. *Journal of Physiology-London*, **567**(3), 723–735, 2005.
 - [203] Li, Y., Zhao, Z., Song, J., Feng, Y., Wang, Y., Li, X., Liu, Y. and Yang, P. Cyclic force upregulates mechano-growth factor and elevates cell proliferation in 3D cultured skeletal myoblasts. *Archives of Biochemistry and Biophysics*, **490**(2), 171–176, 2009.

- [204] Kook, S. H., Lee, H. J., Chung, W. T., Hwang, I. H., Lee, S. A., Kim, B. S. and Lee, J. C. Cyclic mechanical stretch stimulates the proliferation of C2C12 myoblasts and inhibits their differentiation via prolonged activation of p38 MAPK. *Molecules and Cells*, **25**(4), 479–486, 2008.
- [205] Kumar, A., Murphy, R., Robinson, P., Wei, L. E. I. and Boriek, A. M. Cyclic mechanical strain inhibits skeletal myogenesis through activation of focal adhesion kinase, Rac-1 GTPase, and NF- κ B transcription factor. *FASEB J.*, **18**(13), 1524–1535, 2004.
- [206] Kuang, W., Tan, J., Duan, Y., Duan, J., Wang, W., Jin, F., Jin, Z., Yuan, X. and Liu, Y. Cyclic stretch induced miR-146a upregulation delays C2C12 myogenic differentiation through inhibition of Numb. *Biochemical and Biophysical Research Communications*, **378**(2), 259–263, 2009.
- [207] Desai, L. P., White, S. R. and Waters, C. M. Cyclic Mechanical Stretch Decreases Cell Migration by Inhibiting Phosphatidylinositol 3-Kinase- and Focal Adhesion Kinase-mediated JNK1 Activation. *Journal of Biological Chemistry*, **285**(7), 4511–4519, 2010.
- [208] Otis, J. S., Burkholder, T. J. and Pavlath, G. K. Stretch-induced myoblast proliferation is dependent on the COX2 pathway. *Experimental Cell Research*, **310**(2), 417–425, 2005.
- [209] Murphy, R., Kumar, A. and Boriek, A. M. The effect of mechanical stretch on proliferation and differentiation of C2C12 cells. In *Experimental Biology 2004 Meeting*, pages A743–A743, Washington, DC, 2004.
- [210] Haddad, F. and Adams, G. R. Selected Contribution: Acute cellular and molecular responses to resistance exercise. *Journal of Applied Physiology*, **93**(1), 394–403, 2002.
- [211] Tidball, J. G. Mechanical signal transduction in skeletal muscle growth and adaptation. *Journal of Applied Physiology*, **98**(5), 1900–1908, 2005.
- [212] Ahmed, W. W., Wolfram, T., Goldyn, A. M., Bruellhoff, K., Rioja, B. A., Möller, M., Spatz, J. P., Saif, T. A., Groll, J. and Kemkemer, R. Myoblast morphology and organization on biochemically micro-patterned hydrogel coatings under cyclic mechanical strain. *Biomaterials*, **31**(2), 250–258, 2010.
- [213] Yuan, X., Luo, S., Lin, Z. and Wu, Y. Cyclic stretch translocates the α 2-subunit of the Na pump to plasma membrane in skeletal muscle cells in vitro. *Biochemical and Biophysical Research Communications*, **348**(2), 750–757, 2006.
- [214] Abe, S., Rhee, S., Iwanuma, O., Hiroki, E., Yanagisawa, N., Sakiyama, K. and Ide, Y. Effect of Mechanical Stretching on Expressions of Muscle Specific Transcription Factors MyoD, Myf-5, Myogenin and MRF4 in Proliferated Myoblasts. *Anatomia Histologia Embryologia*, **38**(4), 305–310, 2009.
- [215] Iwanuma, O., Abe, S., Hiroki, E., Kado, S., Sakiyama, K., Usami, A. and Ide, Y. Effects of mechanical stretching on caspase and IGF-1 expression during the proliferation process of myoblasts. *Zoological Science*, **25**(3), 242–247, 2008.
- [216] Goldspink, C., Yang, S. Y., Skarli, M. and Vrbova, G. Local growth regulation is associated with an isoform of IGF-1 that is expressed in normal muscles but not in dystrophic mdx or dydy mouse muscles when subjected to stretch. *Journal of Physiology-London*, **495P**, P162–P163, 1996.
- [217] Wong, M., Siegrist, M. and Goodwin, K. Cyclic tensile strain and cyclic hydrostatic pressure differentially regulate expression of hypertrophic markers in primary chondrocytes. *Bone*, **33**(4), 685–693, 2003.

-
- [218] Cheng, B.-B., Yan, Z.-Q., Yao, Q.-P., Shen, B.-R., Wang, J.-Y., Gao, L.-Z., Li, Y.-Q., Yuan, H.-T., Qi, Y.-X. and Jiang, Z.-L. Association of SIRT1 expression with shear stress induced endothelial progenitor cell differentiation. *Journal of Cellular Biochemistry*, **113**(12), 3663–3671, 2012.
 - [219] Brown, T. D. Techniques for mechanical stimulation of cells in vitro: a review. *Journal of Biomechanics*, **33**(1), 3–14, 2000.
 - [220] Hasegawa, S., Sato, S., Saito, S., Suzuki, Y. and Brunette, D. D. M. Mechanical stretching increases the number of cultured bone cells synthesizing DNA and alters their pattern of protein synthesis. *Calcified Tissue International*, **37**(4), 431–436, 1985.
 - [221] Basdra, E. K., Kohl, A. and Komposch, G. Mechanical stretching of periodontal ligament fibroblasts—a study on cytoskeletal involvement. *Journal of orofacial orthopedics = Fortschritte der Kieferorthopädie: Organ/official journal Deutsche Gesellschaft für Kieferorthopädie*, **57**(1), 24–30, 1996.
 - [222] Felix, J. A., Woodruff, M. L. and Dirksen, E. R. Stretch increases inositol 1,4,5-trisphosphate concentration in airway epithelial cells. *American journal of respiratory cell and molecular biology*, **14**(3), 296–301, 1996.
 - [223] Vandeburgh, H. H. and Karlisch, P. Longitudinal growth of skeletal myotubes in vitro in a new horizontal mechanical cell stimulator. *In vitro cellular & developmental biology: journal of the Tissue Culture Association*, **25**(7), 607–616, 1989.
 - [224] Soma, S., Matsumoto, S. and Takano-Yamamoto, T. Enhancement by conditioned medium of stretched calvarial bone cells of the osteoclast-like cell formation induced by parathyroid hormone in mouse bone marrow cultures. *Archives of Oral Biology*, **42**(3), 205–211, 1997.
 - [225] Andersen, K. and Norton, L. A device for the application of known simulated orthodontic forces to human cells in vitro. *Journal of Biomechanics*, **24**(7), 649–654, 1991.
 - [226] Matsuo, T., Uchida, H. and Matsuo, N. Bovine and porcine trabecular cells produce prostaglandin F₂ alpha in response to cyclic mechanical stretching. *Japanese journal of ophthalmology*, **40**(3), 289–296, 1996.
 - [227] Kamotani, Y., Bersano-Begey, T., Kato, N., Tung, Y.-C., Huh, D., Song, J. W. and Takayama, S. Individually programmable cell stretching microwell arrays actuated by a Braille display. *Biomaterials*, **29**(17), 2646–2655, 2008.
 - [228] Colombo, A., Cahill, P. A. and Lally, C. An analysis of the strain field in biaxial Flexcell membranes for different waveforms and frequencies. *Proceedings of the Institution of Mechanical Engineers Part H-Journal of Engineering in Medicine*, **222**(H8), 1235–1245, 2008.
 - [229] Winston, F. K., Macarak, E. J., Gorfien, S. F. and Thibault, L. E. A system to reproduce and quantify the biomechanical environment of the cell. *Journal of Applied Physiology*, **67**(1), 397–405, 1989.
 - [230] Ellis, E. F., McKinney, J. S., Willoughby, K. A., Liang, S. and Povlishock, J. T. A new model for rapid stretch-induced injury of cells in culture: characterization of the model using astrocytes. *Journal of neurotrauma*, **12**(3), 325–339, 1995.
 - [231] Schaffer, J. L., Rizen, M., L'Italien, G. J., Benbrahim, A., Megerman, J., Gerstenfeld, L. C. and Gray, M. L. Device for the application of a dynamic biaxially uniform and isotropic strain to a flexible cell culture membrane. *Journal of orthopaedic research: official publication of the Orthopaedic Research Society*, **12**(5), 709–719, 1994.

- [232] Hung, C. and Williams, J. A method for inducing equi-biaxial and uniform strains in elastomeric membranes used as cell substrates. *Journal of Biomechanics*, **27**(2), 227–232, 1994.
- [233] Sotoudeh, M., Jalali, S., Usami, S., Shyy, J. Y. and Chien, S. A strain device imposing dynamic and uniform equi-biaxial strain to cultured cells. *Annals of biomedical engineering*, **26**(2), 181–189, 1998.
- [234] Lee, A. A., Delhaas, T., Waldman, L. K., MacKenna, D. A., Villarreal, F. J. and McCulloch, A. D. An equibiaxial strain system for cultured cells. *American Journal of Physiology - Cell Physiology*, **271**(4), C1400–C1408, 1996.
- [235] Somjen, D., Binderman, I., Berger, E. and Harell, A. Bone remodelling induced by physical stress is prostaglandin E2 mediated. *Biochimica et Biophysica Acta (BBA) - General Subjects*, **627**(1), 91–100, 1980.
- [236] Meikle, M. C., Reynolds, J. J., Sellers, A. and Dingle, J. T. Rabbit cranial sutures in vitro: A new experimental model for studying the response of fibrous joints to mechanical stress. *Calcified Tissue International*, **28**(1), 137–144, 1979.
- [237] Leung, D., Glagov, S. and Mathews, M. A new in vitro system for studying cell response to mechanical stimulation: Different effects of cyclic stretching and agitation on smooth muscle cell biosynthesis. *Experimental Cell Research*, **109**(2), 285–298, 1977.
- [238] Ives, C. L., Eskin, S. G. and McIntire, L. V. Mechanical effects on endothelial cell morphology: In vitro assessment. *In Vitro Cellular & Developmental Biology*, **22**(9), 500–507, 1986.
- [239] De Witt, M. T., Handley, C. J., Oakes, B. W. and Lowther, D. A. In vitro response of chondrocytes to mechanical loading. The effect of short term mechanical tension. *Connective tissue research*, **12**(2), 97–109, 1984.
- [240] Murray, D. W. and Rushton, N. The effect of strain on bone cell prostaglandin E2 release: a new experimental method. *Calcified tissue international*, **47**(1), 35–39, 1990.
- [241] Neidlinger-Wilke, C., Wilke, H.-J. and Claes, L. Cyclic stretching of human osteoblasts affects proliferation and metabolism: A new experimental method and its application. *Journal of Orthopaedic Research*, **12**(1), 70–78, 1994.
- [242] Xu, J., Liu, M., Liu, J., Caniggia, I. and Post, M. Mechanical strain induces constitutive and regulated secretion of glycosaminoglycans and proteoglycans in fetal lung cells. *Journal of Cell Science*, **109**(6), 1605–1613, 1996.
- [243] Smalt, R., Mitchell, F. T., Howard, R. L. and Chambers, T. J. Induction of NO and prostaglandin E2 in osteoblasts by wall-shear stress but not mechanical strain. *American Journal of Physiology - Endocrinology And Metabolism*, **273**(4), E751–E758, 1997.
- [244] Mitton, K., Tumminia, S., Arora, J., Zelenka, P., Epstein, D. and Russell, P. Transient Loss of α B-Crystallin: An Early Cellular Response to Mechanical Stretch. *Biochemical and Biophysical Research Communications*, **235**(1), 69–73, 1997.
- [245] Komuro, I., Kaida, T., Shibazaki, Y., Kurabayashi, M., Katoh, Y., Hoh, E., Takaku, F. and Yazaki, Y. Stretching cardiac myocytes stimulates protooncogene expression. *Journal of Biological Chemistry*, **265**(7), 3595–3598, 1990.
- [246] Decker, M. L., Janes, D. M., Barclay, M. M., Harger, L. and Decker, R. S. Regulation of adult cardiocyte growth: effects of active and passive mechanical loading. *American Journal of Physiology - Heart and Circulatory Physiology*, **272**(6), H2902–H2918, 1997.

-
- [247] Bottlang, M., Simnacher, M., Schmitt, H., Brand, R. A. and Claes, L. A cell strain system for small homogeneous strain applications. *Biomedizinische Technik. Biomedical engineering*, **42**(11), 305–309, 1997.
 - [248] Wang, J. G., Miyazu, M., Xiang, P., Li, S. N., Sokabe, M. and Naruse, K. Stretch-induced cell proliferation is mediated by FAK-MAPK pathway. *Life Sciences*, **76**(24), 2817–2825, 2005.
 - [249] Morioka, M., Parameswaran, H., Naruse, K., Kondo, M., Sokabe, M., Hasegawa, Y., Suki, B. and Ito, S. Microtubule Dynamics Regulate Cyclic Stretch-Induced Cell Alignment in Human Airway Smooth Muscle Cells. *PLoS ONE*, **6**(10), e26384, 2011.
 - [250] Norton, L. A., Andersen, K. L., Arenholt-Bindslev, D., Andersen, L. and Melsen, B. A methodical study of shape changes in human oral cells perturbed by a simulated orthodontic strain in vitro. *Archives of Oral Biology*, **40**(9), 863–872, 1995.
 - [251] Neidlinger-Wilke, C., Grood, E. S., Wang, J. H. C., Brand, R. A. and Claes, L. Cell alignment is induced by cyclic changes in cell length: studies of cells grown in cyclically stretched substrates. *Journal of Orthopaedic Research*, **19**(2), 286–293, 2001.
 - [252] Salameh, A., Wustmann, A., Karl, S., Blanke, K., Apel, D., Rojas-Gomez, D., Franke, H., Mohr, F. W., Janousek, J. and Dhein, S. Cyclic Mechanical Stretch Induces Cardiomyocyte Orientation and Polarization of the Gap Junction Protein Connexin43. *Circ Res*, **106**(10), 1592–1602, 2010.
 - [253] Wei, Z., Deshpande, V. S., McMeeking, R. M. and Evans, A. G. Analysis and interpretation of stress fiber organization in cells subject to cyclic stretch. *Journal of biomechanical engineering*, **130**(3), 031009, 2008.
 - [254] Engelmayr, G. C., Soletti, L., Vigmostad, S. C., Budilarto, S. G., Federspiel, W. J., Chandran, K. B., Vorp, D. A. and Sacks, M. S. A Novel Flex-Stretch-Flow Bioreactor for the Study of Engineered Heart Valve Tissue Mechanobiology. *Annals of Biomedical Engineering*, **36**(5), 700–712, 2008.
 - [255] Powell, C. A., Smiley, B. L., Mills, J. and Vandenburgh, H. H. Mechanical stimulation improves tissue-engineered human skeletal muscle. *American Journal of Physiology-Cell Physiology*, **283**(5), C1557–C1565, 2002.
 - [256] Gauvin, R., Parenteau-Bareil, R., Larouche, D., Marcoux, H., Bisson, F., Bonnet, A., Auger, F. A., Bolduc, S. and Germain, L. Dynamic mechanical stimulations induce anisotropy and improve the tensile properties of engineered tissues produced without exogenous scaffolding. *Acta Biomaterialia*, **7**(9), 3294–3301, 2011.
 - [257] Liao, I. C., Liu, J. B., Bursac, N. and Leong, K. W. Effect of Electromechanical Stimulation on the Maturation of Myotubes on Aligned Electrospun Fibers. In *Annual Meeting of the Biomedical-Engineering-Society*, pages 133–145, St Louis, MO, 2008. Springer.
 - [258] Madden, J. D. W., Vandesteeg, N. A., Anquetil, P. A., Madden, P. G. A., Takshi, A., Pytel, R. Z., Lafontaine, S. R., Wieringa, P. A. and Hunter, I. W. Artificial muscle technology: Physical principles and naval prospects. In *13th International Symposium on Unmanned Untethered Submersible Technology*, pages 706–728, Durham, NH, 2003.
 - [259] Pei, Q., Pelrine, R., Rosenthal, M. A., Stanford, S., Prahlad, H. and Kornbluh, R. D. Recent progress on electroelastomer artificial muscles and their application for biomimetic robots. *Proceedings of the SPIE*, **5385**, 41–50, 2004.
 - [260] BarCohen, Y., Pelrine, R., Kornbluh, R., Pei, Q. B., Stanford, S., Oh, S. J., Eckerle, J., Full, R., Rosenthal, M. and Meijer, K. Dielectric elastomer artificial muscle actuators: Toward biomimetic motion. In *Smart Structures and Materials 2002 Conference*, pages 126–137, San Diego, Ca, 2002.

- [261] Shankar, R., Ghosh, T. K. and Spontak, R. J. Dielectric elastomers as next-generation polymeric actuators. *Soft Matter*, **3**(9), 1116–1129, 2007.
- [262] Ladegaard Skov, A. and Sommer-Larsen, P. Chapter 3 - Physical and chemical properties of dielectric elastomers. In Carpi, F., Rossi, D. D., Kornbluh, R., Pelrine, R., Peter Sommer-LarsenA2 Federico Carpi, D. D. R. and Sommer-Larsen, P., editors, *Dielectric Elastomers as Electromechanical Transducers*, pages 23–32. Elsevier, Amsterdam, 2008.
- [263] Kofod, G., Sommer-Larsen, P., Kornbluh, R. and Pelrine, R. Actuation Response of Polyacrylate Dielectric Elastomers. *Journal of Intelligent Material Systems and Structures*, **14**(12), 787–793, 2003.
- [264] Pelrine, R. and Kornbluh, R. Chapter 1 - Electromechanical transduction effects in dielectric elastomers: actuation, sensing, stiffness modulation and electric energy generation. In Carpi, F., Rossi, D. D., Kornbluh, R., Pelrine, R., Peter Sommer-LarsenA2 Federico Carpi, D. D. R. and Sommer-Larsen, P., editors, *Dielectric Elastomers as Electromechanical Transducers*, pages 1–12. Elsevier, Amsterdam, 2008.
- [265] Carpi, F., Chiarelli, P., Mazzoldi, A. and De Rossi, D. Electromechanical characterisation of dielectric elastomer planar actuators: comparative evaluation of different electrode materials and different counterloads. *Sensors and Actuators a-Physical*, **107**(1), 85–95, 2003.
- [266] Clerc, J., Giraud, G., Laugier, J. and Luck, J. The electrical conductivity of binary disordered systems, percolation clusters, fractals and related models. *Advances in Physics*, **39**(3), 191–309, 1990.
- [267] Kofod, G. and Sommer-Larsen, P. Chapter 7 - Compliant electrodes: solutions, materials and technologies. In Carpi, F., Rossi, D. D., Kornbluh, R., Pelrine, R., Peter Sommer-LarsenA2 Federico Carpi, D. D. R. and Sommer-Larsen, P., editors, *Dielectric Elastomers as Electromechanical Transducers*, pages 69–76. Elsevier, Amsterdam, 2008.
- [268] Klüppel, M., Schuster, R. H. and Heinrich, G. Structure and Properties of Reinforcing Fractal Filler Networks in Elastomers. *Rubber Chemistry and Technology*, **70**(2), 243–255, 1997.
- [269] Aschwanden, M. and Stemmer, A. Low voltage, highly tunable diffraction grating based on dielectric elastomer actuators. *Proceedings of the SPIE*, **6524**, 65241N–65241N, 2007.
- [270] Benslimane, M., Gravesen, P. and Sommer-Larsen, P. Mechanical properties of dielectric elastomer actuators with smart metallic compliant electrodes. *Proceedings of the SPIE*, **4695**, 150–157, 2002.
- [271] Pelrine, R. E., Kornbluh, R. D. and Joseph, J. P. Electrostriction of polymer dielectrics with compliant electrodes as a means of actuation. *Sensors and Actuators a-Physical*, **64**(1), 77–85, 1998.
- [272] Claus, R. O., Goff, R. M., Homer, M., Hill, A. B. and Lalli, J. H. Ultralow modulus electrically conducting electrode materials. *Proceedings of the SPIE*, **6168**, 61681O–61681O, 2006.
- [273] Rosset, S., Niklaus, M., Dubois, P. and Shea, H. R. Metal Ion Implantation for the Fabrication of Stretchable Electrodes on Elastomers. *Advanced Functional Materials*, **19**(3), 470–478, 2009.
- [274] Choi, H. R., Jung, K. M., Koo, J. C., Nam, J. D., Lee, Y. K. and Cho, M. S. Electrostatically Driven Soft Polymer Actuator Based on Dielectric Elastomer. *Key Engineering Materials*, **297-300**, 622–627, 2005.
- [275] Kornbluh, R. and Pelrine, R. Chapter 4 - High-performance acrylic and silicone elastomers. In Carpi, F., Rossi, D. D., Kornbluh, R., Pelrine, R., Peter Sommer-LarsenA2 Federico Carpi, D. D. R. and Sommer-Larsen, P., editors, *Dielectric Elastomers as Electromechanical Transducers*, pages 33–42. Elsevier, Amsterdam, 2008.

-
- [276] Pelrine, R. and Kornbluh, R. Introduction: History of dielectric elastomer actuators. In Carpi, F., Rossi, D. D., Kornbluh, R., Pelrine, R., Peter Sommer-LarsenA2 Federico Carpi, D. D. R. and Sommer-Larsen, P., editors, *Dielectric Elastomers as Electromechanical Transducers*, pages xi–xiii. Elsevier, Amsterdam, 2008.
 - [277] Aschwanden, M., Friedlos, R. and Stemmer, A. Polymeric, electrically tunable optical elements based on artificial muscles. In *20th Annual Meeting of the IEEE-Lasers-and-Electro-Optics-Society*, pages 204–205, Lake Buena Vista, FL, 2007.
 - [278] Vincenzini, P., BarCohen, Y., Carpi, F., Dubois, P., Rosset, S., Niklaus, M., Dadras, M. and Shea, H. Metal Ion Implanted Compliant Electrodes in Dielectric Electroactive Polymer (EAP) Membranes. In *3rd International Conference on Smart Materials, Structures and Systems*, pages 18–25, Acireale, ITALY, 2008.
 - [279] Rosset, S., Niklaus, A., Dubois, P. and Shea, H. R. Mechanical characterization of a dielectric elastomer microactuator with ion-implanted electrodes. *Sensors and Actuators a-Physical*, **144**(1), 185–193, 2008.
 - [280] Bar-Cohen, Y., Rosset, S., Niklaus, M., Stojanov, V., Felber, A., Dubois, P. and Shea, H. R. Ion-implanted compliant and patternable electrodes for miniaturized dielectric elastomer actuators - art. no. 69270W. In *Conference on Electroactive Polymer Actuators and Devices (EAPAD 2008)*, pages W9270–W9270, San Diego, CA, 2008.
 - [281] Chen, L. Z., Liu, C. H., Hu, C. H. and Fan, S. S. Electrothermal actuation based on carbon nanotube network in silicone elastomer. *Applied Physics Letters*, **92**(26), 263104, 2008.
 - [282] Langer, R. and Vacanti, J. P. Tissue engineering. *Science*, **260**(5110), 920–926, 1993.
 - [283] Yang, J., Yamato, M., Shimizu, T., Sekine, H., Ohashi, K., Kanzaki, M., Ohki, T., Nishida, K. and Okano, T. Reconstruction of functional tissues with cell sheet engineering. *Biomaterials*, **28**(34), 5033–5043, 2007.
 - [284] Cao, Y., Vacanti, J. P., Paige, K. T., Upton, J. and Vacanti, C. A. Transplantation of chondrocytes utilizing a polymer-cell construct to produce tissue-engineered cartilage in the shape of a human ear. *Plastic and reconstructive surgery*, **100**(2), 297–302; discussion 303–304, 1997.
 - [285] Vacanti, C. A., Bonassar, L. J., Vacanti, M. P. and Shufflebarger, J. Replacement of an Avulsed Phalanx with Tissue-Engineered Bone. *New England Journal of Medicine*, **344**(20), 1511–1514, 2001.
 - [286] Atala, A., Bauer, S. B., Soker, S., Yoo, J. J. and Retik, A. B. Tissue-engineered autologous bladders for patients needing cystoplasty. *The Lancet*, **367**(9518), 1241–1246, 2006.
 - [287] Poh, M., Boyer, M., Solan, A., Dahl, S. L., Pedrotty, D., Banik, S. S., McKee, J. A., Klinger, R. Y., Counter, C. M. and Niklason, L. E. Blood vessels engineered from human cells. *The Lancet*, **365**(9477), 2122–2124, 2005.
 - [288] Shin’oka, T., Imai, Y. and Ikada, Y. Transplantation of a Tissue-Engineered Pulmonary Artery. *New England Journal of Medicine*, **344**(7), 532–533, 2001.
 - [289] Yamato, M. and Okano, T. Cell sheet engineering. *Materials Today*, **7**(5), 42–47, 2004.
 - [290] Matsuda, N., Shimizu, T., Yamato, M. and Okano, T. Tissue engineering based on cell sheet technology. *Advanced Materials*, **19**(20), 3089–3099, 2007.

- [291] Koh, G. Y., Klug, M. G., Soonpaa, M. H. and Field, L. J. Differentiation and long-term survival of C2C12 myoblast grafts in heart. *Journal of Clinical Investigation*, **92**(3), 1548–1554, 1993.
- [292] Nishida, K., Yamato, M., Hayashida, Y., Watanabe, K., Maeda, N., Watanabe, H., Yamamoto, K., Nagai, S., Kikuchi, A., Tano, Y. and Okano, T. Functional bioengineered corneal epithelial sheet grafts from corneal stem cells expanded ex vivo on a temperature-responsive cell culture surface. *Transplantation*, **77**(3), 379–385, 2004.
- [293] Memon, I. A., Sawa, Y., Fukushima, N., Matsumiya, G., Miyagawa, S., Taketani, S., Sakakida, S. K., Kondoh, H., Aleshin, A. N., Shimizu, T., Okano, T. and Matsuda, H. Repair of impaired myocardium by means of implantation of engineered autologous myoblast sheets. *The Journal of Thoracic and Cardiovascular Surgery*, **130**(5), 1333–1341, 2005.
- [294] Haraguchi, Y., Shimizu, T., Yamato, M., Kikuchi, A. and Okano, T. Electrical coupling of cardiomyocyte sheets occurs rapidly via functional gap junction formation. *Biomaterials*, **27**(27), 4765–4774, 2006.
- [295] Shimizu, T., Yamato, M., Isoi, Y., Akutsu, T., Setomaru, T., Abe, K., Kikuchi, A., Umezu, M. and Okano, T. Fabrication of Pulsatile Cardiac Tissue Grafts Using a Novel 3-Dimensional Cell Sheet Manipulation Technique and Temperature-Responsive Cell Culture Surfaces. *Circulation Research*, **90**(3), e40–e48, 2002.
- [296] Masuda, S., Shimizu, T., Yamato, M. and Okano, T. Cell sheet engineering for heart tissue repair. *Advanced Drug Delivery Reviews*, **60**(2), 277–285, 2008.
- [297] Giraud, M. N., Armbruster, C., Carrel, T. and Tevæarai, H. T. Current state of the art in myocardial tissue engineering. *Tissue Engineering*, **13**(8), 1825–1836, 2007.
- [298] Reinecke, H., MacDonald, G. H., Hauschka, S. D. and Murry, C. E. Electromechanical coupling between skeletal and cardiac muscle: Implications for infarct repair. *Journal of Cell Biology*, **149**(3), 731–740, 2000.
- [299] Elloumi-Hannachi, I., Yamato, M. and Okano, T. Cell sheet engineering: a unique nanotechnology for scaffold-free tissue reconstruction with clinical applications in regenerative medicine. *Journal of Internal Medicine*, **267**(1), 54–70, 2010.
- [300] Haraguchi, Y., Shimizu, T., Yamato, M. and Okano, T. Scaffold-free tissue engineering using cell sheet technology. *RSC Advances*, **2**(6), 2184–2190, 2012.
- [301] Guerra, L., Dellambra, E., Panacchia, L. and Paionni, E. Tissue Engineering for Damaged Surface and Lining Epithelia: Stem Cells, Current Clinical Applications, and Available Engineered Tissues. *Tissue Engineering Part B: Reviews*, **15**(2), 91–112, 2009.
- [302] Hannachi, I. E., Yamato, M. and Okano, T. Cell sheet technology and cell patterning for biofabrication. *Biofabrication*, **1**(2), 022002, 2009.
- [303] Sekine, H., Shimizu, T., Yang, J., Kobayashi, E. and Okano, T. Pulsatile Myocardial Tubes Fabricated With Cell Sheet Engineering. *Circulation*, **114**(1 suppl), I–87–I–93, 2006.
- [304] Sekine, H., Shimizu, T. and Okano, T. Myocardial tissue engineering: toward a bioartificial pump. *Cell and Tissue Research*, **347**(3), 775–782, 2012.
- [305] Yamada, N., Okano, T., Sakai, H., Karikusa, F., Sawasaki, Y. and Sakurai, Y. Thermo-responsive polymeric surfaces; control of attachment and detachment of cultured cells. *Die Makromolekulare Chemie, Rapid Communications*, **11**(11), 571–576, 1990.

-
- [306] Hou, H., Kim, W., Grunlan, M. and Han, A. A thermoresponsive hydrogel poly(N-isopropylacrylamide) micropatterning method using microfluidic techniques. *Journal of Micromechanics and Microengineering*, **19**(12), 127001, 2009.
 - [307] Guillaume-Gentil, O., Semenov, O., Roca, A. S., Groth, T., Zahn, R., Vörös, J. and Zenobi-Wong, M. Engineering the Extracellular Environment: Strategies for Building 2D and 3D Cellular Structures. *Advanced Materials*, **22**(48), 5443–5462, 2010.
 - [308] Guillaume-Gentil, O., Akiyama, Y., Schuler, M., Tang, C., Textor, M., Yamato, M., Okano, T. and Vörös, J. Polyelectrolyte Coatings with a Potential for Electronic Control and Cell Sheet Engineering. *Advanced Materials*, **20**(3), 560–565, 2008.
 - [309] Iler, R. Multilayers of colloidal particles. *Journal of Colloid and Interface Science*, **21**(6), 569–594, 1966.
 - [310] Decher, G., Hong, J. and Schmitt, J. Buildup of ultrathin multilayer films by a self-assembly process: III. Consecutively alternating adsorption of anionic and cationic polyelectrolytes on charged surfaces. *Thin Solid Films*, **210–211, Part 2**(0), 831–835, 1992.
 - [311] Decher, G. Fuzzy Nanoassemblies: Toward Layered Polymeric Multicomposites. *Science*, **277**(5330), 1232–1237, 1997.
 - [312] Schneider, A., Francius, G., Obeid, R., Schwinte, P., Hemmerle, J., Frisch, B., Schaaf, P., Voegel, J. C., Senger, B. and Picart, C. Polyelectrolyte multilayers with a tunable Young's modulus: Influence of film stiffness on cell adhesion. *Langmuir*, **22**(3), 1193–1200, 2006.
 - [313] Shi, X., Qin, L., Zhang, X., He, K., Xiong, C., Fang, J., Fang, X. and Zhang, Y. Elasticity of cardiac cells on the polymer substrates with different stiffness: an atomic force microscopy study. *Physical Chemistry Chemical Physics*, **13**(16), 7540–7545, 2011.
 - [314] Lavalle, P., Voegel, J.-C., Vautier, D., Senger, B., Schaaf, P. and Ball, V. Dynamic Aspects of Films Prepared by a Sequential Deposition of Species: Perspectives for Smart and Responsive Materials. *Advanced Materials*, **23**(10), 1191–1221, 2011.
 - [315] Richert, L., Engler, A. J., Discher, D. E. and Picart, C. Elasticity of native and cross-linked polyelectrolyte multilayer films. *Biomacromolecules*, **5**(5), 1908–1916, 2004.
 - [316] Richert, L., Boulmedais, F., Lavalle, P., Mutterer, J., Ferreux, E., Decher, G., Schaaf, P., Voegel, J.-C. and Picart, C. Improvement of Stability and Cell Adhesion Properties of Polyelectrolyte Multilayer Films by Chemical Cross-Linking. *Biomacromolecules*, **5**(2), 284–294, 2004.
 - [317] Ren, K. F., Crouzier, T., Roy, C. and Picart, C. Polyelectrolyte multilayer films of controlled stiffness modulate myoblast cell differentiation. *Advanced Functional Materials*, **18**(9), 1378–1389, 2008.
 - [318] Graf, N., Thomasson, E., Tanno, A., Vörös, J. and Zambelli, T. Spontaneous Formation of a Vesicle Multilayer on Top of an Exponentially Growing Polyelectrolyte Multilayer Mediated by Diffusing Poly-L-lysine. *The Journal of Physical Chemistry B*, **115**(43), 12386–12391, 2011.
 - [319] Graf, N., Tanno, A., Dochter, A., Rothfuchs, N., Vörös, J. and Zambelli, T. Electrochemically driven delivery to cells from vesicles embedded in polyelectrolyte multilayers. *Soft Matter*, **8**(13), 3641–3648, 2012.
 - [320] Ouyang, L., Malaisamy, R. and Bruening, M. L. Multilayer polyelectrolyte films as nanofiltration membranes for separating monovalent and divalent cations. *Journal of Membrane Science*, **310**(1–2), 76–84, 2008.

- [321] Adusumilli, M. and Bruening, M. L. Variation of Ion-Exchange Capacity, ζ Potential, and Ion-Transport Selectivities with the Number of Layers in a Multilayer Polyelectrolyte Film. *Langmuir*, **25**(13), 7478–7485, 2009.
- [322] Guillaume-Gentil, O., Graf, N., Boulmedais, F., Schaaf, P., Vörös, J. and Zambelli, T. Global and local view on the electrochemically induced degradation of polyelectrolyte multilayers: from dissolution to delamination. *Soft Matter*, **6**(17), 4246–4254, 2010.
- [323] Guillaume-Gentil, O., Gabi, M., Zenobi-Wong, M. and Vörös, J. Electrochemically switchable platform for the micro-patterning and release of heterotypic cell sheets. *Biomedical Microdevices*, **13**(1), 221–230, 2011.
- [324] Itabashi, Y., Miyoshi, S., Kawaguchi, H., Yuasa, S., Tanimoto, K., Furuta, A., Shimizu, T., Okano, T., Fukuda, K. and Ogawa, S. A New Method for Manufacturing Cardiac Cell Sheets Using Fibrin-Coated Dishes and Its Electrophysiological Studies by Optical Mapping. *Artificial Organs*, **29**(2), 95–103, 2005.
- [325] Ko, I. K., Kato, K. and Iwata, H. A thin carboxymethyl cellulose culture substrate for the cellulase-induced harvesting of an endothelial cell sheet. *Journal of biomaterials science. Polymer edition*, **16**(10), 1277–1291, 2005.
- [326] Sakai, S., Ogushi, Y. and Kawakami, K. Enzymatically crosslinked carboxymethylcellulose–tyramine conjugate hydrogel: Cellular adhesiveness and feasibility for cell sheet technology. *Acta Biomaterialia*, **5**(2), 554–559, 2009.
- [327] Nagai, N., Yunoki, S., Satoh, Y., Tajima, K. and Munekata, M. A method of cell-sheet preparation using collagenase digestion of salmon atelocollagen fibrillar gel. *Journal of Bioscience and Bioengineering*, **98**(6), 493–496, 2004.
- [328] Ito, A., Ino, K., Kobayashi, T. and Honda, H. The effect of RGD peptide-conjugated magnetite cationic liposomes on cell growth and cell sheet harvesting. *Biomaterials*, **26**(31), 6185–6193, 2005.
- [329] Shimizu, K., Ito, A., Yoshida, T., Yamada, Y., Ueda, M. and Honda, H. Bone tissue engineering with human mesenchymal stem cell sheets constructed using magnetite nanoparticles and magnetic force. *Journal of Biomedical Materials Research Part B: Applied Biomaterials*, **82B**(2), 471–480, 2007.
- [330] Shimizu, K., Ito, A., Lee, J.-K., Yoshida, T., Miwa, K., Ishiguro, H., Numaguchi, Y., Murohara, T., Kodama, I. and Honda, H. Construction of multi-layered cardiomyocyte sheets using magnetite nanoparticles and magnetic force. *Biotechnology and Bioengineering*, **96**(4), 803–809, 2007.
- [331] Fujita, H., Shimizu, K., Yamamoto, Y., Ito, A., Kamihira, M. and Nagamori, E. Fabrication of scaffold-free contractile skeletal muscle tissue using magnetite-incorporated myogenic C2C12 cells. *Journal of Tissue Engineering and Regenerative Medicine*, **4**(6), 437–443, 2010.
- [332] Minsky, M. Memoir on inventing the confocal scanning microscope. *Scanning*, **10**(4), 128–138, 1988.
- [333] Müller, M. *Introduction to Confocal Fluorescence Microscopy*. SPIE Publications, Bellingham, Washington, 2006.
- [334] Sandison, D. R. and Webb, W. W. Background rejection and signal-to-noise optimization in confocal and alternative fluorescence microscopes. *Appl. Opt.*, **33**(4), 603–615, 1994.
- [335] Binnig, G., Quate, C. F. and Gerber, C. Atomic Force Microscope. *Physical Review Letters*, **56**(9), 930–933, 1986.

-
- [336] Sarid, D. *Scanning force microscopy: with applications to electric, magnetic, and atomic forces*. Oxford University Press, Inc., New York, New York, 1994.
 - [337] Bowen, W. R., Lovitt, R. W. and Wright, C. J. Application of atomic force microscopy to the study of micromechanical properties of biological materials. *Biotechnology Letters*, **22**(11), 893–903, 2000.
 - [338] Francis, L. W., Lewis, P. D., Wright, C. J. and Conlan, R. S. Atomic force microscopy comes of age. *Biology of the Cell*, **102**(2), 133–143, 2010.
 - [339] Ushiki, T., Hitomi, J., Ogura, S., Umemoto, T. and Shigeno, M. Atomic force microscopy in histology and cytology. *Archives of Histology and Cytology*, **59**(5), 421–431, 1996.
 - [340] Muller, D. J. and Dufrene, Y. F. Atomic force microscopy as a multifunctional molecular toolbox in nanobiotechnology. *Nat Nano*, **3**(5), 261–269, 2008.
 - [341] Kasas, S., Gotzos, V. and Celio, M. R. Observation of living cells using the atomic force microscope. *Biophysical Journal*, **64**(2), 539–544, 1993.
 - [342] Ludwig, T., Kirmse, R., Poole, K. and Schwarz, U. S. Probing cellular microenvironments and tissue remodeling by atomic force microscopy. *Pflugers Archiv-European Journal of Physiology*, **456**(1), 29–49, 2008.
 - [343] Alkaisi, M. M., Muys, J. J. and Evans, J. J. Single cell imaging with AFM using Biochip/Bioimprint technology. *International Journal of Nanotechnology*, **6**(3-4), 355–368, 2009.
 - [344] Meyer, E. Atomic force microscopy. *Progress in Surface Science*, **41**(1), 3–49, 1992.
 - [345] Jalili, N. and Laxminarayana, K. A review of atomic force microscopy imaging systems: application to molecular metrology and biological sciences. *Mechatronics*, **14**(8), 907–945, 2004.
 - [346] Seo, Y. and Jhe, W. Atomic force microscopy and spectroscopy. *Reports on Progress in Physics*, **71**(1), 016101, 2008.
 - [347] Meister, A., Gabi, M., Behr, P., Studer, P., Vörös, J., Niedermann, P., Bitterli, J., Polesel-Maris, J., Liley, M., Heinzlmann, H. and Zambelli, T. FluidFM: Combining Atomic Force Microscopy and Nanofluidics in a Universal Liquid Delivery System for Single Cell Applications and Beyond. *Nano Letters*, **9**(6), 2501–2507, 2009.
 - [348] Dörig, P., Stiefel, P., Behr, P., Sarajlic, E., Bijl, D., Gabi, M., Vörös, J., Vorholt, J. A. and Zambelli, T. Force-controlled spatial manipulation of viable mammalian cells and micro-organisms by means of FluidFM technology. *Applied Physics Letters*, **97**(2), 023701, 2010.
 - [349] Jozefczuk, J. and Adjaye, J. Chapter Six - Quantitative Real-Time PCR-Based Analysis of Gene Expression. In Jameson, D., Westerhoff, H. V. and Verma, M., editors, *Methods in Enzymology*, volume 500, pages 99–109. Academic Press, 2011.
 - [350] Arya, M., Shergill, I. S., Williamson, M., Gommersall, L., Arya, N. and Patel, H. R. H. Basic principles of real-time quantitative PCR. *Expert Review of Molecular Diagnostics*, **5**(2), 209–219, 2005.
 - [351] Livak, K. J. and Schmittgen, T. D. Analysis of Relative Gene Expression Data Using Real-Time Quantitative PCR and the delta delta CT Method. *Methods*, **25**(4), 402–408, 2001.
 - [352] Peirson, S. N., Butler, J. N. and Foster, R. G. Experimental validation of novel and conventional approaches to quantitative real-time PCR data analysis. *Nucleic Acids Research*, **31**(14), e73, 2003.

- [353] Marx, K. A. Quartz Crystal Microbalance: A Useful Tool for Studying Thin Polymer Films and Complex Biomolecular Systems at the Solution-Surface Interface. *Biomacromolecules*, **4**(5), 1099–1120, 2003.
- [354] Rodahl, M., Hook, F., Krozer, A., Brzezinski, P. and Kasemo, B. Quartz crystal microbalance setup for frequency and Q-factor measurements in gaseous and liquid environments. *Review of Scientific Instruments*, **66**(7), 3924–3930, 1995.
- [355] Schram, D. C. Plasma processing and chemistry. *Pure and Applied Chemistry*, **74**(3), 369–380, 2002.
- [356] Kim, J., Chaudhury, M. K. and Owen, M. J. Hydrophobic Recovery of Polydimethylsiloxane Elastomer Exposed to Partial Electrical Discharge. *Journal of Colloid and Interface Science*, **226**(2), 231–236, 2000.
- [357] Adams, C. L., Chen, Y.-T., Smith, S. J. and James Nelson, W. Mechanisms of Epithelial Cell-Cell Adhesion and Cell Compaction Revealed by High-resolution Tracking of E-Cadherin- Green Fluorescent Protein. *The Journal of Cell Biology*, **142**(4), 1105–1119, 1998.
- [358] Wartenberg, M., Dönmez, F., Ling, F. C., Acker, H., Hescheler, J. and Sauer, H. Tumor-induced angiogenesis studied in confrontation cultures of multicellular tumor spheroids and embryoid bodies grown from pluripotent embryonic stem cells. *The FASEB Journal*, **15**(6), 995–1005, 2001.
- [359] Dufrene, Y. F., Evans, E., Engel, A., Helenius, J., Gaub, H. E. and Muller, D. J. Five challenges to bringing single-molecule force spectroscopy into living cells. *Nat Meth*, **8**(2), 123–127, 2011.
- [360] Müller, D. J. and Dufrêne, Y. F. Force nanoscopy of living cells. *Current Biology*, **21**(6), R212–R216, 2011.
- [361] Abdulreda, M. H. and Moy, V. T. Investigation of SNARE-Mediated Membrane Fusion Mechanism Using Atomic Force Microscopy. *Japanese journal of applied physics (2008)*, **48**(8), 08JA03–08JA03–10, 2009.
- [362] Hosokawa, Y., Hagiya, M., Iino, T., Murakami, Y. and Ito, A. Noncontact estimation of inter-cellular breaking force using a femtosecond laser impulse quantified by atomic force microscopy. *Proceedings of the National Academy of Sciences*, **108**(5), 1777–1782, 2011.
- [363] Ounkomol, C., Yamada, S. and Heinrich, V. Single-Cell Adhesion Tests against Functionalized Microspheres Arrayed on AFM Cantilevers Confirm Heterophilic E- and N-Cadherin Binding. *Biophysical Journal*, **99**(12), L100–L102, 2010.
- [364] Simon, A. and Durrieu, M.-C. Strategies and results of atomic force microscopy in the study of cellular adhesion. *Micron*, **37**(1), 1–13, 2006.
- [365] Weder, G., Guillaume-Gentil, O., Matthey, N., Montagne, F., Heinzelmann, H., Vörös, J. and Liley, M. The quantification of single cell adhesion on functionalized surfaces for cell sheet engineering. *Biomaterials*, **31**(25), 6436–6443, 2010.
- [366] Weder, G., Blondiaux, N., Giazson, M., Matthey, N., Klein, M., Pugin, R., Heinzelmann, H. and Liley, M. Use of Force Spectroscopy to Investigate the Adhesion of Living Adherent Cells. *Langmuir*, **26**(11), 8180–8186, 2010.
- [367] Baumgartner, W., Schütz, G. J., Wiegand, J., Golenhofen, N. and Drenckhahn, D. Cadherin function probed by laser tweezer and single molecule fluorescence in vascular endothelial cells. *Journal of Cell Science*, **116**(6), 1001–1011, 2003.

-
- [368] Zhang, X., Chen, A., De Leon, D., Li, H., Noiri, E., Moy, V. T. and Goligorsky, M. S. Atomic force microscopy measurement of leukocyte-endothelial interaction. *American Journal of Physiology - Heart and Circulatory Physiology*, **286**(1), H359–H367, 2004.
 - [369] Klaus, L., Pospieszalska, M. K. and Ley, K. Chapter 8 Modeling Leukocyte Rolling. In *Current Topics in Membranes*, volume 64, pages 221–273. Academic Press, 2009.
 - [370] Liu, J., Weller, G. E. R., Zern, B., Ayyaswamy, P. S., Eckmann, D. M., Muzykantov, V. R. and Radhakrishnan, R. Computational model for nanocarrier binding to endothelium validated using in vivo, in vitro, and atomic force microscopy experiments. *Proceedings of the National Academy of Sciences*, **107**(38), 16530–16535, 2010.
 - [371] Hiratsuka, S., Goel, S., Kamoun, W. S., Maru, Y., Fukumura, D., Duda, D. G. and Jain, R. K. Endothelial focal adhesion kinase mediates cancer cell homing to discrete regions of the lungs via E-selectin up-regulation. *Proceedings of the National Academy of Sciences*, **108**(9), 3725–3730, 2011.
 - [372] Zahler, S., Kupatt, C. and Becker, B. F. Endothelial preconditioning by transient oxidative stress reduces inflammatory responses of cultured endothelial cells to TNF- α . *The FASEB Journal*, **14**(3), 555–564, 2000.
 - [373] Yago, T., Shao, B., Miner, J. J., Yao, L., Klopocki, A. G., Maeda, K., Coggeshall, K. M. and McEver, R. P. E-selectin engages PSGL-1 and CD44 through a common signaling pathway to induce integrin α L β 2-mediated slow leukocyte rolling. *Blood*, **116**(3), 485–494, 2010.
 - [374] Bachtarzi, H., Stevenson, M., Šubr, V., Seymour, L. W. and Fisher, K. D. E-selectin is a viable route of infection for polymer-coated adenovirus retargeting in TNF- α -activated human umbilical vein endothelial cells. *Journal of Drug Targeting*, **19**(8), 690–700, 2011.
 - [375] Ley, K., Laudanna, C., Cybulsky, M. I. and Nourshargh, S. Getting to the site of inflammation: the leukocyte adhesion cascade updated. *Nat Rev Immunol*, **7**(9), 678–689, 2007.
 - [376] Sumagin, R., Prizant, H., Lomakina, E., Waugh, R. E. and Sarelius, I. H. LFA-1 and Mac-1 Define Characteristically Different Intraluminal Crawling and Emigration Patterns for Monocytes and Neutrophils In Situ. *The Journal of Immunology*, **185**(11), 7057–7066, 2010.
 - [377] Cheng, Q., McKeown, S. J., Santos, L., Santiago, F. S., Khachigian, L. M., Morand, E. F. and Hickey, M. J. Macrophage Migration Inhibitory Factor Increases Leukocyte-Endothelial Interactions in Human Endothelial Cells via Promotion of Expression of Adhesion Molecules. *J Immunol*, **185**(2), 1238–1247, 2010.
 - [378] Liu, Z. J., Sniadecki, N. J. and Chen, C. S. Mechanical Forces in Endothelial Cells during Firm Adhesion and Early Transmigration of Human Monocytes. *Cellular and Molecular Bioengineering*, **3**(1), 50–59, 2010.
 - [379] Chaplin, D. D. Overview of the immune response. *Journal of Allergy and Clinical Immunology*, **125**(2), S3–S23, 2010.
 - [380] Makó, V., Czúcz, J., Weiszhar, Z., Herczenik, E., Matkó, J., Prohászka, Z. and Cervenak, L. Proinflammatory activation pattern of human umbilical vein endothelial cells induced by IL-1 β , TNF- α , and LPS. *Cytometry Part A*, **77A**(10), 962–970, 2010.
 - [381] Frommhold, D., Kamphues, A., Hepper, I., Pruenster, M., Lukic, I. K., Socher, I., Zablotzkaya, V., Buschmann, K., Lange-Sperandio, B., Schymeinsky, J., Ryschich, E., Poeschl, J., Kupatt, C., Nawroth, P. P., Moser, M., Walzog, B., Bierhaus, A. and Sperandio, M. RAGE and ICAM-1 cooperate in mediating leukocyte recruitment during acute inflammation in vivo. *Blood*, **116**(5), 841–849, 2010.

- [382] McEver, R. P. and Zhu, C. Rolling Cell Adhesion. *Annual Review of Cell and Developmental Biology*, **26**(1), 363–396, 2010.
- [383] Cinamon, G., Shinder, V. and Alon, R. Shear forces promote lymphocyte migration across vascular endothelium bearing apical chemokines. *Nat Immunol*, **2**(6), 515–522, 2001.
- [384] Wayman, A. M., Chen, W., McEver, R. P. and Zhu, C. Triphasic Force Dependence of E-Selectin/Ligand Dissociation Governs Cell Rolling under Flow. *Biophysical Journal*, **99**(4), 1166–1174, 2010.
- [385] Hickey, M., Reinhardt, P., Ostrovsky, L., Jones, W., Jutila, M., Payne, D., Elliott, J. and Kubes, P. Tumor necrosis factor- α induces leukocyte recruitment by different mechanisms in vivo and in vitro. *The Journal of Immunology*, **158**(7), 3391–3400, 1997.
- [386] Gedeit, R. G. Tumor necrosis factor-induced E-selectin expression on vascular endothelial cells. *Critical Care Medicine*, **24**(9), 1543–1546, 1996.
- [387] Einstein, A. *Investigations on the Theory of Brownian Movement*. Courier Dover Publications, 1956.
- [388] Fenz, S. F., Smith, A.-S., Merkel, R. and Sengupta, K. Inter-membrane adhesion mediated by mobile linkers: Effect of receptor shortage. *Soft Matter*, **7**(3), 952–962, 2011.
- [389] Copuroglu, M. and Sen, M. A comparative study of UV aging characteristics of poly(ethylene-co-vinyl acetate) and poly(ethylene-co-vinyl acetate)/carbon black mixture. *Polymers for Advanced Technologies*, **16**(1), 61–66, 2005.
- [390] Liu, M. and Horrocks, A. R. Effect of Carbon Black on UV stability of LLDPE films under artificial weathering conditions. *Polymer Degradation and Stability*, **75**(3), 485–499, 2002.
- [391] Horrocks, A. R., Mwila, J., Miraftab, M., Liu, M. and Chohan, S. S. The influence of carbon black on properties of orientated polypropylene 2. Thermal and photodegradation. *Polymer Degradation and Stability*, **65**(1), 25–36, 1999.
- [392] Kim, H. J., Liu, X. D., Kobayashi, T., Kohyama, T., Wen, F. Q., Romberger, D. J., Conner, H., Gilmour, P. S., Donaldson, K., MacNee, W. and Rennard, S. I. Ultrafine carbon black particles inhibit human lung fibroblast-mediated collagen gel contraction. *American Journal of Respiratory Cell and Molecular Biology*, **28**(1), 111–121, 2003.
- [393] Horrocks, A. R. and Liu, M. G. UV stabilising synergies between carbon black and hindered light stabilisers in linear low density polyethylene films. In *2nd International Conference on Modification, Degradation and Stabilization of Polymers*, pages 199–219, Budapest, Hungary, 2003. Wiley-VCH Verlag GmbH.
- [394] Sh, M. S., Khatibi, E., Sarpoolaki, H. and Fard, F. G. An investigation of dispersion and stability of carbon black nano particles in water via UV-Visible Spectroscopy. *International Journal of Modern Physics B*, **22**(18-19), 3172–3178, 2008.
- [395] Akbari, S. and Shea, H. R. An array of 100 μm x 100 μm dielectric elastomer actuators with 80% strain for tissue engineering applications. *Sensors and Actuators A: Physical*, **186**(0), 236–241, 2012.
- [396] Akbari, S., Niklaus, M. and Shea, H. Arrays of EAP micro-actuators for single-cell stretching applications. page 76420H, 2010.
- [397] Akbari, S. and Shea, H. R. Microfabrication and characterization of an array of dielectric elastomer actuators generating uniaxial strain to stretch individual cells. *Journal of Micromechanics and Microengineering*, **22**(4), 045020, 2012.

-
- [398] Mauersberger, B., Mickwitz, C. U., Zipper, J., Axt, J. and Heder, G. Studies on the cytotoxicity of poly-L-arginine, poly-L-lysine and DEAE-dextran in L-cells and mouse embryonic fibroblasts. *Experimentelle Pathologie*, **13**(4-5), 268–273, 1977.
- [399] Fischer, D., Li, Y., Ahlemeyer, B., Krieglstein, J. and Kissel, T. In vitro cytotoxicity testing of polycations: influence of polymer structure on cell viability and hemolysis. *Biomaterials*, **24**(7), 1121–1131, 2003.
- [400] El-Safory, N. S. and Lee, C.-K. Cytotoxic and antioxidant effects of unsaturated hyaluronic acid oligomers. *Carbohydrate Polymers*, **82**(4), 1116–1123, 2010.
- [401] Guillaume-Gentil, O., Abbruzzese, D., Thomasson, E., Vörös, J. and Zambelli, T. Chemically Tunable Electrochemical Dissolution of Noncontinuous Polyelectrolyte Assemblies: An In Situ Study Using ecAFM. *ACS Applied Materials & Interfaces*, **2**(12), 3525–3531, 2010.
- [402] Guillaume-Gentil, O., Zahn, R., Lindhoud, S., Graf, N., Vörös, J. and Zambelli, T. From nanodroplets to continuous films: how the morphology of polyelectrolyte multilayers depends on the dielectric permittivity and the surface charge of the supporting substrate. *Soft Matter*, **7**(8), 3861–3871, 2011.
- [403] Boudou, T., Crouzier, T., Auzély-Velty, R., Glinel, K. and Picart, C. Internal Composition versus the Mechanical Properties of Polyelectrolyte Multilayer Films: The Influence of Chemical Cross-Linking. *Langmuir*, **25**(24), 13809–13819, 2009.

Curriculum Vitae

Personal

Name: Elsa Charlotta Thomasson
Date of Birth: November 11, 1982
Nationality: Swedish
Present Address: Tramstrasse 32
CH-8050 Zurich
Switzerland

Education

2007 – 2013 Doctoral student at the laboratory of biosensors and bioelectronics,
Department of Information Technology and Electrical Engineering,
Swiss Federal Institute of Technology (ETH) Zurich
2002 – 2007 Diploma in Engineering Physics, Chalmers University of
Technology, Gothenburg, Sweden
2001 – 2002 History of European Literature, University of Gothenburg, Sweden
1998 – 2001 Gymnasium Degree from the science program, Hvitfeldtska Gym-
nasiet, Gothenburg, Sweden

Experience

2007 Research Assistant at the Institute for Surface Science and Tech-
nology, ETH, Zurich, Switzerland

- 2006 – 2007 Master Thesis at the Institute for Surface Science and Technology, ETH, Zurich, Switzerland (5 months) Title: Wet Particle Lithography- Patterning Proteins Totally in Liquid
- 2005 ABB Kabeldon, Alingsås, Sweden (3 months) Internship, industrial work

Publications

Presentations

- 2012 Ion-induced cell sheet detachment from standard cell culture surfaces coated with polyelectrolytes (*oral presentation*)
E. Thomasson, R. Zahn, O. Guillaume-Gentil, J. Vörös, T. Zambelli
 E-MRS Spring Meeting, May 15–17, 2012, Strasbourg, France
- 2009 Unravelling SAC Dependent Behaviour in C2C12 Myoblasts during Myogenesis with Stretching Conditions (*poster presentation*)
E. Thomasson, J. Vörös and Alfredo Franco-Obregón
 ESB's 22nd European Conference on Biomaterials , September 7–11, 2009, Lausanne, Switzerland
- Unravelling SAC Dependent Behaviour In C2C12 Myoblasts During Myogenesis With Stretching Conditions (*poster presentation*)
E. Thomasson, J. Vörös and Alfredo Franco-Obregón
 2nd TERMIS World Congress, August 31–September 3, 2009, Seoul, South Korea
- 2008 Unraveling Cytoskeletal Transduction during Myogenesis with EAP Bioactuator (*oral presentation*)
E. Thomasson, M. Aschwanden, R. Enning, A. Stemmer, A. Franco-Obregón
 3rd International Conference on Smart Materials Structures Systems, June 8–13, 2008, Acireale, Italy

Unraveling Cytoskeletal Transduction during Myogenesis with EAP Bioactuator (*poster presentation*)

E. Thomasson, M. Aschwanden, R. Enning, A. Stemmer, A. Franco-Obregón
8th World Biomaterial Congress, May 28–June 01, 2008, Amsterdam, Netherlands

Stretch Induced Cell Sheet Alignment (*oral presentation*)

E. Thomasson, M. Aschwanden, R. Enning, A. Stemmer, J. Vörös, A. Franco-Obregón
SSB's 14th Swiss Conference in Biomaterials, May 8, 2008, Basel, Switzerland

2007 Real Time Analyses of Myogenesis in Behaving Myoblasts (*oral presentation*)

E. Thomasson, B. Städler, T. Blättler, J. Vörös, A. Franco-Obregón
TERMIS-AP, December 3–5, 2007, Tokyo, Japan

Real Time Analyses of Myogenesis in Behaving Myoblasts – Combining Atomic Force Microscopy with Confocal Laser Scanning Microscopy (*poster presentation*)

E. Thomasson, B. Städler, T. Blättler, L. Jacot-Descombes, J. Vörös, A. Franco-Obregón
JPK 6th International Workshop, October 9, 2007, Berlin, Germany

Real Time Analyses of Myogenesis in Behaving Myoblasts (*poster presentation*)

E. Thomasson, B. Städler, T. Blättler, J. Vörös, A. Franco-Obregón
Biosurf VII, August 29–31, 2007, Zurich, Switzerland

Wet Particle Lithography – Patterning Proteins Totally in Liquid (*poster presentation*)

E. Thomasson, T. M. Blättler, M. Röllinghoff, J. Vörös, M. Textor
ESF research conference on Biological Surfaces and Interfaces, July 1–6, 2007, Sant Feliu de Guixols, Spain

Journal Articles

E. Thomasson, L. Yu, G. Csucs, J. Vörös, G. Palazzolo, Structural Interpretation of the Cytoskeletal Support Requiring Adherens Junctions at the Fusion Site during Myogenesis, submitted to *Cytoskeleton*.

R. Zahn, **E. Thomasson**, O. Guillaume-Gentil, J. Vörös, T. Zambelli, Ion-induced cell sheet detachment from standard cell culture surfaces coated with polyelectrolytes, *Biomaterials* **2012**, 33(12): 3421–3427.

N. Graf, **E. Thomasson**, A. Tanno, J. Vörös, T. Zambelli, Spontaneous Formation of a Vesicle Multilayer on Top of an Exponentially Growing Polyelectrolyte Multilayer Mediated by Diffusing Poly-l-lysine, *Journal of Physical Chemistry B* **2011**, 115(43): 12386–12391

O. Guillaume-Gentil, D. Abbruzzese, **E. Thomasson**, J. Vörös, and T. Zambelli, Chemically tunable electrochemical dissolution of noncontinuous polyelectrolyte assemblies: an in situ study using ecAFM, *ACS Applied Materials & Interfaces* **2010**, 2(12):3525–3531

Supervision of Student Projects

- 2011 Live Imaging of Myoblast Fusion with Atomic Force Microscopy and Confocal Laser Scanning Microscopy (*master thesis*)
Li-ting Yu

- 2008 Stretch Induced Cell Sheet Alignment (*semester project*)
Radu Ilinca

- 2007 Simultaneous Confocal and Atomic Force Microscopic Imaging of Fusing eGFP-actin expressing Myoblasts (*semester project*)
Loïc Jacot-Descombes